



AGR TRISO Fuel Fission Product Release Data Summary

September 2023

John D. Stempien, PhD
Lu Cai, PhD
Paul A. Demkowicz, PhD



*INL is a U.S. Department of Energy National Laboratory
operated by Battelle Energy Alliance, LLC*

DISCLAIMER

This information was prepared as an account of work sponsored by an agency of the U.S. Government. Neither the U.S. Government nor any agency thereof, nor any of their employees, makes any warranty, expressed or implied, or assumes any legal liability or responsibility for the accuracy, completeness, or usefulness, of any information, apparatus, product, or process disclosed, or represents that its use would not infringe privately owned rights. References herein to any specific commercial product, process, or service by trade name, trade mark, manufacturer, or otherwise, does not necessarily constitute or imply its endorsement, recommendation, or favoring by the U.S. Government or any agency thereof. The views and opinions of authors expressed herein do not necessarily state or reflect those of the U.S. Government or any agency thereof.

AGR TRISO Fuel Fission Product Release Data Summary

John D. Stempien, PhD
Lu Cai, PhD
Paul A. Demkowicz, PhD

September 2023

Idaho National Laboratory
Advanced Reactor Technologies
Idaho Falls, Idaho 83415

<http://www.art.inl.gov>

Prepared for the
U.S. Department of Energy
Office of Nuclear Energy
Under DOE Idaho Operations Office
Contract DE-AC07-05ID14517

Page intentionally left blank

INL ART Program


AGR TRISO Fuel Fission Product Release Data

Summary

INL/RPT-23-74651
Revision 0

September 2023

Technical Reviewer: (Confirmation of mathematical accuracy, and correctness of data and appropriateness of assumptions.)




Adriaan A. Riet, PhD
AGR Computational Scientist

9/15/2023

Date

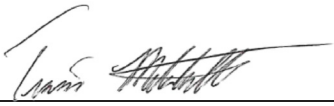
Approved by:



Gerhard Strydom, PhD
ART GCR National Technical Director

9/15/2023

Date



Travis R. Mitchell
ART Program Manager

9/15/2023

Date



Michelle T. Sharp
INL Quality Assurance

9/15/2023

Date

ACKNOWLEDGEMENTS

The work summarized here is the result of collaborative efforts spanning more than a decade of post-irradiation examination (PIE) and separated by thousands of miles between Idaho National Laboratory (INL) and Oak Ridge National Laboratory (ORNL). This report largely draws from the AGR-1 and AGR-2 final PIE reports and the reports and articles upon which they were based. Major contributors to the PIE results compiled here include Dr. John Hunn (ORNL), Dr. Robert Morris (ORNL), Dr. Jason Harp (formerly INL, currently ORNL), and Dr. Fred Montgomery (ORNL). Dr. David Petti (INL) contributed useful comments and discussions and prompted the beginning of this report more than 5 years ago. The following current and retired INL staff are also acknowledged for their contributions to fission product mass balances, safety tests, and compact destructive exams: Scott Ploger, Dr. Edward Reber, Cad Christensen, Les Scott, David Laug, Philip Winston, and Martin Kearns. Finally, staff at the INL Hot Fuel Examination Facility, INL Analytical Laboratory, ORNL Irradiated Fuels Examination Laboratory, and ORNL Nuclear Analytical Chemistry and Isotopics Laboratory are gratefully acknowledged.

Page intentionally left blank

CONTENTS

ACKNOWLEDGEMENTS.....	iii
ACRONYMS.....	x
1. INTRODUCTION.....	1
1.1 AGR Irradiation Tests.....	1
1.1.1 AGR-1 Description	2
1.1.2 AGR-2 Description	3
1.1.3 AGR-3/4 Description	4
1.2 Descriptions of Available PIE Data and Sample Lists.....	5
1.2.1 AGR-1	5
1.2.2 AGR-2	8
1.2.3 AGR-3/4.....	9
1.3 Conventions and Definitions.....	9
1.3.1 Fission-product activities and fractions	9
1.3.2 SiC Failure versus TRISO Failure	10
1.3.3 Limitations of Experimental Measurements, Exams, and Safety Tests	10
2. AS-IRRADIATED PIE DATA SUMMARY	11
2.1 Matrix Inventory of Fission Products from DLBL	11
2.2 Fission-Product Release from Compacts Based on Mass Balance	15
2.2.1 AGR-1 Mass Balance.....	16
2.2.2 AGR-2 Mass Balance.....	19
2.2.3 AGR-3/4 Mass Balance	21
3. SAFETY TEST DATA SUMMARY	24
3.1 AGR-1 Safety Test Total Releases and Particle Failures.....	24
3.2 AGR-2 Safety Test Total Releases and Failures.....	25
3.3 AGR-1 and AGR-2 UCO Safety Test Time-Dependent Release Data	26
3.3.1 Ag-110m	26
3.3.2 Cs-134.....	29
3.3.3 Eu-154 and Sr-90	31
3.3.4 Kr-85	35
3.4 Range of Release of Key Nuclides across AGR-1 and AGR-2 UCO Fuel	35
3.5 Discussion of Temperature-Transient versus Isothermal Testing.....	36
4. FISSION-PRODUCT RELEASE RATES FROM UCO FUEL	40
4.1 SiC and TRISO Failure Rates in UCO Fuel.....	40
4.2 In-pile Compact Release Rates	42
4.3 Accumulation of Fission Products in Compact Matrix	46
4.4 In-pile through-SiC Release Rates	49

4.5	Release Rates from High-Temperature Safety Testing.....	49
4.5.1	Cs-134 Safety Test Release Rates.....	49
4.5.2	Ag-110m Safety-Test Release Rates.....	55
4.5.3	Eu-154 Safety Test Release Rates.....	59
4.5.4	Sr-90 Safety Test Release Rates	63
5.	SUMMARY AND CONCLUSIONS.....	68
6.	REFERENCES.....	69

FIGURES

Figure 1.	TAVA irradiation temperatures versus burnup for compacts from the AGR-1, 2, and 3/4 irradiations.	2
Figure 2.	Image of an AGR-3/4 fuel compact (left) and x-ray side-view image (right) (Hunn, Trammell, and Montgomery 2011).....	4
Figure 3.	Axial cutaway diagram of a standard AGR-3/4 irradiation capsule.....	4
Figure 4.	Summary of the fission-product inventory measured from DLBL of AGR-1 and 2 compacts.	15
Figure 5.	Capsule fractions of key fission products measured outside of the fuel compacts in AGR-1 Capsules 1-6.....	17
Figure 6.	AGR-2 mass balances versus compact TAVA temperature.....	19
Figure 7.	AGR-3/4 Ag-110m and Cs-134 mass balances versus compact TAVA temperature.	21
Figure 8.	AGR-3/4 Eu-154 and Sr-90 mass balances versus compact TAVA temperature.	22
Figure 9.	Summary of the time-dependent Ag-110m release fractions as a function of the hold time at the specified test temperature.	28
Figure 10.	Summary of the time-dependent Cs-134 release fractions as a function of the hold time at the specified test temperature.	30
Figure 11.	Summary of the time-dependent Eu-154 release fractions as a function of the hold time at the specified test temperature.	33
Figure 12.	Summary of the time-dependent Sr-90 release fractions as a function of the hold time at the specified test temperature.	34
Figure 13.	Summary of the ranges of fission product release for key nuclides from AGR-1 and AGR-2 UCO fuel (Stempien et al. 2021).	36
Figure 14.	(a) Release fraction of Ag-110m from AGR-1 transient test of compared to isothermal tests of three other AGR-1 fuel compacts and (b) release rates of Ag-110m from the same tests (Stempien et al. 2016).	37
Figure 15.	(a) Release fraction of Cs-134 from AGR-1 transient test compared to isothermal tests of three other AGR-1 fuel compacts and (b) release rates of Cs-134 from the same tests (Stempien et al. 2016).....	38

Figure 16. (a) Release fraction of Eu-154 from AGR-1 transient test compared to isothermal tests of three other AGR-1 fuel compacts and (b) release rates of Eu-154 from the same tests (Stempien et al. 2016).....	39
Figure 17. Summary of cumulative radionuclide releases from the simultaneous transient test of three Capsule 5 UCO compacts.	40
Table 16. Summary of SiC- and TRISO-failure fractions after irradiation and after safety testing for AGR-1 and 2 individually and for their combination into a single population.....	41
Figure 18. Plot of observed and SiC- and TRISO-failure fraction and the upper 95% confidence limits from the combined results from the AGR-1 and AGR-2 irradiations and safety tests. UCO fuel only.	42
Figure 19. Compact release rates for Ag-110m. Data points come from AGR-1 Capsules 1-6; AGR-2 Capsules 2, 5, and 6; and AGR-3/4 Capsules 3, 4, 7, 8, and 10.....	44
Figure 20. Compact release rates for Cs-134. Data points come from AGR-1 Capsules 5 and 6 and AGR-2 Capsules 2, 5, and 6.....	44
Figure 21. Compact release rates for Eu-154. Data points come from AGR-1 Capsules 1-6; AGR-2 Capsules 2 and 5; and AGR-3/4 Capsule 7.....	45
Figure 22. Compact release rates for Sr-90. Data points come from AGR-1 Capsules 1-6; AGR-2 Capsules 2, 5, and 6; and AGR-3/4 Capsule 7.....	45
Figure 23. Rate of Ag-110m buildup in the fuel-compact matrix and OPyC from AGR-1 compacts subjected to as-irradiated DLBL that did not have any SiC or TRISO failures.	47
Figure 24. Rate of Cs-134 buildup in the fuel-compact matrix and OPyC from AGR-1 and 2 compacts subjected to as-irradiated DLBL.....	47
Figure 25. Rate of Eu-154 buildup in the fuel-compact matrix and OPyC from AGR-1 and 2 compacts subjected to as-irradiated DLBL.....	48
Figure 26. Rate of Sr-90 buildup in the fuel-compact matrix and OPyC from AGR-1 and 2 compacts subjected to as-irradiated DLBL.....	48
Figure 27. Release fractions and release rates for AGR-1 Compact 4-3-3 and AGR-2 Compact 5-2-1, showing typical 1600°C Cs-134 release behavior in the absence of any SiC or TRISO failures.....	50
Figure 28. Release fractions and release rates for AGR-1 Compact 4-1-2 and AGR-1 Compact 3-3-2, each of which suffered a single SiC failure at the beginning of the test.	50
Figure 29. Release fractions and release rates for AGR-1 Compact 3-2-3 and AGR-2 Compact 6-2-1, at 1800°C. The AGR-1 Compact 3-2-3 test had 11 SiC failures.....	51
Figure 30. Release fractions and release rates for AGR-1 Compact 4-4-1 and AGR-2 Compact 2-2-1, at 1800°C.....	52
Figure 31. Compact release fraction versus time for two safety tests.....	53
Figure 32. Average pseudo-steady-state release rates of Cs-134 from AGR-2 and 1 fuel compacts subjected to safety testing at temperatures of 1600, 1700, and 1800°C at INL and ORNL.	54
Figure 33. Cumulative fractional release of Ag-110m and release rates (calculated as the slopes between adjacent cumulative releases) for two compacts.	56

Figure 34. Pseudo-steady-state release rates of Ag-110m from AGR-2 and AGR-1 fuel compacts subjected to safety testing at temperatures of 1600, 1700, and 1800°C at INL and ORNL.	57
Figure 35. Pseudo-steady-state release rate of Ag-110m from AGR-2 and AGR-1 fuel compacts subjected to safety testing at temperatures of 1600, 1700, and 1800°C at INL and ORNL.	58
Figure 36. Examples of Eu-154 release vs time data from three different safety tests and the linear fits applied to establish average rates of release.	59
Figure 37. Eu-154 pseudo-steady-state release rates from 1600°C AGR-1 and AGR-2 safety tests versus compact TAVA irradiation temperature.	61
Figure 38. Eu-154 pseudo-steady-state release rates from 1700 and 1800°C AGR-1 and AGR-2 safety tests versus compact TAVA irradiation temperature.	61
Figure 39. Pseudo-steady state Eu-154 release rates versus inverse safety test temperatures including exponential fits for different groupings of compacts based on TAVA temperature.	62
Figure 40. Examples of Sr-90 release vs time data from three different safety tests and the linear fits applied to establish average release rates at the isothermal holds.	63
Figure 41. Cumulative fractional release and release rates for unique tests with late increases in Sr-90 release rate.	65
Figure 42. Sr-90 pseudo-steady-state release rates from AGR-1 and 2 safety tests versus compact TAVA irradiation temperature.	66
Figure 43. Pseudo-steady-state Sr-90 release rates from 1700 and 1800°C AGR-1 and 2 safety tests versus compact TAVA irradiation temperature.	66
Figure 44. Sr-90 pseudo-steady-state release rates versus inverse safety-test temperatures, including exponential fits for compacts with irradiation temperatures > or < 1200°C.	67

TABLES

Table 1. Description of AGR-1 TRISO coating types.	2
Table 2. AGR-1 fuel type loadings and capsule-average irradiation properties.	3
Table 3. AGR-2 fuel kernel types and capsule-average irradiation properties.	3
Table 4. AGR-3/4 capsule types, FB and Std, type of ring material surrounding the AGR-3/4 fuel compacts, and the average burnup, fast-neutron fluence, and TAVA irradiation temperature of the fuel in each capsule.	5
Table 5. AGR-1 fuel compacts used for as-irradiated DLBL analyses.	6
Table 6. Summary of safety tests of AGR-1 fuel compacts.	7
Table 7. AGR-2 compacts subjected to as-irradiated DLBL.	8
Table 8. List of AGR-2 compacts used in safety tests.	9
Table 9. Fraction of compact inventory (M/C) determined from the DLBL solutions in as-irradiated compacts from AGR-1 and AGR-2.	13

Table 10. Summary of the numbers of particles with in-pile failed SiC and failed TRISO coatings, the number of particles determined to have as-fabricated defects, and the number of particles accidentally damaged during DLBL examinations.	14
Table 11. Summary of major condensable fission-product inventories measured on the AGR-1 irradiation test-train components outside of the fuel compacts.	18
Table 12. Summary of major condensable fission-product inventories measured on the AGR-2 irradiation test-train components outside of the fuel compacts.	20
Table 13. Summary of major condensable fission-product inventories measured on the AGR-3/4 irradiation test train components outside of the fuel compacts.....	23
Table 14. Summary of total release of key radionuclides and numbers of SiC and TRISO failures at the completion of each AGR-1 isothermal safety test (Demkowicz et al. 2015a).	25
Table 15. Summary of total release of key radionuclides and numbers of SiC and TRISO failures at the completion of each AGR-2 isothermal safety test (Stempien et al. 2021).	26

ACRONYMS

AGR	Advanced Gas Reactor
ART	Advanced Reactor Technologies
ATR	Advanced Test Reactor
AVG	Arbeitsgemeinschaft Versuchsreaktor
C	Calculated value
CCCTF	Core Conduction Cooldown Test Facility
DLBL	Deconsolidation leach burn leach
DTF	Designed-to-fail
DUF	Dispersed uranium fraction
EOI	End of irradiation
EFPD	Effective-full-power days
FACS	Fuel Accident Condition Simulator
FB	Fuel body
FIMA	Fissions per initial metal atom
HTGR	High-temperature gas-cooled reactor
INL	Idaho National Laboratory
IPyC	Inner pyrolytic carbon
M	Measured value
M/C	Measured-to-calculated ratio
MDA	Minimum detectable activity
OPyC	Outer pyrolytic carbon
ORNL	Oak Ridge National Laboratory
PIE	Post-irradiation examination
TA	Time-averaged
TAVA	Time-average volume-average
TRISO	Tristructural isotropic
UCO	Uranium oxycarbide (a heterogeneous mixture of uranium carbide and uranium oxide)

Page intentionally left blank

AGR TRISO Fuel Fission Product Release Data Summary

1. INTRODUCTION

The Advanced Gas Reactor (AGR) Fuel Development and Qualification Program has been charged with research and development of tristructural isotropic (TRISO) coated-particle fuel for use in high-temperature reactors in the US (INL 2022). The AGR program includes work on TRISO fuel fabrication, irradiation performance, and post-irradiation safety testing. All four of the AGR irradiation experiments have been completed, and post-irradiation examination (PIE) has been completed for two of them (AGR-1 and AGR-2). PIE of the AGR-3/4 and AGR-5/6/7 experiments is ongoing as of this writing. Data accumulated from PIE activities are being used to support fuel qualification and reactor licensing, comparisons with predictive models, and as the bases for empirical models of fuel behavior and fission-product transport.

Knowledge of fission-product retention in and release from the fuel under normal and off-normal conditions is needed for reactor safety analyses. This is particularly critical in the case of coated-particle fuel used in high-temperature reactors relying on the functional containment strategy (Petti et al. 2013) in which the fuel itself is the primary barrier to fission-product release. Much of AGR PIE focuses on detecting and quantifying key fission products outside of the fuel. Upon completion of an AGR irradiation test, the irradiation test train is disassembled, and fuel compacts and capsule components are analyzed for fission-product inventories. Next, select irradiated fuel compacts are subjected to post-irradiation heating tests (often referred to as “safety tests”) at high temperatures characteristic of conduction cool-down events in high-temperature gas-cooled reactors (HTGRs). Safety tests enable the determination of fission-product releases as a function of irradiation conditions (e.g., irradiation temperature, fluence, and burnup), safety-test temperature (typically between 1600 and 1800°C), and elapsed safety-test time. Safety tests are also used to establish the rates of TRISO-coating failure at typical accident temperatures (Stempien et al. 2021, Demkowicz et al. 2015a).

In this report, data on fission-product release from fuel determined via a variety of experimental methods will be summarized, and empirical relationships will be made with respect to time and temperature where possible. This includes in-pile fission product release and release during post-irradiation safety testing. It also includes the fission-product content measured during destructive exams of fuel compacts via a process called deconsolidation-leach-burn-leach (DLBL). The frequencies of silicon carbide (SiC) failure and TRISO-coating failure from irradiation and post-irradiation safety testing will also be summarized.

1.1 AGR Irradiation Tests

Fission-product data will be considered from in-pile and PIE results from three AGR irradiations: AGR-1, 2, and 3/4. The fourth and final AGR irradiation, AGR-5/6/7, is in the midst of PIE. The range of burnups and the time-average volume-average (TAVA) irradiation temperatures spanned by all compacts in the AGR-1, 2, and 3/4 tests are plotted in Figure 1.

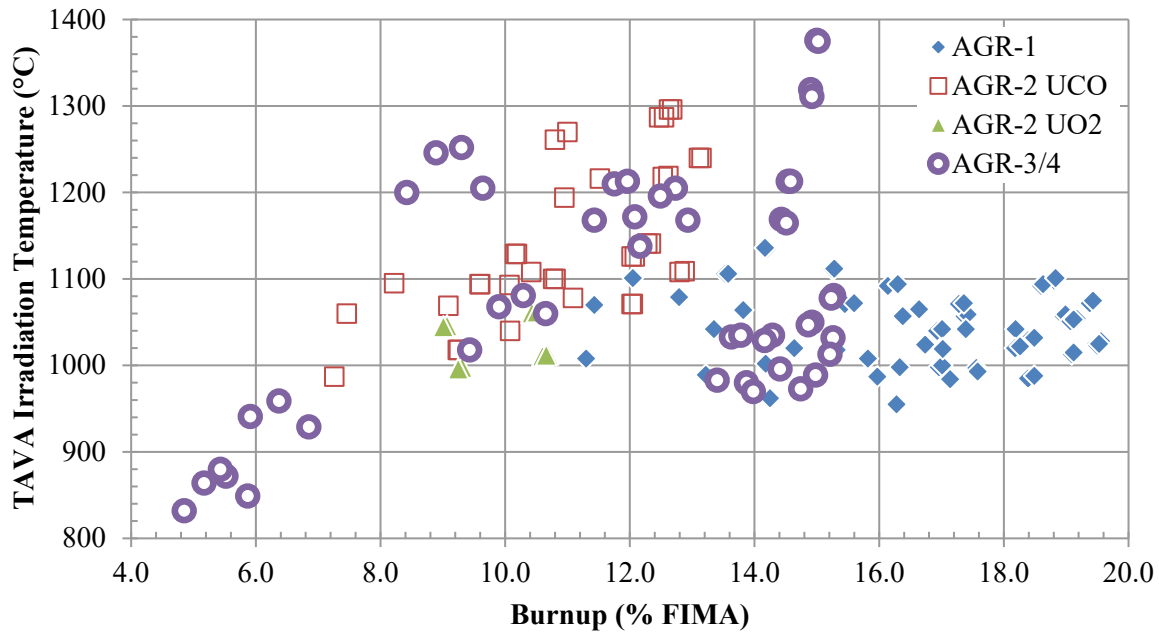


Figure 1. TAVA irradiation temperatures versus burnup for compacts from the AGR-1, 2, and 3/4 irradiations. AGR-1 burnups and temperatures from Sterbentz (2013) and Hawkes (2014a), respectively. AGR-2 burnups and temperatures from Sterbentz (2014) and Hawkes (2014b), respectively. AGR-3/4 burnups and temperatures from Sterbentz (2015) and Hawkes (2016), respectively.

1.1.1 AGR-1 Description

The AGR-1 irradiation test consisted of six capsules, each with 12 fuel compacts. Each compact contained approximately 4100 TRISO-coated uranium-oxycarbide (UCO) fuel particles, and particle packing fractions ranged from 36.0 to 37.5%, depending on the type (described below). Here UCO is used as shorthand for a heterogeneous mixture of uranium carbide and uranium oxide in the fuel kernel. These kernels were nominally 350 μm in diameter. The AGR-1 final PIE report summarizes key as-fabricated properties of the fuel particles and compacts (Demkowicz et al. 2015a). Four types of TRISO coatings were used in this test: Baseline, Variant 1, Variant 2, and Variant 3. Table 1 describes the similarities and differences among the types. Variant 3 was the only AGR-1 type that used argon dilution to promote deposition of a more-uniform and equiaxed SiC grain structure (Gerczak et al. 2016; Phillips, Barnes, and Hunn 2010). The fuel compacts had end caps, i.e., unfueled areas approximately 1.5 mm thick at the top and the bottom, composed only of graphitic matrix to protect the particles from damage (Collin 2015a). The irradiation conditions (e.g., temperature and burnup) for each compact in this test are summarized in Collin (2015a). Table 2 summarizes which AGR-1 capsules contained which fuel type and the capsule-average irradiation conditions.

Table 1. Description of AGR-1 TRISO coating types (Hunn, Jellison, and Lowden 2008; Demkowicz et al. 2015a).

AGR-1 Type	Description
Baseline	Coating properties similar to German reference properties
1	Like baseline, but with IPyC deposited at 25°C higher temperature
2	Like baseline, but IPyC deposited with a coating gas fraction of 0.45, instead of 0.30
3	Like baseline, but SiC deposited at 1425°C instead of 1500°C and using Ar and H ₂ for fluidization in the coater instead of H ₂ alone. This is supposed to promote formation of a more-uniform and equiaxed grain structure.

Table 2. AGR-1 fuel type loadings and capsule-average irradiation properties. Information from Collin (2015a).

AGR-1 Capsule Number	Variant	Burnup (% FIMA)	Fast Fluence (1×10^{25} , $E > 0.18$ MeV)	TAVA Temperature (°C)
6	Baseline	13.36	2.65	1087
5	Variant 1	16.50	3.52	1023
4	Variant 3	18.23	3.98	1070
3	Baseline	18.64	4.07	1028
2	Variant 2	17.84	3.77	1002
1	Variant 3	15.33	3.02	1054

1.1.2 AGR-2 Description

AGR-2 was the second of four irradiations that were conducted in the AGR program. The AGR-2 test included two different types of TRISO fuel fabricated in the U.S. The first type was UCO, the main focus of this fuel qualification program, and the second type was uranium oxide (UO₂). The TRISO-coating conditions for both types of kernels were derived from the AGR-1, Variant 3 fuel (described above). The AGR-2 UCO fuel kernels and UO₂ fuel kernels were 427 μm and 508 μm in diameter, respectively. AGR-2 UCO fuel compacts had an estimated 3176 particles per compact, giving a packing fraction of 36.8%. AGR-2 UO₂ compacts had an average of 1543 particles per compact, equating to a packing fraction of 23.5%. While AGR-1 fuel was produced at the laboratory scale, the AGR-2 coatings were fabricated using an industrial-scale coater and represented an important step in the establishment of an industrial-scale fuel-fabrication capability. As-fabricated fuel properties are summarized in Stempien et al. (2021) and the irradiation conditions are summarized in Collin (2018). The peak burnups of AGR-1 (enriched to 19.7% U-235) were higher than AGR-2 (enriched to 14.0% U-235), and AGR-2 fuel TAVA irradiation temperatures ranged from about 1000–1300°C compared to 950–1135°C for AGR-1. This constituted a temperature-margin test of fuel-irradiation performance. The “AGR-2 Irradiation Test Final As-Run Report” summarizes the irradiation conditions and fuel properties from this test (Collin 2018). Table 3 contains selected capsule-averaged irradiation conditions and denotes which capsules contained UCO TRISO fuel and UO₂ TRISO fuel. Only Capsules 2, 3, 5, and 6 contained U.S. AGR program fuel.

Table 3. AGR-2 fuel kernel types and capsule-average irradiation properties. Information from Collin (2018). Capsules 1 and 4 did not contain AGR Program fuel.

AGR-2 Capsule Number	Kernel Type	Burnup (% FIMA)	Fast Fluence (1×10^{25} , $E > 0.18$ MeV)	TAVA Temperature (°C)
Capsule 6	UCO	9.30	2.39	1074
Capsule 5	UCO	11.68	3.18	1101
Capsule 3	UO ₂	10.10	3.35	1032
Capsule 2	UCO	12.17	3.25	1252

1.1.3 AGR-3/4 Description

The AGR-3/4 irradiation experiment was designed to investigate the migration of fission products in fuel-compact graphitic matrix and reactor-grade graphite components. Each AGR-3/4 fuel compact contained an estimated 1898 TRISO-coated UCO particles, similar to AGR-1 baseline fuel (Collin 2015b, Hunn and Lowden 2007, Hunn et al. 2014e) and 20 designed-to-fail (DTF) particles. DTF particles consisted of kernels coated only with a thin (20- μm -thick) pyrocarbon layer. This layer was intentionally fabricated with a high optical anisotropy, such that it would be likely to fail during the irradiation (Collin 2015b, Hunn and Miller 2009, Kercher et al. 2011) and result in 20 exposed fuel kernels per compact. As shown at right in Figure 2, the DTF particles (highlighted in red) were aligned roughly along the compact's radial centerline. DTF particles provided a known source of fission products to migrate radially outward in the compacts and into the surrounding concentric rings of graphite and/or matrix material. There were three concentric rings around a stack of four fuel compacts in each capsule. From the inside to the outside, these are called the inner ring, outer ring, and sink ring. Two types of capsules were used in AGR-3/4: standard (Std) and fuel body (FB) (Collin 2015b, Stempien et al. 2018). The Std capsule type is depicted in Figure 3, where the outer ring is open on its top and bottom. FBs, on the other hand, had floors and a lid that screwed on to the top of the outer ring. Driver-particle and DTF-particle properties have been summarized by Collin (2015b). Complete kernel and particle characterization and fabrication data are compiled in several publications (Kercher and Hunn 2006, Hunn and Lowden 2007, Hunn and Miller 2009, Kercher et al. 2011). Table 4 summarizes the materials used in each AGR-3/4 capsule, the capsule type, and the capsule-averaged irradiation conditions in the fuel.

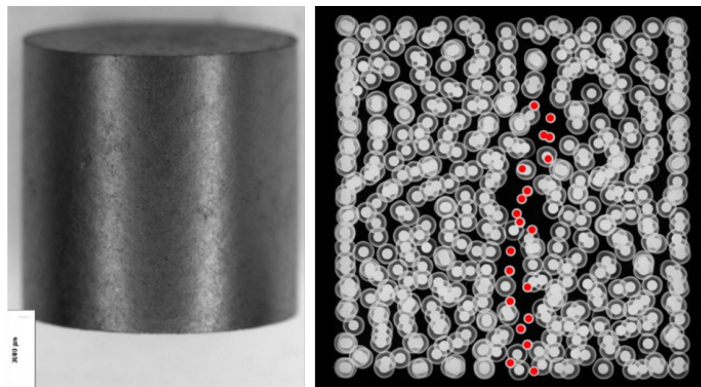


Figure 2. Image of an AGR-3/4 fuel compact (left) and x-ray side-view image (right) (Hunn, Trammell, and Montgomery 2011). DTF particles are highlighted with red dots in the x-ray image.

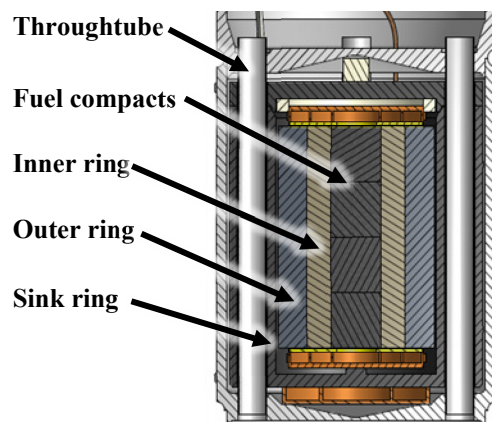


Figure 3. Axial cutaway diagram of a standard AGR-3/4 irradiation capsule.

Table 4. AGR-3/4 capsule types, FB and Std, type of ring material surrounding the AGR-3/4 fuel compacts, and the average burnup, fast-neutron fluence, and TAVA irradiation temperature of the fuel in each capsule. Except for the Capsule 4 FB, only standard capsules were disassembled to establish a mass balance of fission products released from the fuel compacts. AGR-3/4 burnups and fluences from Sterbentz (2015). Temperatures from Hawkes (2016).

Capsule No.	Capsule Type	Ring Material			Average Irradiation Conditions in Fuel Compacts		
		Inner	Outer	Sink	Burnup (% FIMA)	Fast Fluence (1×10^{25} , $E > 0.18$ MeV)	TAVA Temperature (°C)
1	Std	Matrix	PCEA	PCEA	6.14	1.76	927
2	FB	Matrix	PCEA	PCEA	10.07	3.21	1057
3	Std	PCEA	PCEA	PCEA	12.58	4.22	1177
4	FB	Matrix	PCEA	PCEA	14.21	4.85	1008
5	Std	Matrix	PCEA	PCEA	14.87	5.19	1015
6	FB	Matrix	PCEA	PCEA	15.24	5.31	1051
7	Std	Matrix	PCEA	PCEA	14.96	5.27	1345
8	Std	IG-110	IG-110	PCEA	14.51	5.08	1190
9	FB	Matrix	IG-110	PCEA	13.67	4.65	1008
10	Std	PCEA	PCEA	PCEA	11.8	3.94	1191
11	FB	Matrix	PCEA	PCEA	9.06	2.87	1226
12	Std	Matrix	PCEA	PCEA	5.35	1.5	854

1.2 Descriptions of Available PIE Data and Sample Lists

1.2.1 AGR-1

AGR-1 PIE data include the inventory of fission products outside of the fuel compacts, measured on the irradiation-capsule components (e.g., graphite compact holder, capsule spacers, capsule shell, etc.) (Demkowicz et al. 2013). Certain compacts were selected for as-irradiated DLBL analysis in order to determine the inventory of fission products retained in the compact matrix outside of the SiC layer. Individual deconsolidated particles were also analyzed for their post-irradiation inventory of gamma-emitting fission products (Demkowicz et al. 2015a). Table 5 lists the compacts used in as-irradiated DLBL analyses. References given in Table 5 describe the experimental methods employed. A number of compacts were selected for isothermal safety testing at temperatures generally ranging from 1600 to 1800°C. One safety test used the time-versus-temperature profile characteristic of a depressurized conduction cool-down event in HTGRs, and one test varied the temperature with a number of holds at temperatures between 1000 and 1600°C. Table 3 summarizes the AGR-1 safety tests that were completed. Tests conducted at Idaho National Laboratory (INL) were performed in the fuel accident-condition simulator (FACS) furnace, and tests performed at Oak Ridge National Laboratory (ORNL) used the Core Conduction-Cooldown Test Facility (CCCTF). Table 6 lists the post-irradiation safety tests of AGR-1 compacts and references specifically dedicated to those tests that describe the equipment and methods used in those tests. A number of reports and articles written by AGR staff summarize all major AGR-1 PIE results (Demkowicz et al. 2015a), the in-pile performance (Demkowicz et al. 2016), and the post-irradiation safety tests (Morris et al. 2016).

Table 5. AGR-1 fuel compacts used for as-irradiated DLBL analyses. In addition to the final PIE report, which discusses these tests (Demkowicz et al. 2015a), references for the analysis of each fuel compact are also listed.

Compact	Variant	TAVA ^a Temp (°C) ^a	Burnup (% FIMA) ^b	Fast fluence (10 ²⁵ n/m ²) ^b	Reference
6-3-2	Baseline	1070	11.4	2.55	Demkowicz et al. 2012
6-1-1	Baseline	1111	15.3	2.43	Hunn et al. 2012a Hunn et al. 2012b
3-2-1	Baseline	1051	19.1	4.21	Demkowicz et al. 2015b
5-2-1	1	1057	17.4	3.71	Hunn et al. 2012b Hunn et al. 2014a
5-2-3	1	1059	17.4	3.77	Hunn et al. 2014a
5-3-1	1	1040	16.7	3.60	Demkowicz et al. 2015c
4-4-2	3	1024	16.6	3.59	Hunn et al. 2012b Hunn et al. 2013a
4-1-1	3	1072	19.4	4.13	Demkowicz et al. 2015d
1-3-1	3	1092	15.3	3.22	Demkowicz et al. 2015e

a Hawkes 2012

b Sterbentz 2013

Table 6. Summary of safety tests of AGR-1 fuel compacts. Each of these is listed in the final PIE report (Demkowicz et al. 2015a), and references dedicated to each compact or small group of compacts are provided in the right-most column of this table. Some references cover both the safety test and the post-test exams. Some references may only cover the safety test or the post-test exams of the fuel.

Compact	Safety Test Temperature (°C)	Burnup (% FIMA)	Fast Fluence (1×10^{25} , E>0.18 MeV)	TAVA Irradiation Temperature (°C)	AGR-1 Fuel Type	Lab	Reference
1-1-1 ^a	Transient (min 800, max 1695)	15.19	2.81	1017	3	INL	Stempien et al. 2016
1-1-3 ^a		15.32	2.86	1018	3	INL	
1-4-2 ^a		14.93	3.01	1045	3	INL	
3-2-2	1600	17.02	3.79	1019	Baseline	ORNL	Hunn et al. 2012c and 2012d
3-2-3	1800	19.12	4.28	1053	Baseline	ORNL	Hunn et al. 2014b
3-3-1	1700	19.07	4.23	1051	Baseline	ORNL	Hunn et al. 2012e and 2013b
3-3-2	1600	17.02	3.8	1020	Baseline	ORNL	Hunn et al. 2012b and 2012c
4-1-2	1600	17.39	3.72	1042	3	ORNL	Hunn et al. 2013c and 2014c
4-2-2 ^b	Varying holds (1000 to 1600)	16.64	3.73	1065	3	ORNL	Hunn et al. 2014d and 2015a
4-3-2	1800	16.38	3.68	1057	3	INL	Demkowicz et al. 2015f
4-3-3	1600	18.63	4.16	1094	3	INL	Demkowicz et al. 2015f and 2015g
4-4-1	1800	18.96	3.99	1057	3	ORNL	Hunn et al. 2013b and 2013c
4-4-3	1700	18.99	4.06	1059	3	ORNL	Hunn et al. 2013c and 2014c
5-1-1	1700	18.22	3.76	1041	1	ORNL	Hunn et al. 2015c
5-1-3	1800	18.19	3.82	1042	1	ORNL	Hunn et al. 2013d and 2014b
5-3-3	1600	17.01	3.65	1042	1	ORNL	Hunn et al. 2013d and 2014b
6-2-1	1600	14.2	2.87	1135	Baseline	ORNL	Hunn et al. 2012c and 2013b
6-4-1	1600	13.35	2.43	1041	Baseline	INL	Demkowicz et al. 2015a and 2015f
6-4-3	1600	13.35	2.46	1041	Baseline	ORNL	Baldwin et al. 2014 Hunn et al. 2012b

^a Compacts 1-1-1, 1-1-3, and 1-4-2 were tested simultaneously using a temperature-versus-time profile mimicking a depressurized conduction cooldown event in an HTGR.

^b Compact 4-2-2 was tested by varying the temperature up and down between 1000 and 1600°C to probe the behavior of silver.

1.2.2 AGR-2

As with AGR-1, PIE data from AGR-2 include the quantification of fission products outside of the fuel compacts, as determined from measurements of the irradiation-capsule components (Stempien and Demkowicz 2020). Some compacts were selected for as-irradiated DLBL analysis to determine the inventory of fission products retained in the compact matrix outside of the SiC layer and for gamma counting individual particles to determine their post-irradiation inventories of fission products (see Table 7). A number of compacts were selected for isothermal safety testing at temperatures of 1600 or 1800°C for UCO fuel and 1500°C, 1600°C, or 1700°C for UO₂ fuel (see Table 8). Most of these safety-tested compacts were also subjected to post-test DLBL. Three AGR-2 compacts were tested under a temperature transient nearly identical to that performed as part of AGR-1.

Table 7. AGR-2 compacts subjected to as-irradiated DLBL. These are discussed in the final PIE report (Stempien et al. 2021), and individual references that fed the final PIE report are included here.

Compact	Kernel	Temperature (°C) ^a			Burnup ^b (% FIMA)	Fast Fluence ^b (10 ²⁵ n/m ²)	References
		TAVA	TA _{min} ^d	TA _{max} ^e			
3-1-2	UO ₂	1012	903	1084	10.66	3.45	Hunn et al. 2018b, 2020b
3-3-1	UO ₂	1062	997	1104	10.46	3.49	Hunn et al. 2018b, 2020b
2-2-1	UCO	1287	1185	1353	12.47	3.35	Hunn et al. 2018b
2-2-3	UCO	1261	1161	1335	10.80	2.99	Hunn et al. 2018a, 2018b
5-2-3	UCO	1108	1003	1184	10.42	3.00	Hunn et al. 2018a, 2018b
5-3-3	UCO	1093	986	1172	10.07	2.91	Hunn et al. 2018b
5-4-2	UCO	1071	927	1168	12.03	3.14	Hunn et al. 2018b, 2018c
6-2-3	UCO	1095	1012	1157	8.22	2.30	Hunn et al. 2018b
6-3-3	UCO	1060	970	1134	7.46	2.14	Hunn et al. 2018b
6-4-1 ^c	UCO	1018	891	1106	9.24	2.20	Stempien 2020

a. Hawkes 2014b

b. Sterbentz 2014

c. DLBL of Compact 6-4-1 at INL was completed before gamma counting a small subset of particles. All other AGR-2 compacts were analyzed at ORNL, where particles were separated from the matrix and counted before particle burn-leach, and ~10% of the particles were withheld from the particle burn-leach for microstructural analysis or as a TRISO particle archive. Particle burn-leach results were scaled to account for the 10% of particles withheld. Implicit in this the assumption that the 90% analyzed are representative of the compact as are the 10% withheld.

d. Time averaged (TA) minimum temperature.

e. Time averaged maximum temperature.

Table 8. List of AGR-2 compacts used in safety tests. The safety test results were discussed in aggregate in the AGR-2 PIE report (Stempien et al. 2021), and individual reports for each test are given in the “references” columns here.

Compact	Kernel	Safety Test (°C)	Temperature (°C) ^a		Burnup ^b (% FIMA)	Fast Fluence ^b (10 ²⁵ n/m ² , E>0.18 MeV)	References
			TAVA	TA _{max} ^c			
2-1-2	UCO	1800	1219	1324	12.62	3.25	Hunn et al. 2019b
2-2-2	UCO	1600	1287	1354	12.55	3.39	Hunn et al. 2016a, 2018b; Morris et al. 2018
2-3-1	UCO	1600	1296	1360	12.63	3.42	Hunn et al. 2017, 2018b
2-3-2	UCO	1800	1296	1360	12.68	3.46	Hunn et al. 2018d, 2018b
3-1-1	UO ₂	1500	1011	1083	10.6	3.41	Hunn et al. 2020a, 2020b
3-3-2	UO ₂	1600	1062	1105	10.54	3.53	Hunn et al. 2015b, 2018b, 2020b; Morris et al. 2018
3-4-1	UO ₂	1700	1013	1085	10.62	3.47	Hunn et al. 2018d, 2020b
3-4-2	UO ₂	1600	1013	1085	10.69	3.50	Hunn et al. 2015b, 2020b, 2018b; Morris et al. 2018
5-2-1	UCO	1600	1141	1209	12.28	3.38	Hunn et al. 2019a
5-2-2	UCO	1600	1141	1210	12.34	3.39	Hunn et al. 2016a, 2018b; Morris et al. 2018
5-4-1	UCO	1800	1071	1168	12.05	3.12	Hunn et al. 2016a, 2018b
6-2-1	UCO	1800	1129	1183	10.16	2.60	Hunn et al. 2019a
6-2-2	UCO	1600	1129	1183	10.19	2.61	Hunn et al. 2019a
6-4-2	UCO	1600	1018	1106	9.26	2.21	Hunn et al. 2017, 2018b, 2018e
6-4-3	UCO	1800	987	1080	7.26	1.94	Hunn et al. 2019c, 2018b
5-1-1	UCO	transient	1108	1202	12.8	3.41	Hunn, Morris, and Burns 2019
5-1-2	UCO		1109	1203	12.88	3.42	
5-3-1	UCO		1126	1197	12.03	3.28	

a. Hawkes 2014b

b. Sterbentz 2014

c. Time-averaged maximum temperature

1.2.3 AGR-3/4

Of the 12 AGR-3/4 irradiation capsules, eight were disassembled so that the fuel compacts and capsule internals could be accessed. This included all the Std capsules and the Capsule 4 FB. This allowed a determination of the mass balances of fission products outside of the fuel compacts in each capsule (Stempien et al. 2018). The mass balance provides a means of assessing the release of fission products from the fuel compacts during irradiation. The AGR-3/4 fission-product mass balance is made up of the fission-product inventories measured on all components of the test train except the fuel compacts themselves and the stainless-steel capsule shells (Stempien et al. 2018). The components analyzed included foils, felts, spacers, through tubes, inner rings, outer rings, and sink rings. Because the sink rings were kept at low temperatures during irradiation, it was assumed that any fission products that transported beyond the outer ring would be captured in the sink ring. Thus, the stainless-steel capsule shells were not analyzed. Several elements of AGR-3/4 PIE are still being completed or analyzed and are not yet ready for use in this study. This includes compact destructive exams and heating tests in the FACS furnace. A number of as-irradiated compacts were subjected to radial DLBL. Others were heated in the FACS furnace with test temperatures ranging from 1000 to 1600°C. Another group of compacts was reirradiated in the Neutron Radiography Reactor prior to heating in the FACS furnace.

1.3 Conventions and Definitions

1.3.1 Fission-product activities and fractions

This report focuses on fission-product behavior in AGR TRISO fuel. The focus will be on gamma-emitting Ag-110m, Cs-134, Cs-137, Eu-154, and Eu-155, and beta-emitting Sr-90. Activities for each

nuclide measured in the experiments were decay-corrected back to the date and time of the end of the appropriate irradiation (i.e., AGR-1, AGR-2, or AGR-3/4) plus one day. AGR-1 data were decay-corrected to November 7, 2009, at 6:00 AM MT. Data collected for AGR-2 were decay-corrected to October 17, 2013, at 11:00 AM MT, and measured AGR-3/4 radionuclide activities were decay-corrected to April 13, 2014, at 5:00 AM MT. Decay corrections were made using the following equation:

$$A = A_0 e^{-\lambda t} \quad (1)$$

Where A is the measured activity at a time t seconds after end-of-irradiation (EOI) plus one day, A_0 is the decay-corrected activity at $t = 0$, and λ is the decay constant. The decay constant is defined as $\lambda = \ln(2)/t_{1/2}$, where $t_{1/2}$ is the half-life. Half-lives for each nuclide were taken from the ENDF/B-VII.1 library downloaded on July 9, 2013 (Chadwick et al. 2011). In instances where no activity was detected for a given nuclide, minimum detectable activities (MDAs) were determined. For analyses regarding nuclide retention or release, it was useful to convert the measured nuclide inventories (M_x , where x is the specific isotope) to ratios of the measured nuclide inventories to the calculated nuclide inventories in the related compact (M_x/C_{compact}) or capsule (M_x/C_{capsule}). For example, to compute M_x/C_{compact} (also referred to as the compact fraction), measured activities of gamma- and beta-emitting nuclides were divided by the total activities of these nuclides predicted by physics calculations (e.g., Sterbentz 2013, 2014, and 2015) to exist in the fuel at the end of the irradiation. Both the measured activities and the activities from physics calculations were decay-corrected to EOI plus one day.

1.3.2 SiC Failure versus TRISO Failure

The retention of key fission products in TRISO fuel depends on the integrity of the TRISO coatings. Some elements, like Ce, are largely retained in the fuel kernel even in the presence of TRISO coating defects; however, other elements like Cs are best retained by fuel with an intact SiC layer. Fission gases can be retained by any single intact TRISO coating layer, whether it is inner pyrolytic carbon (IPyC), silicon carbide (SiC), or outer pyrolytic carbon (OPyC) layers. A SiC failure is any irradiation-induced degradation of the SiC layer resulting in loss of fission-product retention while at least one PyC layer simultaneously remains intact. A particle with a SiC failure will release Cs to at least some degree, but it will still retain fission gases because it has at least one hermetic PyC layer remaining. A TRISO failure is defined as a loss of hermeticity in all three dense-coating (i.e., IPyC, SiC, and OPyC) layers. Such a particle would release both condensable fission products like Cs and fission gases. All TRISO failures have a failed SiC layer, and the Cs release from a failed SiC layer is generally as severe as the Cs release from a full TRISO failure. For that reason, in some contexts of this report, particles with SiC failure and particles with TRISO failure will simply be called particles with SiC failures as an expedient. It will be stated explicitly when this is being done.

1.3.3 Limitations of Experimental Measurements, Exams, and Safety Tests

The data summarized herein were collected from a variety of different methods. Descriptions of each method can be found in the references cited within this report. It is important to point out that this report summarizes data from many reports and articles, and it is not possible to include all the discussions for each sample from that body of work. Key limitations and nuances of the data will be described in the following sections.

Some limitations regarding inventory fractions (M/C) and safety tests are worth noting early on. The gamma measurement values (M) are commonly given a 5% systematic error on top of the random error from counting statistics, which may be larger or smaller than 5%. The physics calculations (C) that are used to normalize the measured values have some biases as well. For example, available data indicate that Ag-110m production in some of the fuel compacts at the axial centers of AGR-1 (i.e., Capsules 2 through 4) and AGR-2 (i.e., Capsule 3) is underpredicted by up to 10% in AGR-1 (Demkowicz et al. 2015a) and up to 17% in AGR-2 (Harp, Demkowicz, and Stempien 2020). Eu-154 production is overpredicted by 10–20% across all capsules in AGR-1 (Demkowicz et al. 2015a) and by 15–29% across all capsules in

AGR-2 (Harp, Demkowicz, and Stempien 2020). Greater emphasis is placed on Eu-154 results than Eu-155 results here. Eu-154 has higher-energy gamma rays that are often more-readily detectible (and typically with lower error) than Eu-155 in AGR PIE. The measured Cs-137 and Cs-134 are generally in good agreement, but due to trace contamination of the longer-lived Cs-137 in the hot cell, Cs-137 readings are usually biased higher than those for Cs-134. Thus, Cs-134 will be used to represent Cs in this report.

In the post-irradiation safety tests, condensable fission products are collected on condensation plates in the FACS furnace and deposition cups in the CCCTF furnace. These plates and cups are exchanged throughout a test and then gamma counted and examined for Sr-90 upon removal from the furnace. Dozens of plates may be exchanged at known time intervals throughout the test. The radionuclide inventories on each plate require correction by collection efficiencies for each element in order to estimate the inventory that was released from the fuel. Collection efficiencies are defined as the inventory of a given element collected on the plate or cup divided by the total inventory released from the fuel; they account for the inventory that is lost to other areas inside the furnace. In applying a single collection efficiency for each element, the assumption is that the collection efficiency is constant throughout the test. Furthermore, because of the CCCTF construction, a collection efficiency can be determined for each test. In contrast, the FACS furnace has one set of efficiencies experimentally determined at 1600°C and used for both 1600 and 1800°C FACS tests. Only one 1800°C test has been conducted in the FACS furnace (specifically, AGR-1, Compact 4-3-2).

2. AS-IRRADIATED PIE DATA SUMMARY

In TRISO fuels, the SiC layer receives significant attention because it is the primary barrier to the release of metallic fission products such as Cs; however, each structure in the TRISO fuel system is a barrier to fission-product release. This includes the kernel, buffer, TRISO coatings, and graphitic matrix surrounding the particles in the TRISO fuel element (e.g., compact or pebble). Any intact PyC coating will retain fission gases even if the SiC has been breached. Furthermore, the matrix is an important final barrier to fission-product release from a TRISO fuel element. For example, small amounts of fission-product Eu and Sr may be released through intact TRISO coatings if irradiation temperatures are sufficiently high over a sufficient duration. DLBL of irradiated fuel has shown that much of this is retained in the compact matrix. The mass balance, that is the quantification of fission products on the components outside of the fuel, indicates the total amount of condensable fission products released from the fuel during irradiation. Considering the DLBL results together with the mass balance is one way to estimate total release from the TRISO particles.

2.1 Matrix Inventory of Fission Products from DLBL

The compact matrix is an important part of the coated-particle fuel system. The graphitic matrix surrounds and protects the particles, acts as a heat-transfer medium, provides some neutron moderation, and has been shown to retain some fission products that may have diffused out of the particles. The type of matrix in the AGR-1, 2, and 3/4 fuel compacts is similar to the A3-3 formulation historically referred to as the German TRISO program's reference matrix (Gerczak et al. 2022). A different type of matrix may behave differently than the AGR A3-3 style of matrix.

In this section, data collected from DLBL will be used to determine the fission-product inventory in the compact matrix and particle OPyC layers (outside of the SiC layers) as a function of irradiation conditions. Table 9 summarizes the available DLBL data. The data presented here are the total inventories from the sum of all the samples from all the DLBL steps. Table 10 summarizes the numbers of in-pile failed TRISO particles, in-pile failed SiC particles, particles that were defective as-fabricated, and particles that were accidentally damaged during the DLBL process. In Table 9 and Table 10, rows that are shaded indicate compacts with damaged, defective, or failed particles. The data in Table 9 and Table 10 were assembled from data compilations provided by Demkowicz et al. (2015a) and Stempien et al.

(2021). The unshaded rows in Table 9 and Table 10 denote compacts with no observed damage whatsoever (neither from in-pile failure nor from damage incurred during DLBL). In these compacts, the inventories determined from DLBL directly reflect the inventory that diffused through intact IPyC and SiC coatings and was trapped in the OPyC and matrix in these compacts. Any small contribution from as-fabricated dispersed uranium is also reflected in these values. In the shaded rows, the DLBL inventories reflect the combination of what diffused through the intact particles plus what was released from in-pile failed SiC or in-pile failed TRISO or leached from particles damaged during DLBL. Thus, in these cases, the contributions from intact particle release cannot be distinguished from contributions due to release from damaged particles, especially for elements such as Ag, Eu, and Sr, which may transport through intact coatings in significant quantities. Another limitation of the DLBL process is that Ag-110m may be under-recovered if it is driven off during the burn (750°C) or leach steps (~100°C).

In AGR-1, the dispersed uranium fraction (DUF) in the compacts after fabrication (also referred to as uranium contamination) was $<4\text{E-}7$ (Demkowicz et al. 2015a). The only values from AGR-1 post-irradiation DLBL that were comparable to the DUF were for Ce-144 and Cs-134 in Compact 4-1-1; therefore, those values likely reflect dispersed uranium and not small releases from TRISO particles. The DUF in as-fabricated AGR-2 fuel was about an order of magnitude higher at $3.9\text{E-}6$. AGR-2 UCO DLBL data points that are similar in magnitude to the DUF include Ce-144 in Compact 6-4-1, and Cs-134 in Compacts 2-2-1 and 6-4-1. Thus, any small amount of Cs-134 in Compacts 2-2-1 and 6-4-1 cannot be distinguished from what may have been present from fission in dispersed uranium in the OPyC and matrix. The dispersed uranium present at the time of fabrication dictates the lower limit of intact particle release that can be determined. If intact particle release were actually at a lower level than the DUF, that intact-particle release would be too small to quantify. Another effect that could possibly affect the detection of low levels of fission products is if fission products were to transport out of one compact and contaminate a neighboring compact. Such an effect cannot be quantified; therefore, it is neglected here.

Figure 4 is a plot summarizing the compact fractional inventories measured in the compact matrix and OPyC in all AGR-1 and AGR-2 compacts subjected to as-irradiated DLBL that did not have failed SiC or failed TRISO particles. There are some indications of increases in the matrix inventory with increased irradiation temperature. Section 4.3 describes how these data are fitted with Arrhenius functions to estimate the rate of fission-product accumulation in the matrix.

Table 9. Fraction of compact inventory (M/C) determined from the DLBL solutions in as-irradiated compacts from AGR-1 and AGR-2. Note that in AGR-1, a compact fraction of 2.4E-4 corresponds to a single particle's inventory. In AGR-2 UCO compacts, a fraction of 3.2E-4 corresponds to a single particle's inventory. In AGR-2 UO₂ compacts, a fraction of 6.5E-5 corresponds to a single particle's inventory. Shading indicates compacts with damaged, defective, or failed particles as described in Table 10.

Experiment	Compact	Fuel Type	Kernel	TAVA (°C)	TA min (°C)	TA max (°C)	Burnup (% FIMA)	Fast Fluence (10 ²⁵ n/m ²)	Ag-110m	Ce-144	Cs-134	Eu-154	Sr-90
AGR-1	6-3-2	Baseline	UCO	1070	974	1144	11.43	2.38	2.20E-4	1.70E-4	7.30E-5	5.90E-3	4.30E-4
	6-1-1	Baseline		1111	969	1194	15.25	3.00	1.70E-1	6.90E-4	2.10E-5	1.50E-2	5.90E-4
	3-2-1	Baseline		1051	897	1143	19.07	4.21	6.90E-3	4.00E-6	3.00E-6	7.80E-4	1.50E-6
	5-2-3	1		1059	933	1141	17.42	3.77	3.30E-3	1.50E-3	4.40E-5	6.00E-3	3.10E-3
	5-2-1	1		1057	925	1140	17.37	3.71	3.90E-3	1.60E-3	4.80E-5	5.80E-3	1.90E-3
	5-3-1	1		1040	908	1122	16.93	3.60	9.10E-3	3.40E-4	2.50E-6	1.20E-3	1.90E-4
	4-4-2	3		1024	866	1139	16.74	3.59	2.30E-2	1.30E-5	1.20E-5	5.90E-4	1.60E-5
	4-1-1	3		1072	900	1182	19.38	4.13	3.30E-2	6.60E-7	4.00E-7	2.40E-4	1.70E-6
	1-3-1	3		1092	977	1166	16.14	3.22	3.60E-3	1.50E-4	5.40E-6	6.30E-3	2.60E-3
AGR-2	3-1-2	NA ^a	UO ₂	1012	903	1084	10.66	3.45	<2.7E-3	3.48E-3	1.40E-3	2.48E-3	3.23E-3
	3-3-1			1062	997	1104	10.46	3.49	1.78E-3	3.59E-6	1.16E-5	2.15E-4	7.14E-5
	2-2-1		UCO	1287	1185	1353	12.47	3.35	<2.3E-3	4.28E-4	4.09E-6	1.10E-1	8.16E-2
	2-2-3			1261	1161	1335	10.8	2.99	6.26E-4	1.20E-3	5.70E-4	1.57E-2	1.05E-2
	5-2-3			1108	1003	1184	10.42	3.00	4.69E-4	9.10E-4	2.34E-4	1.37E-3	7.64E-4
	5-3-3			1093	986	1172	10.07	2.91	<1.4E-4	3.55E-4	2.07E-5	6.17E-4	2.68E-4
	5-4-2			1071	927	1168	12.03	3.14	4.69E-3	5.25E-4	1.30E-4	8.38E-4	3.46E-4
	6-2-3			1095	1012	1157	8.22	2.30	<1.3E-3	4.08E-4	1.60E-4	8.59E-4	3.65E-4
	6-3-3			1060	970	1134	7.46	2.14	3.46E-4	1.33E-5	7.82E-6	7.37E-4	1.60E-5
	6-4-1			1018	891	1106	9.24	2.20	<4.8E-4	4.23E-6	7.49E-7	5.09E-4	7.98E-5

a. Only one coating process was used for all the AGR-2 particles. The AGR-2 coating processes were most similar to AGR-1, Variant 3.

Table 10. Summary of the numbers of particles with in-pile failed SiC and failed TRISO coatings, the number of particles determined to have as-fabricated defects, and the number of particles accidentally damaged during DLBL examinations.

Experiment	Compact	Number of Failed SiC	Number of Failed TRISO	Number of TRISO broken during DLBL	Number of As-fabricated TRISO Defects	Total Number of Defective and Failed and Broken TRISO and SiC Particles
AGR-1	6-3-2 ^a	1	0	0	0	1
	6-1-1	0	0	0	0	0
	3-2-1	0	0	0	0	0
	5-2-3 ^b	2	0	0	0	2
	5-2-1 ^b	1	0	0	0	1
	5-3-1	0	0	0	0	0
	4-4-2	0	0	0	0	0
	4-1-1	0	0	0	0	0
	1-3-1	0	0	0	0	0
AGR-2	3-1-2 ^c	0	0	6	0	6
	3-3-1	0	0	0	0	0
	2-2-1	0	0	0	0	0
	2-2-3 ^d	5	0	0	1	6
	5-2-3 ^e	0	1	2	0	3
	5-3-3 ^f	0	1	0	0	1
	5-4-2 ^g	0	0	1	0	1
	6-2-3 ^h	0	2	0	0	2
	6-3-3 ⁱ	1	0	0	0	1
	6-4-1	0	0	0	0	0

- AGR-1 Compact 6-3-2 had a single particle with in-pile failed SiC, and this remained in the particle population when burn-leach was performed; therefore, its kernel was dissolved in the burn-leach solutions. This would skew the estimate of the inventory in the OPyC and matrix of this compact.
- AGR-1 Compacts 5-2-3 and 5-2-1 had two and one particles with in-pile failed SiC coatings, respectively. These were identified after pre-burn leaching steps, but these particles were removed from the population prior to burn-leach analysis. Thus, these kernels were not leached during DLBL. The inventory in the OPyC and matrix of these compacts will be impacted by these SiC failures, however.
- AGR-2 Compact 3-1-2 had six particles accidentally broken during IMGA that were then leached during DLBL.
- AGR-2 Compact 2-2-3 had between three and five in-pile failed-SiC particles. A conservative value of 5 was used. This compact had one particle with an as-fabricated defect. All were leached during DLBL.
- AGR-2 Compact 5-2-3 had one in-pile failed TRISO and two particles that were broken during DLBL, all of which were leached during DLBL. The two particles broken during DLBL are not considered defective or failed.
- AGR-2 Compact 5-3-3 had one in-pile failed TRISO that was leached during DLBL.
- AGR-2 Compact 5-4-2 had one particle accidentally broken during DLBL that was leached during DLBL.
- AGR-2 Compact 6-2-3 had two defective or failed particles whose specific type could not be determined. Thus the number of failed particles in Compact 6-2-3 was 0-2, and they could have been either failed SiC or failed TRISO. Failed TRISO was assumed for conservatism.
- AGR-2 Compact 6-3-3 had one in-pile failed SiC whose kernel was NOT leached into the DLBL solutions.

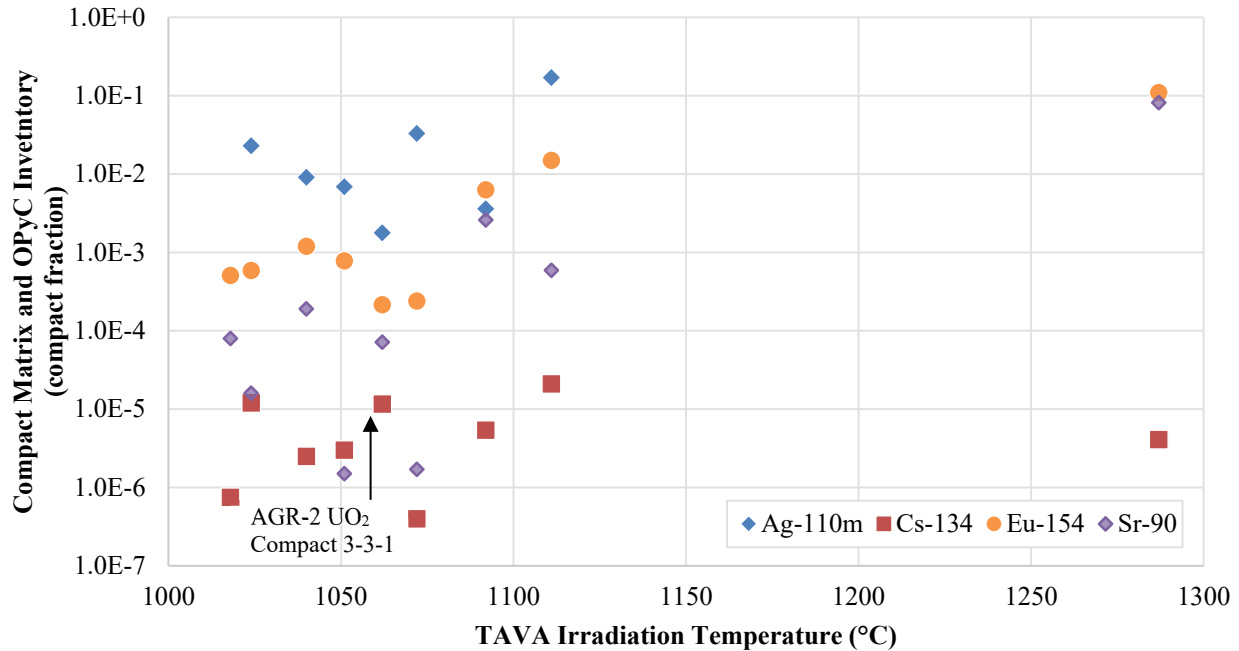


Figure 4. Summary of the fission-product inventory measured from DLBL of AGR-1 and 2 compacts. Only compacts with no defects or failures as listed in Table 9 and Table 10 are plotted here.

2.2 Fission-Product Release from Compacts Based on Mass Balance

After disassembling the irradiation test trains, components within each capsule were analyzed for their fission-product content. Looking at all the components other than the fuel compacts themselves enables a determination of the fission-product inventory that migrated out of the compacts. Because each capsule contained multiple compacts, in the absence of SiC or TRISO failures, the inventories measured on the components cannot be specifically attributed to any single compact. Therefore, the inventories on the components allow for an estimate of the average release from each compact.

The following subsections summarize the fission product inventory measured outside of the fuel compacts for AGR-1, 2, and 3/4. These data include releases from all sources such as intact fuel, as-fabricated dispersed uranium, rare instances of in-pile SiC or TRISO failure, and any fuel particles with as-fabricated defective coatings. Table 10 lists the SiC failures from AGR-1 and the SiC and TRISO failures from AGR-2.

AGR-1 had no TRISO failures and four SiC failures out of about 298,000 particles. Three of these were in AGR-1 Capsule 5, and one was in Capsule 6 (Demkowicz et al. 2015a). The reported number of TRISO failures for the AGR-2 experiment was ≤ 4 , and there were six SiC failures.^a Each AGR-2 capsule contained an estimated 38,112 particles, and there were 114,336 AGR UCO particles in AGR-2. In AGR-2, five SiC particles failed in Capsule 2 (all of them from Compact 2-2-3^b), and one defective as-fabricated particle (also in Compact 2-2-3) was not classified as either a failed SiC or a failed TRISO particle. The AGR-2, Capsule 2 mass-balance data will reflect these failed and defective particles. AGR-2, Capsule 5, contained two failed TRISO particles (one in Compact 5-2-3 and one in Compact 5-3-3). AGR-2, Capsule 6, contained one failed SiC (Compact 6-3-3) and two failed TRISO particles (Compact 6-3-3) (Stempien et al. 2021).

All AGR-3/4 capsules contained 80 DTF particles; therefore, approximately 1% of all the particles in AGR-3/4 were DTF particles. This prevents an analysis of any TRISO-coated driver-particle SiC or TRISO failures. The AGR-3/4 mass balance includes the contributions from DTF and TRISO-coated particles in addition to the other potential sources mentioned earlier.

2.2.1 AGR-1 Mass Balance

Figure 5 shows a plot of the compact fractional inventory of key fission products measured outside of the fuel compacts in each AGR-1 capsule. This fraction also represents the average inventory released from a compact in each capsule. The x-axis is the TAVA temperature for all the fuel in the capsule (see Table 2). No corrections were made for the three failed SiC particles in Capsule 5 or the one failed SiC particle in Capsule 6 (Demkowicz et al. 2015a). Table 11 summarizes the mass balance for each AGR-1 capsule (Demkowicz et al. 2013). It is noteworthy that AGR-1 had a narrower irradiation-temperature range than any other AGR experiment and that the calculated temperature uncertainty for AGR-1 is about the same size as the spread in average irradiation temperatures shown here (Pham, Einerson, and Hawkes 2013).

^a It should be noted that the enumeration of in-pile TRISO failures during PIE was not conclusive in some cases, and the numbers for failed TRISO provided in this report (take from Stempien et al. 2021) are conservative estimates that classified a particle as an in-pile TRISO failure if there was any uncertainty in the nature of the coating failure or defect.

^b Three of the failed SiC particles were confirmed to contain Ni and appeared to have failed from the outside in. This suggests they could have failed from Ni picked up during fabrication, or more likely, Ni from a nearby failed thermocouple in the graphite holder (Stempien et al. 2021). Nevertheless, for conservatism, these particles were considered SiC failures.

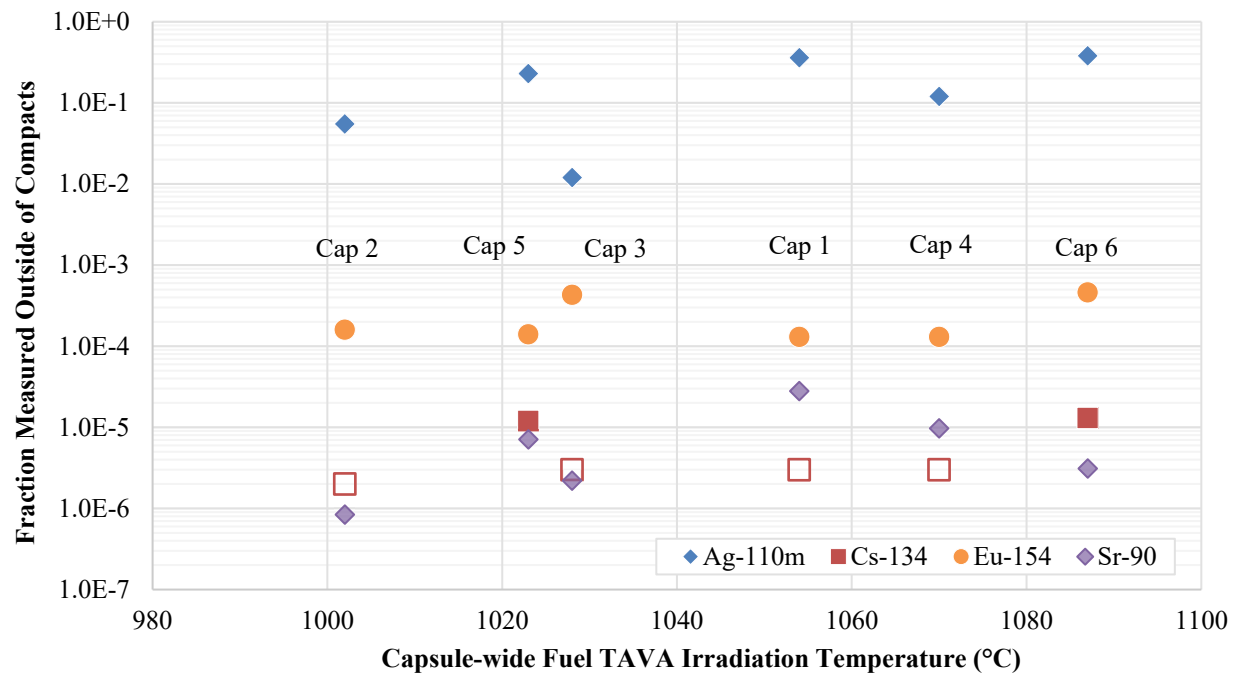


Figure 5. Capsule fractions of key fission products measured outside of the fuel compacts in AGR-1 Capsules 1-6. Open symbols were derived from MDAs.

Table 11. Summary of major condensable fission-product inventories measured on the AGR-1 irradiation test-train components outside of the fuel compacts. Particle equivalents are estimated by multiplying the capsule fraction by the number of particles in each capsule (approximately 49,200 particles per capsule).

Capsule	AGR-1 Fuel Type	Capsule Fraction					Particle Equivalents				
		Ag-110m	Ce-144	Cs-134	Eu-154	Sr-90	Ag-110m	Ce-144	Cs-134	Eu-154	Sr-90
1	3	3.60E-01	<3E-6	<3E-6	1.30E-4	2.80E-5	1.77E+4	<1.5E-1	<1.5E-1	6.40E+0	1.38E+0
2	2	5.50E-2	<2E-6	<2E-6	1.60E-4	8.40E-7	2.71E+3	<9.8E-2	<9.8E-2	7.87E+0	4.13E-2
3	Baseline	1.20E-2	<4E-6	<3E-6	4.30E-4	2.20E-6	5.90E+2	<2.0E-1	<1.5E-1	2.12E+1	1.08E-1
4	3	1.20E-1	<4E-6	<3E-6	1.30E-4	9.70E-6	5.90E+3	<2.0E-1	<1.5E-1	6.40E+0	4.77E-1
5	1	2.30E-1	<2E-6	1.20E-5	1.40E-4	7.10E-6	1.13E+4	<9.8E-2	5.90E-01	6.89E+0	3.49E-1
6	Baseline	3.80E-1	9.70E-6	1.30E-5	4.60E-4	3.10E-6	1.87E+4	4.77E-1	6.40E-1	2.26E+1	1.53E-1

2.2.2 AGR-2 Mass Balance

Figure 6 shows a plot of the compact fractional inventory of key fission products measured outside of the fuel compacts in all the US AGR-2 capsules. This fraction also represents the average compact inventory released in each capsule. The x-axis is the TAVA temperature for all the fuel in the capsule. The values here reflect releases from the fuel compacts from all sources, including the five failed SiC particles and one defective particle in Capsule 2, the two failed TRISO particles in Capsule 5, and the one failed SiC and two failed TRISO particles in Capsule 6 (Stempien et al. 2021). Table 12 summarizes the mass balance for each AGR-2 capsule (Stempien and Demkowicz 2020).

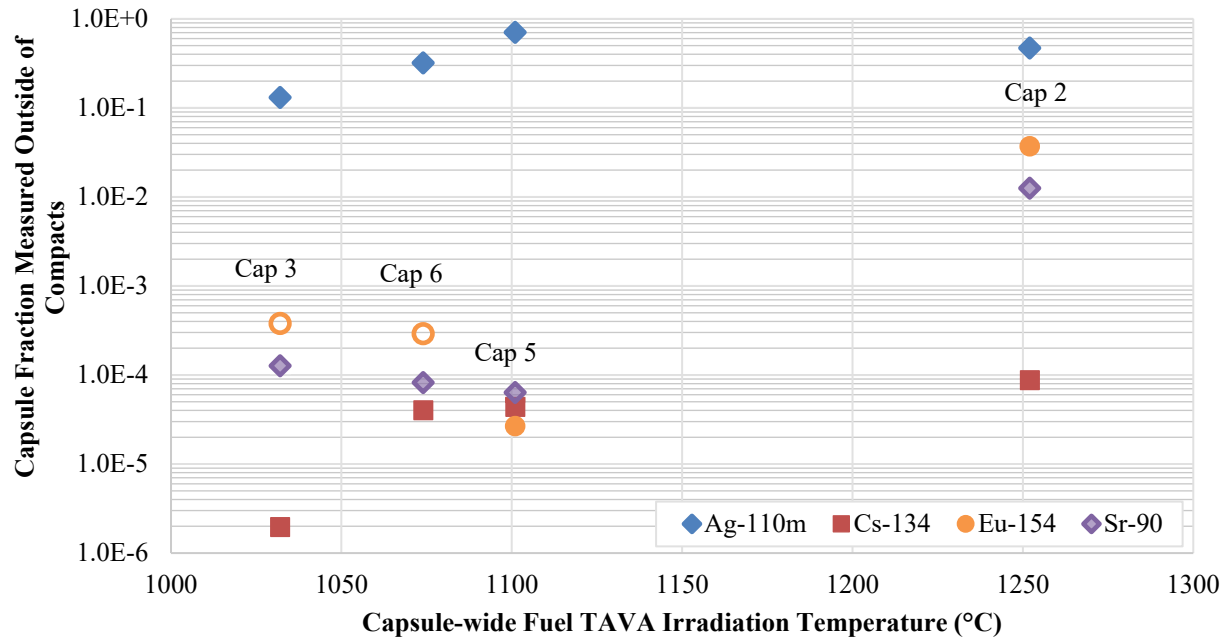


Figure 6. AGR-2 mass balances versus compact TAVA temperature. The open Eu-154 symbols denote values derived from MDAs. Note that Capsules 2, 5, and 6 contained UCO fuel, and Capsule 3 contained UO₂ fuel.

Table 12. Summary of major condensable fission-product inventories measured on the AGR-2 irradiation test-train components outside of the fuel compacts. Particle equivalents are estimated by multiplying the capsule fraction by the number of particles in each capsule (38,112 particles per UCO fuel capsule and 18,516 particles per UO₂ capsule).

Capsule	Fractions							Particle Equivalents					
	Type	Ag-110m	Ce-144	Cs-134	Cs-137	Eu-154	Sr-90	Ag-110m	Ce-144	Cs-134	Cs-137	Eu-154	Sr-90
2	UCO	4.70E-1	1.53E-6	8.74E-5	1.27E-4	3.70E-2	1.25E-2	1.49E+3	4.86E-3	2.78E-1	4.03E-1	1.18E+2	3.97E+1
3	UO ₂	1.31E-1	<2.4E-6	1.96E-6	4.98E-6	<3.8E-4	1.27E-4	2.02E+2	<3.7E-1	3.02E-3	7.68E-3	<5.8E-1	1.96E-1
5	UCO	7.04E-1	<1.5E-6	4.38E-5	7.26E-5	2.66E-5	6.35E-5	2.24E+3	<4.7E-3	1.39E-1	2.31E-1	8.45E-2	2.02E-1
6	UCO	3.20E-1	1.25E-6	4.02E-5	6.47E-5	<2.9E-4	8.21E-5	1.02E+3	3.97E-3	1.28E-1	2.05E-1	<9.2E-1	2.61E-1

2.2.3 AGR-3/4 Mass Balance

The AGR-3/4 fission product mass balance is made up of the fission-product inventories measured on all components of the test train except the fuel compacts themselves and the stainless-steel capsule shells (Section 1.2.3). All the Std AGR-3/4 capsules were completely disassembled for this purpose, but only one of the FB capsules was disassembled to allow this determination (Stempien et al. 2018). Complete mass balances are available for gamma-emitting fission products in the Std capsules; however, in addition to full and complete measurements of Sr-90 on capsule components, the mass balance of beta-emitting Sr-90 also relies on estimates from partial destructive analyses of the inner and outer rings (Stempien 2021).

Approximately one percent of all the particles in AGR-3/4 were DTF particles. The AGR-3/4 mass balance includes the contributions from DTF and TRISO-coated particles in addition to the other potential sources mentioned earlier. The mass balance of Ag-110m and Cs-134 is plotted as a function of the fuel compact TAVA temperature in Figure 7. Figure 8 plots the AGR-3/4 mass balances for Eu-154 and Sr-90. Table 13 summarizes the AGR-3/4 mass balance (Stempien et al. 2018). All Sr-90 values are estimates from partial destructive analyses of the rings. No Eu-154 was detected on the Capsule 4 and 5 components using typical methods (i.e., gamma counting of components, and leaching or burn-leaching small components followed by gamma assay). However, destructive sampling of portions of the inner and outer rings from Capsules 4 and 5 proved to be more sensitive and enabled an estimate of the Eu-154 inventory in those rings (Stempien 2021). Error bars are plotted for each data point based on propagating the measurement error from each individual sample into the sum of all the capsule components comprising the total capsule mass balance (Stempien et al. 2018); however, in most cases the error bars are smaller than the symbols used in the plots (generally less than 10%). The relative error is more significant in the capsules at the top and bottom of the test train where the burnup was lower and measurement sensitivity made quantification of smaller fission product activities more difficult. The error bar on the Capsule 1 Eu-154 mass balance is large because roughly 90% of all the Eu-154 measured outside of the fuel in Capsule 4 was in the inner ring, and that measurement had a larger error from the analysis via the Precision Gamma Scanner (Harp, Stempien, and Demkowicz 2021).

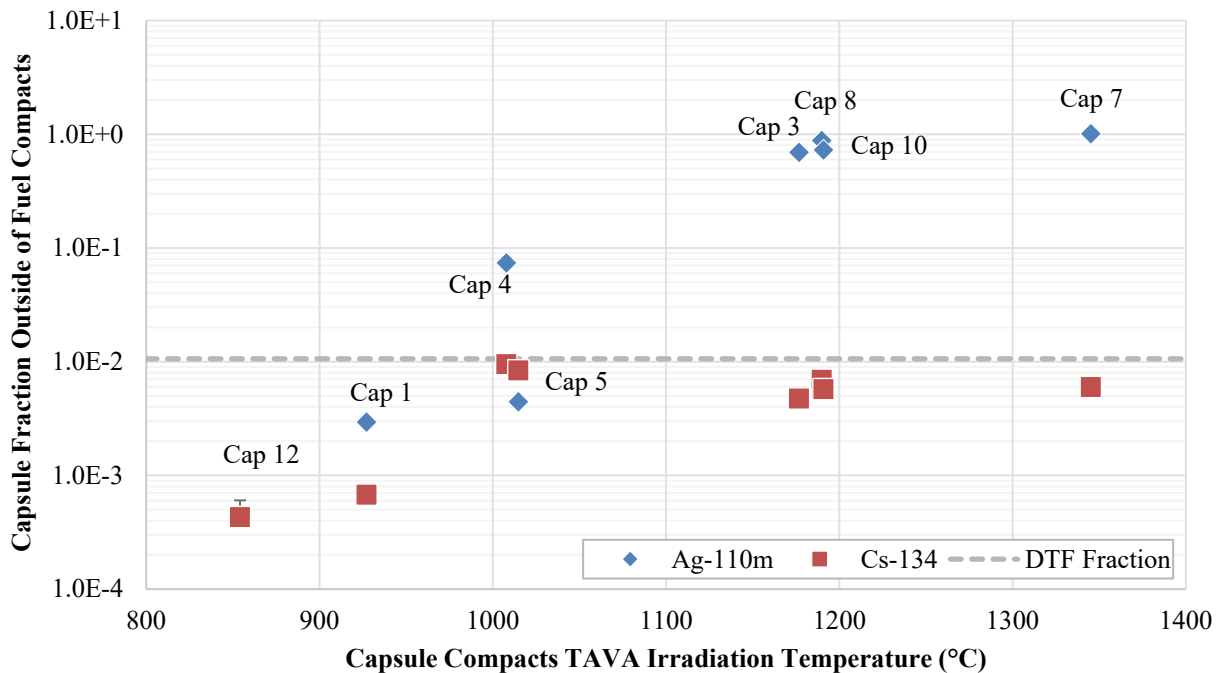


Figure 7. AGR-3/4 Ag-110m and Cs-134 mass balances versus compact TAVA temperature.

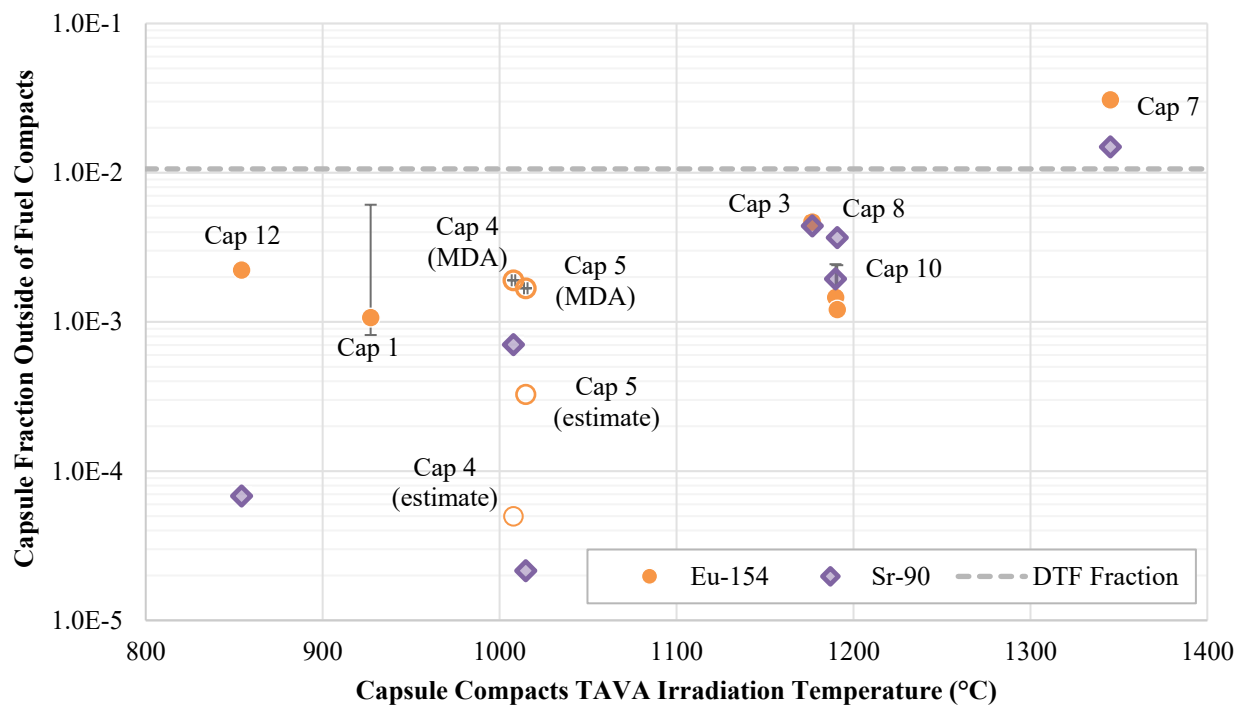


Figure 8. AGR-3/4 Eu-154 and Sr-90 mass balances versus compact TAVA temperature. The open symbols for Eu-154 indicate that they are either derived from MDAs or estimated from incomplete analysis of the inner and outer rings that were physically sampled. All Sr-90 values were estimated from physical sampling results.

Table 13. Summary of major condensable fission-product inventories measured on the AGR-3/4 irradiation test train components outside of the fuel compacts. Particle equivalents are estimated by assuming a total of 7,672 particles per capsule (80 DTF particles and 7,592 TRISO-coated driver particles).

Capsule	Fractions						Particle Equivalents					
	Ag-110m	Ce-144	Cs-134	Cs-137	Eu-154	Sr-90	Ag-110m	Ce-144	Cs-134	Cs-137	Eu-154	Sr-90
1 ^a	2.94E-3	<2.0E-5	6.75E-4	1.26E-3	1.07E-3	4.78E-6	5.65E+0	<3.9E-2	1.30E+0	2.42E+0	2.05E+0	9.16E-3
2 ^b	<6.5E-3	<1.9E-5	5.52E-4	1.26E-3	<1.4E-4	7.66E-6	<1.2E1	<3.7E-2	1.06E+0	2.42E+0	<2.7E-1	1.47E-2
3 ^{a,d}	6.93E-1	7.32E-6	4.74E-3	5.42E-3	4.67E-3	4.40E-3	1.33E+3	1.40E-2	9.09E+0	1.04E+1	8.95E+0	8.43E+0
4 ^c	7.40E-2	<3.1E-5	9.52E-3	9.68E-3	<1.9E-3	1.02E-5	1.42E+2	<5.9E-2	1.83E+1	1.86E+1	<3.6E0	1.96E-2
5 ^{a,d}	4.44E-3	1.15E-5	8.38E-3	8.00E-3	<1.7E-3	2.15E-5	8.52E+0	2.20E-2	1.61E+1	1.53E+1	<3.2E0	4.12E-2
6 ^b	1.70E-3	<2.6E-5	4.33E-4	6.27E-4	3.08E-7	3.53E-6	3.27E+0	<4.9E-2	8.31E-1	1.20E+0	5.91E-4	6.78E-3
7 ^{a,d}	1.01E+0	<1.5E-5	5.98E-3	6.56E-3	3.08E-2	1.49E-2	1.94E+3	<2.8E-2	1.15E+1	1.26E+1	5.91E+1	2.85E+1
8 ^{a,d}	8.82E-1	2.24E-6	6.92E-3	7.95E-3	1.46E-3	1.94E-3	1.69E+3	4.29E-3	1.33E+1	1.52E+1	2.80E+0	3.72E+0
9 ^b	4.15E-3	<2.4E-5	2.91E-4	6.70E-4	2.93E-4	4.80E-6	7.95E+0	<4.6E-2	5.59E-1	1.28E+0	5.63E-1	9.20E-3
10 ^{a,d}	7.29E-1	9.91E-7	5.74E-3	6.65E-3	1.21E-3	3.67E-3	1.40E+3	1.90E-3	1.10E+1	1.28E+1	2.32E+0	7.04E+0
11 ^b	5.44E-2	1.16E-6	3.50E-3	4.21E-3	2.63E-3	1.52E-5	1.04E+2	2.23E-3	6.72E+0	8.07E+0	5.05E+0	2.92E-2
12 ^{a,d}	<4.1E-1	<3.2E-5	4.30E-4	2.19E-3	2.23E-3	6.81E-5	<7.8E2	<6.2E-2	8.24E-1	4.19E+0	4.27E+0	1.31E-1

- Std capsules disassembled and fuel retrieved.
- FB capsules were not disassembled, and fuel was not retrieved; therefore, the mass balance is incomplete in these capsules and lacks inner and outer ring inventories.
- The Capsule 4 FB was disassembled so all the fuel and test train components could be retrieved.
- Sr-90 value estimated from destructive physical sampling of portions of the inner and outer rings (Stempien 2021).

3. SAFETY TEST DATA SUMMARY

Irradiated AGR-1 and AGR-2 UCO TRISO fuel compacts have been subjected to post-irradiation safety tests with isothermal holds at 1600 and 1800°C. (In addition, several AGR-1 tests were conducted at 1700°C.) These tests were conducted to explore the fission-product release characteristics of AGR TRISO fuel at temperatures that may be reached during a depressurized conduction cool-down event. Data on particle-failure statistics under these conditions were also collected (see Section 4.1). AGR-1 safety tests were conducted at ORNL and INL. All AGR-2 safety tests were conducted at ORNL. Some details of these tests were discussed earlier. The final PIE reports from those experiments describe the facilities and processes of these tests (Demkowicz et al. 2015a, Stempien et al. 2021). Those final reports cite numerous reports and articles with additional details about the tests. In this section, the time-dependent releases of fission products are grouped by nuclide for the entire body of AGR-1 and 2 tests.

Nominally, a test consisted of ramping up the furnace temperature up at $\sim 120^{\circ}\text{C/h}$ with a 2-hour pause at 400°C and a 12-hour pause at 1250°C . Above 1250°C , the temperature was ramped at $\sim 50^{\circ}\text{C/h}$ to the safety-test soak temperature. The test temperature was then maintained for 300 h or more, depending on the particular goal. It was then ramped down at a maximum rate of $\sim 600^{\circ}\text{C/h}$ to room temperature. Some tests—namely, AGR-1, Compact 3-3-2, and AGR-2, Compacts 3-4-2, 5-4-1, and 6-2-2—were interrupted for a variety of reasons (e.g., power outages) and restarted. In these tests, the cooldown and reheat periods were not included in the isothermal soak times, but they are included in the total test time.

Table 6 and Table 8 summarized the AGR-1 and AGR-2 compacts used in these tests, respectively. The presence of DTF particles in the AGR-3/4 fuel compacts makes them ill-suited to determining fission product releases from intact fuel; therefore, this section will focus on the results from AGR-1 and 2 safety tests.

3.1 AGR-1 Safety Test Total Releases and Particle Failures

Table 14 summarizes the total release of key fission products at the completion of safety tests of AGR-1 fuel compacts. Some irradiation information (e.g., temperature and burnup) is summarized for each compact in Table 6. Some of these tests were conducted in the FACS furnace at INL, and some were performed in the CCCTF at ORNL. Compacts for which no Kr-85 was detected were tested at ORNL, where a typical Kr-85 detection limit in CCCTF corresponds to an AGR-1 compact fraction of about $1\text{E-}6$ (Demkowicz et al. 2015a).

Table 14. Summary of total release of key radionuclides and numbers of SiC and TRISO failures at the completion of each AGR-1 isothermal safety test (Demkowicz et al. 2015a). Compact fraction is given with no parentheses, and particle equivalents are given in parentheses.

	Test (°C)	Variant	Kr-85	Sr-90	Ag-110m	Cs-134	Eu-154	# of Failures	
								SiC	TRISO
3-2-2	1600	Baseline	N/D	3.00E-5 (1.24E-1)	6.33E-2 (2.62E+2)	2.79E-7 (1.15E-3)	2.81E-4 (1.16E+0)	0	0
3-2-3	1800	Baseline	6.14E-5 (2.54E-1)	1.03E-2 (4.28E+1)	9.93E-2 (4.11E+2)	1.60E-3 (6.62E+0)	1.36E-2 (5.63E+1)	11	0
3-3-1	1700	Baseline	6.45E-6 (2.67E-2)	1.33E-3 (5.53E+0)	5.12E-2 (2.12E+2)	3.59E-4 (1.49E+0)	2.33E-3 (9.66E+0)	4	0
3-3-2	1600	Baseline	N/D	1.33E-3 (5.53E+0)	1.01E-1 (4.17E+2)	2.15E-4 (8.91E-1)	1.92E-3 (7.95E+0)	1	0
4-1-2	1600	3	N/D	1.43E-4 (5.91E-1)	5.80E-2 (2.39E+2)	1.66E-4 (6.85E-1)	3.39E-4 (1.40E+0)	1	0
4-3-2	1800	3	4.69E-4 (1.93E+0)	9.22E-3 (3.80E+1)	1.40E-1 (5.77E+2)	1.21E-3 (5.00E+0)	1.78E-2 (7.36E+1)	3	2
4-3-3	1600	3	1.44E-6 (5.95E-3)	7.59E-4 (3.13E+0)	3.40E-1 (1.40E+3)	6.77E-7 (2.79E-3)	8.17E-4 (3.37E+0)	0	0
4-4-1	1800	3	5.49E-6 (2.27E-2)	9.99E-3 (4.12E+1)	2.34E-1 (9.67E+2)	3.62E-4 (1.49E+0)	1.51E-2 (6.21E+1)	2	0
4-4-3	1700	3	N/D	9.67E-4 (3.99E+0)	1.66E-1 (6.83E+2)	7.29E-7 (3.01E-3)	2.90E-3 (1.20E+1)	0	0
5-1-1	1700	1	1.05E-5 (4.34E-2)	2.48E-3 (1.03E+1)	4.13E-2 (1.71E+2)	3.43E-4 (1.42E+0)	4.11E-3 (1.71E+1)	3	0
5-1-3	1800	1	4.76E-5 (1.98E-1)	1.19E-2 (4.92E+1)	4.35E-2 (1.81E+2)	1.17E-3 (4.87E+0)	1.43E-2 (5.93E+1)	7	0
5-3-3	1600	1	N/D	2.98E-4 (1.24E+0)	2.30E-2 (9.54E+1)	3.80E-6 (1.58E-2)	8.28E-4 (3.44E+0)	0	0
6-2-1	1600	Baseline	4.60E-6 (1.91E-2)	9.08E-4 (3.76E+0)	3.52E-3 (1.46E+1)	4.75E-6 (1.97E-2)	2.89E-3 (1.20E+1)	0	0
6-4-1	1600	Baseline	2.07E-6 (8.57E-3)	1.93E-4 (7.99E-1)	3.25E-2 (1.35E+2)	1.18E-4 (4.87E-1)	2.15E-3 (8.90E+0)	1	0
6-4-3	1600	Baseline	N/D	1.10E-5 (4.56E-2)	1.92E-2 (7.94E+1)	9.41E-7 (3.90E-3)	1.39E-3 (5.77E+0)	0	0

N/D: none-detected

3.2 AGR-2 Safety Test Total Releases and Failures

Table 15 summarizes the total release of key fission products at the completion of safety tests of AGR-2 fuel compacts. A more-complete discussion of these results is available in the AGR-2 PIE final report and supporting references therein (Stempien et al. 2021). Releases of Cs-134 above 0.05 particle-equivalents were associated with either SiC failure or contamination held-over from earlier tests of AGR-2 UO₂ fuel (which experienced many SiC layer failures). Cs-134 releases less than 0.024 particle-equivalents in the 1600°C safety tests of the UCO fuel are so small that they may be dominated by contributions from hot-cell contamination and dispersed uranium in the as-fabricated compacts. The release of Kr-85 was primarily used to monitor for TRISO failure during safety testing, which only occurred in one compact (Compact 2-3-2).

Table 15. Summary of total release of key radionuclides and numbers of SiC and TRISO failures at the completion of each AGR-2 isothermal safety test (Stempien et al. 2021). Compact fraction is given with no parentheses, and particle equivalents are given in parentheses.

	Test Temp (°C)	Kr-85	Sr-90	Ag-110m	Cs-134	Eu-154	Number of Failures	
							SiC	TRISO
3-1-1 ^a	1500	6.49E-6 (0.010)	3.35E-5 (0.052)	6.37E-3 (9.8)	3.62E-4 (0.56)	2.92E-5 (0.045)	1	0
3-3-2 ^a	1600	<1E-6 (<0.002)	1.44E-3 (2.2)	1.73E-2 (27)	2.11E-3 (3.3)	3.77E-4 (0.58)	5–13	0
3-4-1 ^a	1700	4.33E-5 (0.067)	4.47E-2 (69)	8.92E-2 (138)	8.72E-2 (135)	3.06E-3 (4.7)	>>150	0
3-4-2 ^a	1600	<1E-6 (<0.002)	2.70E-3 (4.2)	1.13E-2 (17)	9.29E-3 (14)	3.23E-4 (0.50)	20-108	0
2-1-2 ^b	1800	1.02E-5 (0.032)	1.04E-2 (33)	2.10E-2 (67)	2.34E-4 (0.74)	1.67E-2 (53)	1	0
2-2-2 ^b	1600	5.40E-6 (0.017)	4.09E-2 (130)	7.27E-3 (23)	2.47E-7 (0.0008)	4.67E-2 (148)	0	0
2-3-1 ^b	1600	<7E-7 (<0.002)	8.61E-2 (273)	1.76E-2 (56)	3.96E-6 (0.013)	8.77E-2 (278)	0	0
2-3-2 ^b	1800	4.03E-4 (1.28)	9.85E-2 (313)	2.48E-2 (79)	2.95E-4 (0.94)	1.35E-1 (429)	0	0 ^c
5-2-1 ^b	1600	7.66E-6 (0.24)	2.27E-4 (0.72)	2.12E-2 (67)	4.20E-6 (0.013)	6.82E-4 (2.2)	0	0
5-2-2 ^b	1600	<7E-7 (<0.002)	7.91E-4 (2.5)	1.63E-2 (52)	5.91E-6 (0.019)	1.10E-3 (3.5)	0	0
5-4-1 ^b	1800	<7E-7 (<0.002)	2.34E-3 (7.4)	1.73E-1 (550)	1.03E-4 (0.33)	6.04E-3 (19)	1	0
6-2-1 ^b	1800	8.95E-5 (0.28)	2.01E-3 (6.4)	9.46E-3 (30)	6.64E-4 (2.1)	2.43E-3 (7.7)	3	1
6-2-2 ^b	1600	4.58E-6 (0.015)	2.21E-5 (0.070)	2.79E-3 (8.8)	7.67E-6 (0.024)	1.07E-4 (0.34)	0	0
6-4-2 ^{b,d}	1600	<9E-7 (<0.003)	8.70E-5 (0.28)	3.42E-3 (11)	6.20E-5 (0.20)	2.69E-4 (0.85)	0	0
6-4-3 ^b	1800	5.04E-6 (0.016)	5.37E-5 (0.17)	2.57E-2 (82)	1.97E-5 (0.063)	9.46E-4 (3.0)	0	0

Estimated uncertainty is $\pm 10\%$, and less-than values for Kr-85 are estimated from detector background.

Safety test soak temperatures were held for ~300 h, except for Compact 3-4-1, which was only held for 164 hours due to excessive radionuclide release, and Compact 3-1-1, which was held for 400 hours to observe particle release that initiated after 258 hours.

- Capsule 3 fuel compacts contained UO₂ fuel.
- Capsules 2, 5, and 6 compacts contained UCO fuel.
- Compact 2-3-2 had one TRISO failure traced to attack by Mo contamination that was probably introduced during fabrication. While this particle did release fission products, it is not accounted as a TRISO failure because of this as-fabricated defect from Mo.
- Compact 6-4-2 Cs-134 was affected by cross contamination from a preceding test of AGR-2 UO₂ Compact 3-4-1.

3.3 AGR-1 and AGR-2 UCO Safety Test Time-Dependent Release Data

3.3.1 Ag-110m

Figure 9 summarizes the Ag-110m time-dependent release for AGR-1 and 2. The Ag-110m release behavior is characterized by rapid early release. In most safety tests with isothermal holds $\leq 1700^\circ\text{C}$, most

of the Ag-110m was released during the temperature ramp at the start of the test and shortly after reaching the isothermal hold. In 11 of 15 safety tests with isothermal holds at 1600 or 1700°C, 90% of all the Ag-110m released from such tests had been released between the start of the ramp up from room temperature and 1 h into the isothermal hold at 1600 or 1700°C. The other four tests with isothermal holds in that temperature range had released 90% of the total safety-test release of Ag-110m within 48 h of starting the isothermal hold. Most of the tests with 1800°C holds had not released 90% of their total until after 230 h at 1800°C, on average.

Some of the Ag-110m released during safety testing was inventory that had been released in-pile through intact TRISO coatings that was retained in the OPyC and compact matrix material at the end of irradiation. In some cases (e.g., AGR-2, Compacts 6-4-2 and 2-2-2), it was apparent that much of the measured Ag-110m release occurred via diffusion through intact TRISO coatings during the 12-hour pause at 1250°C prior to ramping to the final test temperature. This is consistent with earlier observations of Ag-110m release from AGR-1 Compact 4-2-2 during a unique test in which the compact was subjected to soaks at different temperatures (Hunn et al. 2014d, Hunn et al. 2015a). Evidence of the restart of the AGR-1 Compact 3-3-2 test is visible with the sharp increase at 53 h after undergoing an additional heating and cooldown phase. The phenomenon of Ag-110m release through intact TRISO coatings was particularly noticeable in the 1800°C tests of UCO compacts where the Ag-110m release continued to increase after 300 hours. Some tests at 1800°C show a notable increase in Ag-110m release (and release rate) after at least 50 h at the target test temperature. Given that the Ag-110m releases at 1800°C were significantly higher than the number of particles with failed SiC or failed TRISO, Ag-110m release through failed coatings was not the primary source. As is discussed further in Section 4.5.2, AGR-1, Variant 3 fuel had the highest Ag-110m release rates at 1800°C, followed by AGR-2, and then other AGR-1 types (i.e., Baseline and Variant 1).

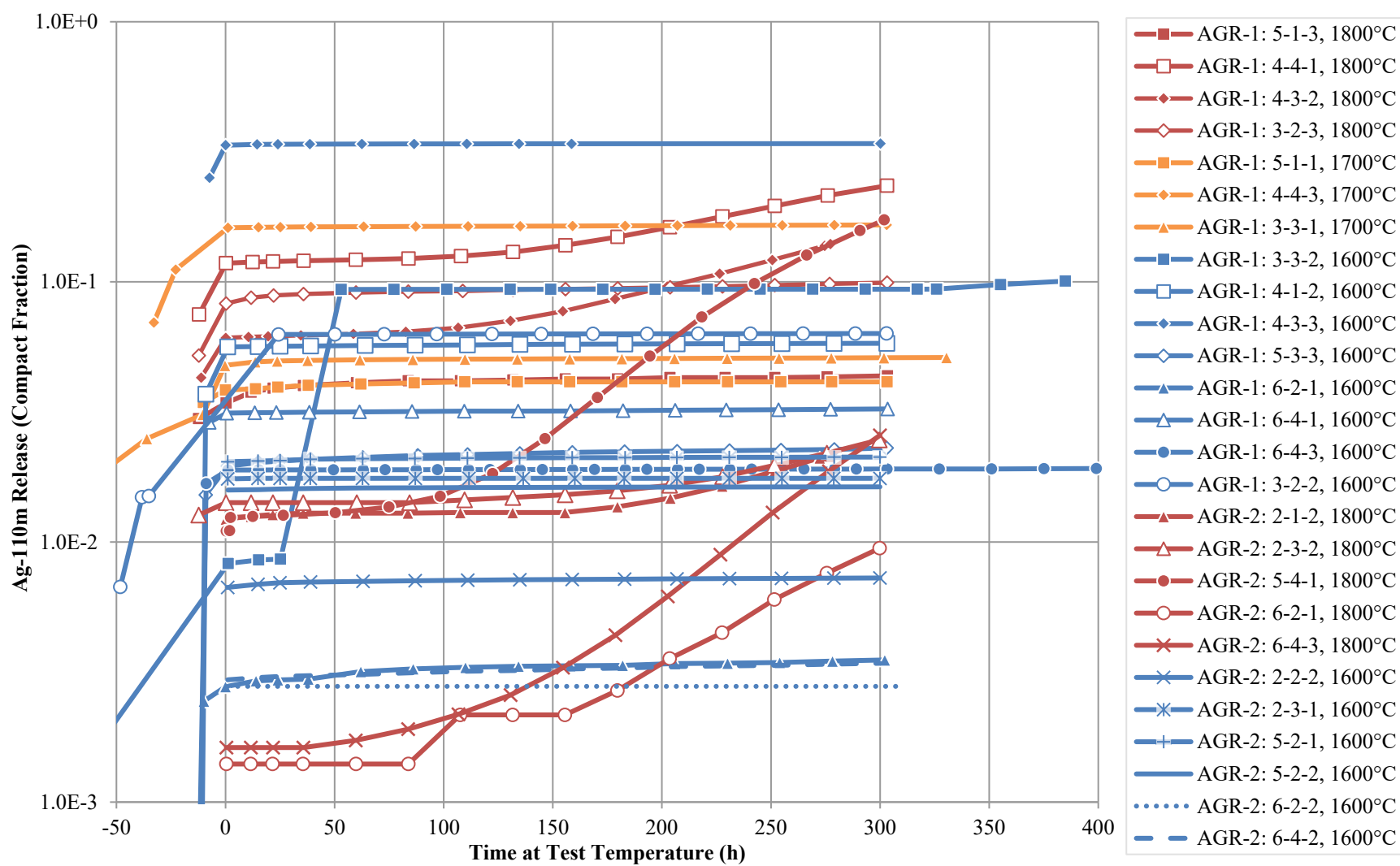


Figure 9. Summary of the time-dependent Ag-110m release fractions as a function of the hold time at the specified test temperature.

3.3.2 Cs-134

The time-dependent Cs-134 release from AGR-1 and AGR-2 compacts during safety tests is shown in Figure 10. Cesium is well retained by TRISO fuel with intact SiC layers. The numbers of SiC and TRISO failures in each safety test are summarized in Table 14 and Table 15 (the statistical frequencies of SiC and TRISO failures from both irradiation and safety testing are discussed in Section 4.1). Most of the tests fall into two categories: (1) final release $>1\text{E-}4$, associated with one or more particles with a failed SiC layer and (2) final release $<1\text{E-}5$, associated with no SiC failures. In AGR-1, there were three SiC failures during 1600°C safety tests and no SiC failures during AGR-2 1600°C tests. The number of SiC failures increased with the safety-test temperature. TRISO failures were less frequent, occurring only in two tests at 1800°C. In the absence of particles with failed SiC layers, cesium releases were due to dispersed uranium in the compact matrix from fabrication, and the measurements were further influenced by cesium picked up from contamination in the hot cell.

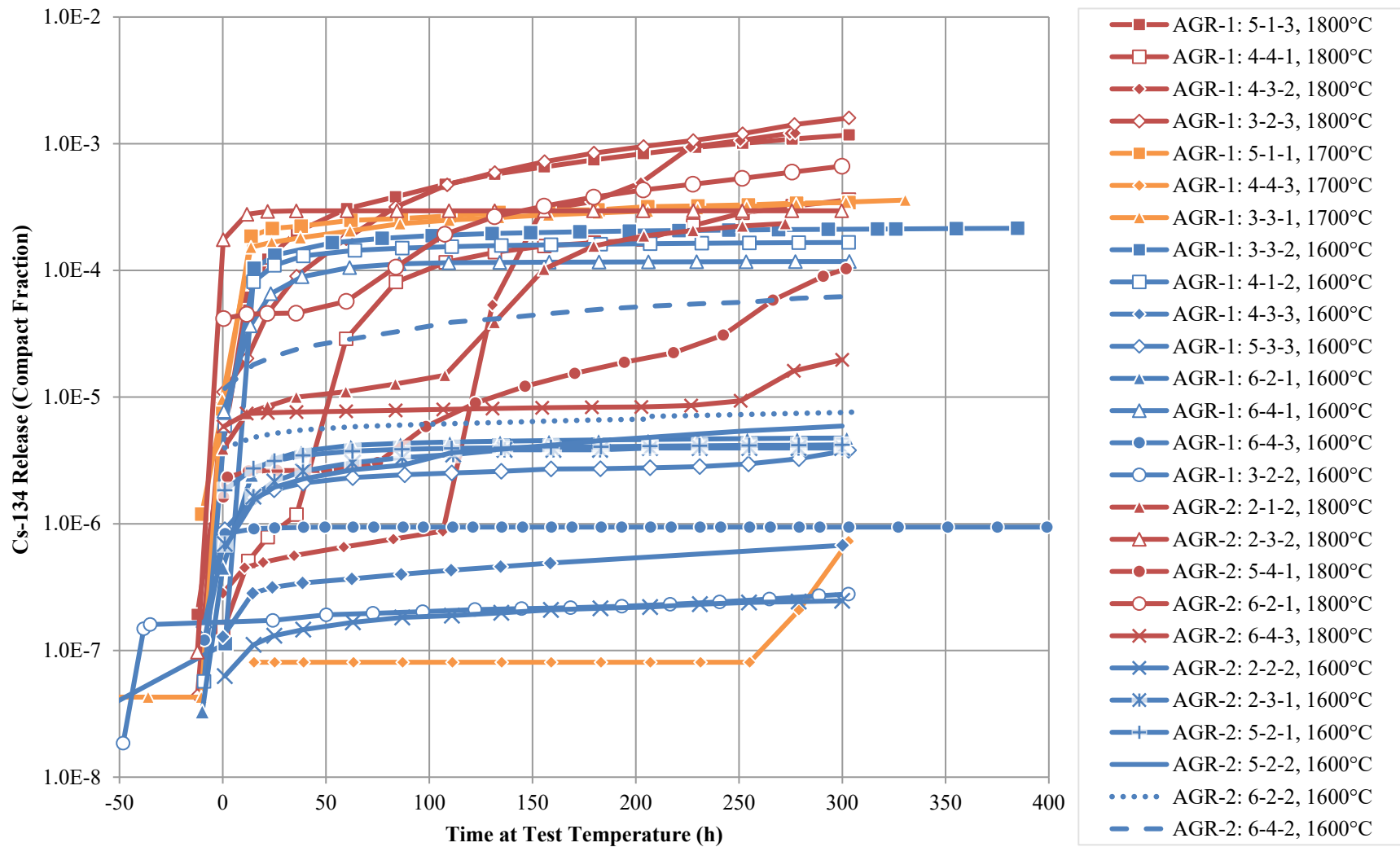


Figure 10. Summary of the time-dependent Cs-134 release fractions as a function of the hold time at the specified test temperature.

3.3.3 Eu-154 and Sr-90

3.3.3.1 Eu-154

Figure 11 shows the time-dependent Eu-154 safety-test releases from AGR-1 and 2. AGR-1 Variant 3 showed signs of more Eu-154 release than other AGR-1 fuel types. The AGR-2 SiC microstructure was most similar to AGR-1 Variant 3. Safety-test releases of Eu were dominated by the inventory that had been released through intact TRISO particles during irradiation that was retained in the compact matrix after irradiation (Stempien et al. 2021). Fuel compacts with higher irradiation temperatures (e.g., AGR-2 Capsule 2 compacts) were shown to have higher matrix inventories of Eu (Demkowicz et al. 2015a, Stempien et al. 2021). In contrast, fuel compacts in the cooler AGR-2 Capsules 5 and 6 had significantly lower TAVA irradiation temperatures (1071–1141°C and 987–1129°C, respectively) than Capsule 2 (1220–1300°C), and Eu releases from safety tests of Capsules 5 and 6 fuel were one to two orders of magnitude lower than in Capsule 2 safety tests (Stempien et al. 2021).

In support of the notion that safety-test releases are dominated by the inventory of Eu-154 in the OPyC and matrix, the quantity of Eu-154 released during safety tests was compared to the inventory of Eu-154 in as-irradiated (i.e., non-safety tested) compacts, which was compared to the inventory in fuel compacts after safety tests. For example, in the as-irradiated state, a compact fraction of $1.10\text{E-}1$ (348.37 particle-equivalents) was measured in AGR-2 Compact 2-2-1 outside of the SiC layers. An Eu-154 fraction of $4.67\text{E-}2$ (148 particle-equivalents) was released from the 1600°C test of AGR-2 Compact 2-2-2, and post-safety test DLBL of AGR-2 Compact 2-2-2 measured a fraction of $5.93\text{E-}2$ (188.22 particle-equivalents) outside of the SiC layers. Summing the measured release of Eu-154 from AGR-2 Compact 2-2-2 with the Eu-154 measured via DLBL of this compact gives a fraction of $1.06\text{E-}1$ (~336 particle-equivalents). This value is very similar to the amount of Eu-154 measured in the as-irradiated twin^c to AGR-2 Compact 2-2-2, AGR-2 Compact 2-2-1, and it indicates that Eu-154 releases from failed SiC layers or from slow diffusion of Eu-154 through intact SiC coatings were only small contributors to Eu-154 release from during the 1600°C safety test of AGR-2 Compact 2-2-2.

Comparisons between AGR-2 Capsule 2 compact twins safety tested at different temperatures showed that the in-pile Eu-154 releases still dominated the safety-test releases at 1800°C (Stempien et al. 2021). In AGR-2 Capsules 5 and 6 compacts, which had lower irradiation temperatures and lower matrix inventories of Eu-154 after irradiation than AGR-2 Capsule 2 compacts, Eu-154 releases from intact particles may comprise a larger portion of the total safety-test release than in the hotter Capsule 2 compacts, especially when those Capsule 5 and 6 compacts are tested at 1800°C. A twin comparison between as-irradiated Compact 5-4-2 and 1800°C safety-tested Compact 5-4-1 indicated that $>10\times$ more Eu-154 was released during 1800°C safety testing of Compact 5-4-1 than what was presumably in the matrix and OPyC at the start of the test, based on what was measured in Compact 5-4-2 (Stempien et al. 2021). In some 1800°C tests, the Eu-154 release increases later in the tests. This was observed with the 1800°C tests of AGR-1 Variant 3 fuel (e.g., Compact 4-4-1 and 4-3-2) and in the 1800°C test of AGR-2 Compact 5-4-1.

Analysis of the results of as-irradiated compact DLBL, safety tests, and post-safety test data from similar compacts indicates that Eu release from failed SiC layers (which had very low failure rates) or from slow diffusion of Eu through intact SiC coatings during the safety test were only small contributors to Eu release from safety-tested UCO fuel compacts (Demkowicz et al. 2015a, Stempien et al. 2021). The only exception was AGR-2 Compact 6-2-1 in which between three and four compromised SiC layers could have contributed to about half of the Eu release.

^c A twin compact means one in the same capsule, at the same level in that capsule, and in an adjacent stack within that capsule.

3.3.3.2 Sr-90

Figure 12 shows the time-dependent Sr-90 fractional release from AGR-1 and 2 compacts. The Sr-90 releases tended to parallel the Eu-154 releases, but at a lower total fraction. Averaged across all AGR-1 and 2 safety tests, the Sr-90:Eu-154 release ratio is 0.51. Similar to the behavior observed for Eu-154, total amounts of Sr-90 released from safety testing were higher from compacts with higher irradiation temperatures due to increased matrix inventories of Sr-90 in fuel that had higher irradiation temperatures (e.g., AGR-1 Compact 6-2-1 and AGR-2 Compacts 2-2-2 and 2-3-1) (Stempien et al. 2021).

In AGR-1 and AGR-2 fuel with lower irradiation temperatures (less than about 1100°C), the matrix inventories of Sr-90 in these compacts may have been small enough that release from intact TRISO coatings could amount to a few percent of the relatively small total Sr-90 releases from a safety test (Stempien et al. 2021). This was apparent in comparing 1600°C safety-tested AGR-2 Compact 6-4-2 with as-irradiated twin AGR-2 Compact 6-4-1. The sum of Sr-90 from safety-test releases and post-safety-test DLBL was more than the matrix inventory of Sr-90 in the as-irradiated compact, suggesting that some small release through intact coatings was occurring at 1600°C. In 1800°C tests of fuel compacts with smaller initial matrix inventories of Sr-90 (i.e., AGR-2 Capsules 5 and 6), the effect was more pronounced. A twin compact comparison between as-irradiated AGR-2 Compact 5-4-2 and 1800°C safety-tested AGR-2 Compact 5-4-1 indicated that ~20× more Sr-90 was released from AGR-2 Compact 5-4-1 during 1800°C safety testing than what was presumably in the matrix and OPyC at the start of the test, based on what was measured in the twin, AGR-2 Compact 5-4-2.

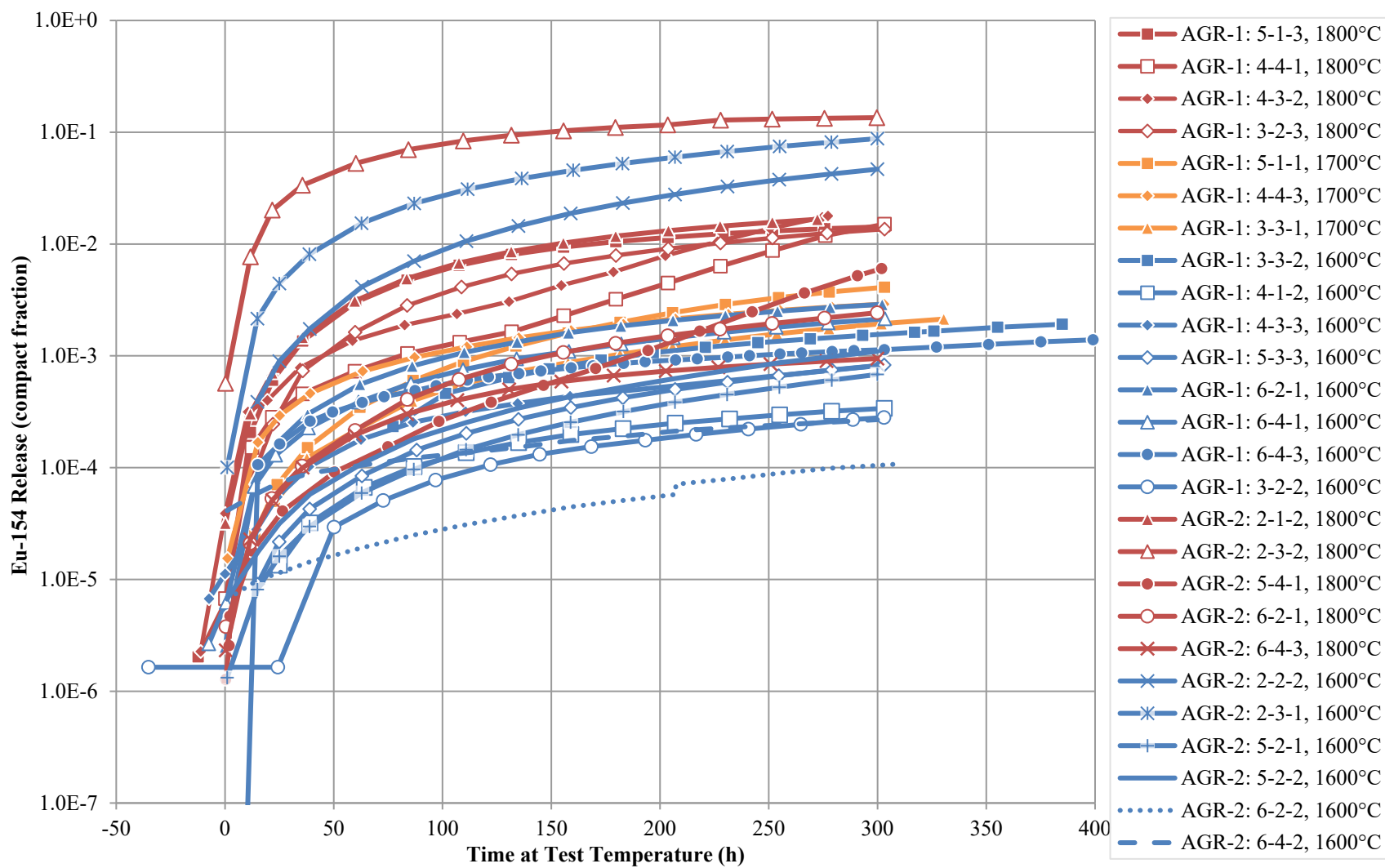


Figure 11. Summary of the time-dependent Eu-154 release fractions as a function of the hold time at the specified test temperature.

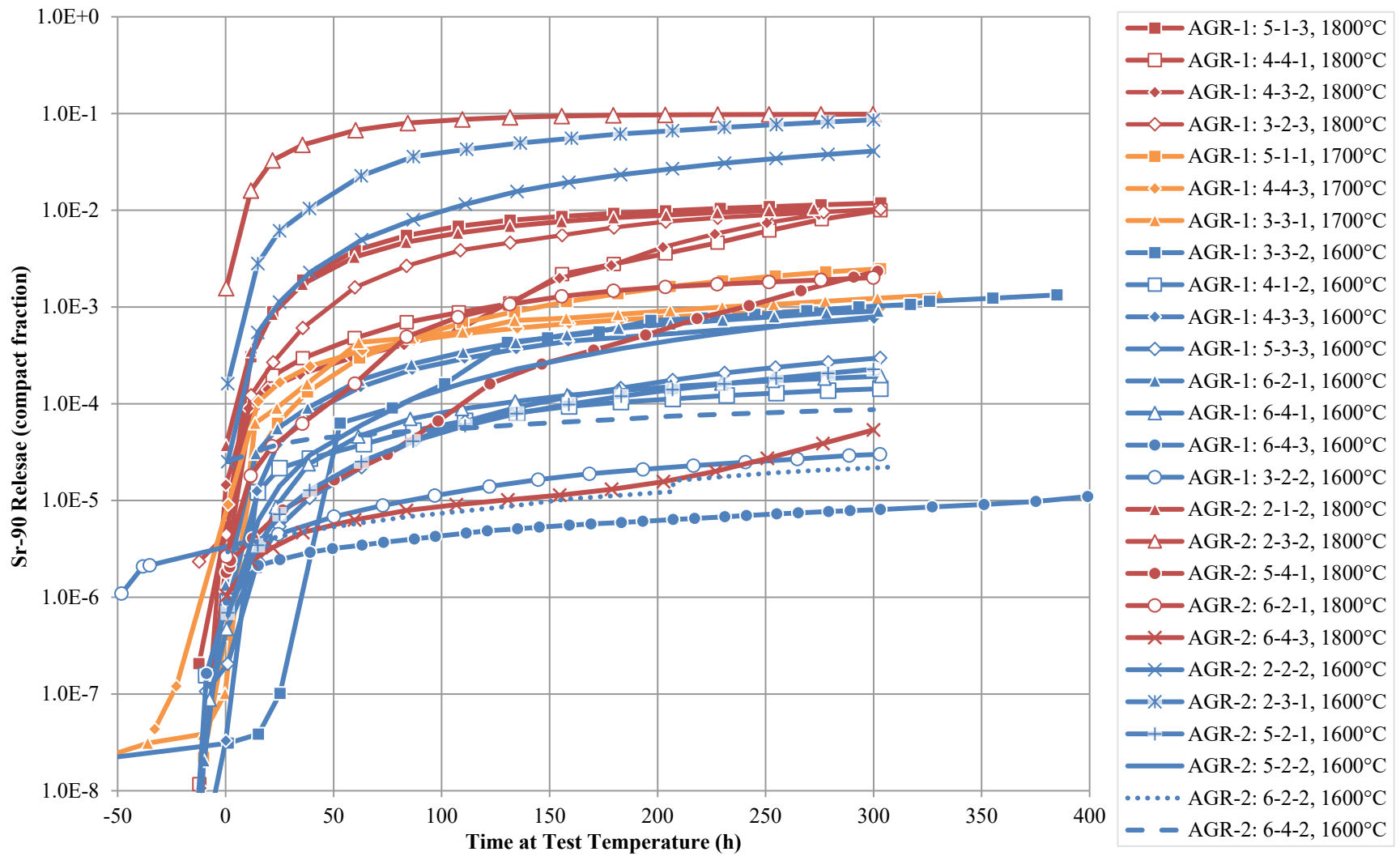


Figure 12. Summary of the time-dependent Sr-90 release fractions as a function of the hold time at the specified test temperature.

3.3.4 Kr-85

Fission-gas isotope Kr-85 is measured in the CCCTF and FACS furnaces when it is carried by a helium sweep gas to cryotrap traps fitted with gamma detectors. It is useful for detecting TRISO failures during the safety tests. In the absence of TRISO failures, very little Kr-85 was measured, and frequently, no Kr-85 was detected during safety tests. In instances where Kr-85 was detected in small amounts—less than a single particle's inventory—it is not clear that it can be reasonably distinguished from small amounts of Kr-85 in leakage from hot-cell contamination (Stempien et al. 2016). Thus, little attention will be given to Kr-85 here. In-pile short-lived fission-gas release-to-birth ratio data were analyzed from AGR-1, 2, and 3/4 (Pham et al. 2019). The isotopes considered were Kr-85m, Kr-87, Kr-88, Xe-135, Xe-135, and Xe-138. The analysis included fission-gas release from both dispersed uranium outside of intact SiC and from exposed kernels as a function of fuel temperature and isotope half-life.

3.4 Range of Release of Key Nuclides across AGR-1 and AGR-2 UCO Fuel

Figure 13 summarizes the range of minimum and maximum measured releases of key nuclides from safety tests of AGR-1 and 2 UCO fuel. AGR-1 ranges are plotted as the base layer, and AGR-2 Capsules 5 and 6 data are overlaid on top of that. The AGR-2 Capsule 2 data are overlaid on top of the AGR-2 Capsules 5 and 6 data. The AGR-2 Capsule 2 fission-product ranges are displayed separately from the other AGR-2 UCO capsules because the high irradiation temperature in Capsule 2 resulted in distinctly higher releases of Sr-90 and Eu-154. AGR-2 Capsule 2 releases of Kr-85, Cs-134 and Ag-110m were similar to those from other tests. Generally, the releases of key radionuclides during the safety tests of AGR-2 UCO fuel compacts were similar to those observed during safety testing of AGR-1 UCO fuel, and the maximum releases from AGR-2 compacts from Capsules 5 and 6 were somewhat lower than AGR-1 at 1800°C.

The representation of the Kr-85 release ranges in Figure 13 is different than that of the other nuclides. In 1600°C safety tests of AGR-2 Compacts 2-3-1, 5-2-2, and 6-4-2 and the 1800°C test of AGR-2 Compact 5-4-1, Kr-85 releases were too low to quantify. In those cases, MDAs were determined, and the true release of Kr-85 in those instances could lie somewhere between zero and the MDA. The bars plotted for Kr-85 span from the lowest MDA (on the bottom) to the highest measured fraction (on the top). In the 1600°C safety tests of two AGR-2 Capsule 2 compacts, a measured fraction of 5.40E-6 was released from Compact 2-2-2. In the 1600°C test of AGR-2 Compact 2-3-1, no Kr-85 release was detected, and the MDA was determined to be equivalent to a fraction of 7E-7. Accordingly, the bar for Kr-85 releases from 1600°C safety testing of these AGR-2 Capsule 2 compacts spans from 7E-7 to 5.40E-6. AGR-2 Compacts 5-2-1, 5-2-2, 6-2-2, and 6-4-2 were safety tested at 1600°C. The highest measured Kr-85 release was 7.66E-6 (from Compact 5-2-1), the lowest was 4.58E-6 (from Compact 6-2-2), and Kr-85 releases from Compacts 5-2-2 and 6-4-2 were below detection with MDAs of 7E-7 and 9E-7, respectively. Therefore, the Kr-85 releases from 1600°C tests of AGR-2 Capsules 5 and 6 fuel are represented by a bar ranging from the lowest MDA (7E-7) to the highest measured value (7.66E-6). When Kr-85 releases in AGR-1 tests were too low to quantify, the same approach was applied.

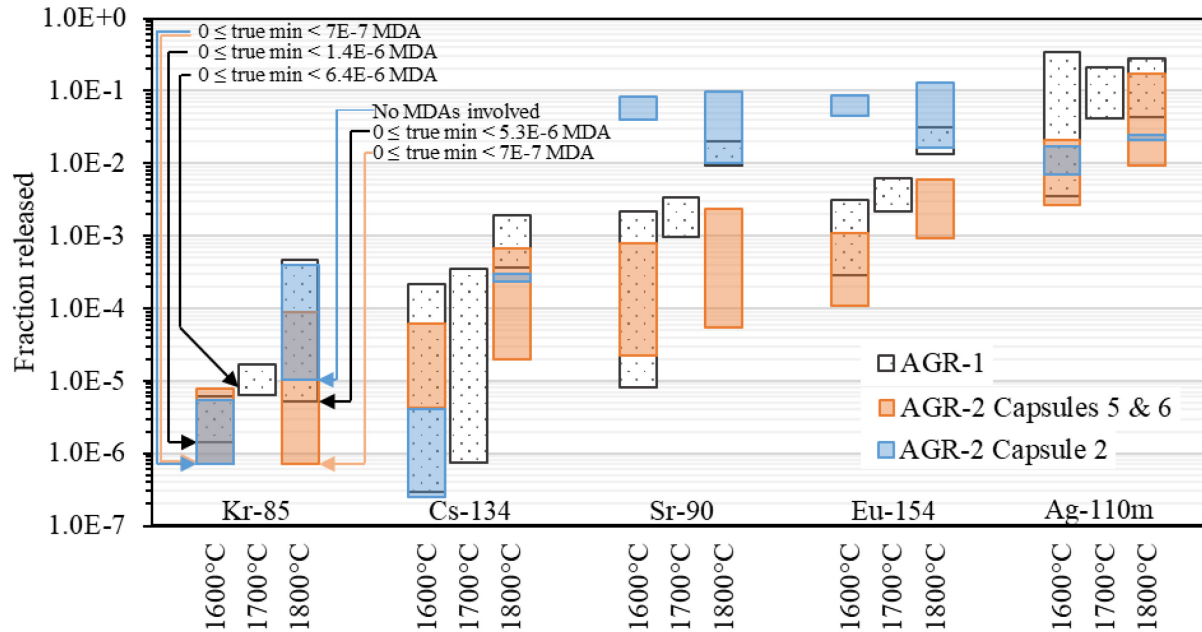


Figure 13. Summary of the ranges of fission product release for key nuclides from AGR-1 and AGR-2 UCO fuel (Stempien et al. 2021).

3.5 Discussion of Temperature-Transient versus Isothermal Testing

From the perspective of time-at-temperature, the high-temperature (1600–1800°C) isothermal tests lasting 300 h are significantly more severe than actual core-conduction cool-down events in traditional HTGRs. During a core-conduction cool-down event, forced coolant circulation ceases, the system depressurizes, and heat removal from the system is primarily by conduction through the reactor vessel into the reactor cavity. The reactor core gradually heats up over tens of hours before decreasing after reaching a peak temperature. Only a small portion of the core sees the peak temperature, with much of the fuel in the core hundreds of degrees cooler.

Another consideration is that a reactor facing a core-conduction cool-down event may contain fuel spanning a range of burnups (e.g., a pebble bed or a prismatic block reloaded one portion at a time). All safety-tested AGR-1 fuel had burnups ranging from 13.4 to 19.1% FIMA, and the majority of AGR-2 safety tests were conducted with fuel with a burnup between 10.2 and 12.9% FIMA. The fuel used in the AGR isothermal tests was not fresh: it had accrued substantial burnup and had already spent hundreds of days at TAVA irradiation temperatures ranging from 1000 to 1300°C.

Twenty-six isothermal safety tests have been performed with AGR-1 and AGR-2 UCO fuel. Two additional tests, one with three AGR-1 fuel compacts (Stempien et al. 2016) and one with three AGR-2 fuel compacts (Hunn, Morris, and Burns 2019) were conducted to mimic the temperature profile of a postulated core-conduction cool-down event so that the results could be compared with those from the isothermal safety tests. The profiles in both the AGR tests were based on an earlier German test that followed the calculated peak core temperature during a core-conduction cool-down event, but with the profile shifted up to give a maximum temperature of 1695°C instead of 1600°C (Schenk, Pitzer, and Knauf 1993). In each of the two AGR-2 temperature transient tests, three compacts were heated simultaneously to increase the total number of particles tested under these conditions.

It was notable that in the German temperature transient test of the TRISO fuel pebble designated Arbeitsgemeinschaft Versuchsreaktor (AVR)-91/31, there were approximately 20 TRISO failures (Schenk, Pitzer, and Knauf 1993). This was a higher failure fraction than had been observed in isothermal tests of similar German fuel. Part of the motivation for the AGR temperature transient tests was to determine whether AGR fuel performed differently during a temperature transient than during high-temperature, isothermal exposure.

Figure 14 shows the total released fraction and the release rates of Ag-110m from the AGR-1 transient test of Compacts 1-4-2, 1-1-3, and 1-1-1 (Stempien et al. 2016). Because all three Capsule 1 compacts were tested simultaneously, the measured activity (after decay correction) was compared to the total predicted activity summed across all three of those compacts. The transient test results are plotted such that time $t = 0$ marks the beginning of the transient rise in temperature. The previously reported isothermal test results for three other AGR-1 fuel compacts are plotted such that time $t = 0$ represents the time at which the isothermal test temperature was reached. Nearly all the silver released from the transient test came during the temperature ramp after the hold at 857°C, prior to reaching the peak test temperature. This indicates relatively rapid, early release of silver that had accumulated in the OPyC and compact graphitic matrix during irradiation. This is consistent with the accompanying data from AGR-1 Compacts 4-3-2, 4-3-3, and 6-4-1. The Ag-110m release rate then increased as the temperature transient dropped into the 1400 to 1100°C range, consistent with the observations from Hunn et al. (2014d and 2015a) during the AGR-1 Compact 4-2-2 test.

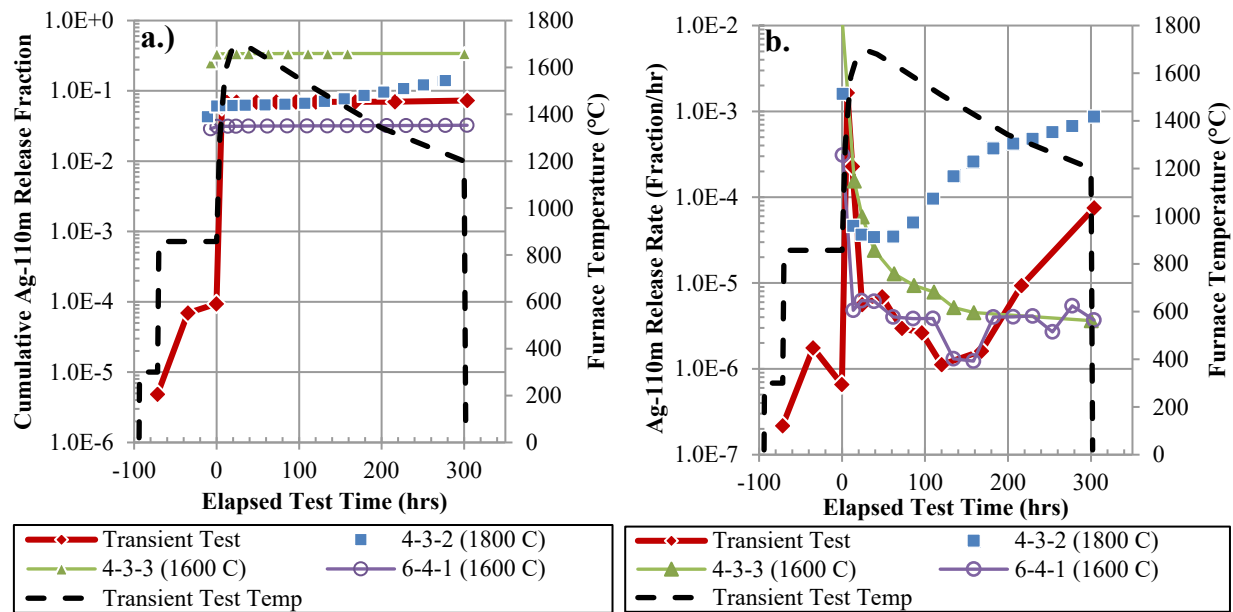


Figure 14. (a) Release fraction of Ag-110m from AGR-1 transient test of compared to isothermal tests of three other AGR-1 fuel compacts and (b) release rates of Ag-110m from the same tests (Stempien et al. 2016).

Figure 15 shows the total released fraction and the release rates of Cs-134 from the AGR-1 transient test of Compacts 1-4-2, 1-1-3, and 1-1-1 and several isothermal AGR-1 tests. Despite a peak temperature of 1695°C, the transient test Cs-134 fractional release is similar to that of the isothermal 1600°C test of AGR-1 Compact 4-3-3. This plot also shows that most cesium release occurred during the ramp to peak temperature following the hold at 857°C. Because little cesium release occurred after peak test temperature, this indicated that cesium released during the transient test was limited primarily to what was produced from as-fabricated dispersed uranium. As-fabricated AGR-1 fuel had a DUF of $<4\text{E-}7$, compared to a total release from the transient test of $4.8\text{E-}7$. Compact 6-4-1 had a single SiC layer failure, and Compact 4-3-2 had three SiC failures and two TRISO failures that dominated their Cs-134 release.

Figure 16 displays the total released fraction and the release rates of Eu-154 from the AGR-1 transient test of Compacts 1-4-2, 1-1-3, and 1-1-1 and several isothermal AGR-1 tests. Here the total release from each test is proportional to average temperature. The Eu-154 release rate from the transient test follows the temperature profile. This comparison highlights the fact that during 1600°C isothermal tests the cumulative Eu-154 release is strongly influenced by the long total duration at the test temperature, during which the release rate remains relatively constant. By contrast, the Eu-154 release rate during the transient test briefly reaches a maximum as the peak temperature is reached and then decreases dramatically as fuel temperature decreases, eventually reaching a value several orders of magnitude below the peak once the furnace temperature has cooled to 1200–1300°C. As a result, Eu-154 release behavior during the isothermal safety tests substantially overpredicts release from fuel at peak core temperature during a depressurized core-conduction cooldown event. The Sr-90 behavior during the transient test was very similar to that of Eu-154 (Stempien et al. 2016), and those results will not be reproduced here.

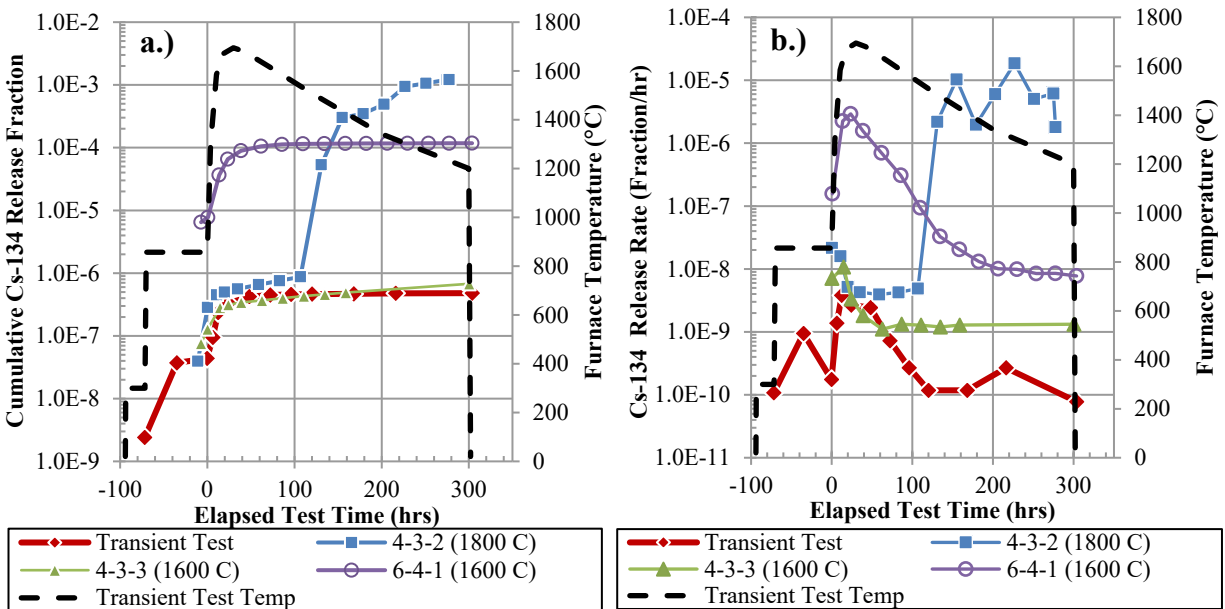


Figure 15. (a) Release fraction of Cs-134 from AGR-1 transient test compared to isothermal tests of three other AGR-1 fuel compacts and (b) release rates of Cs-134 from the same tests (Stempien et al. 2016).

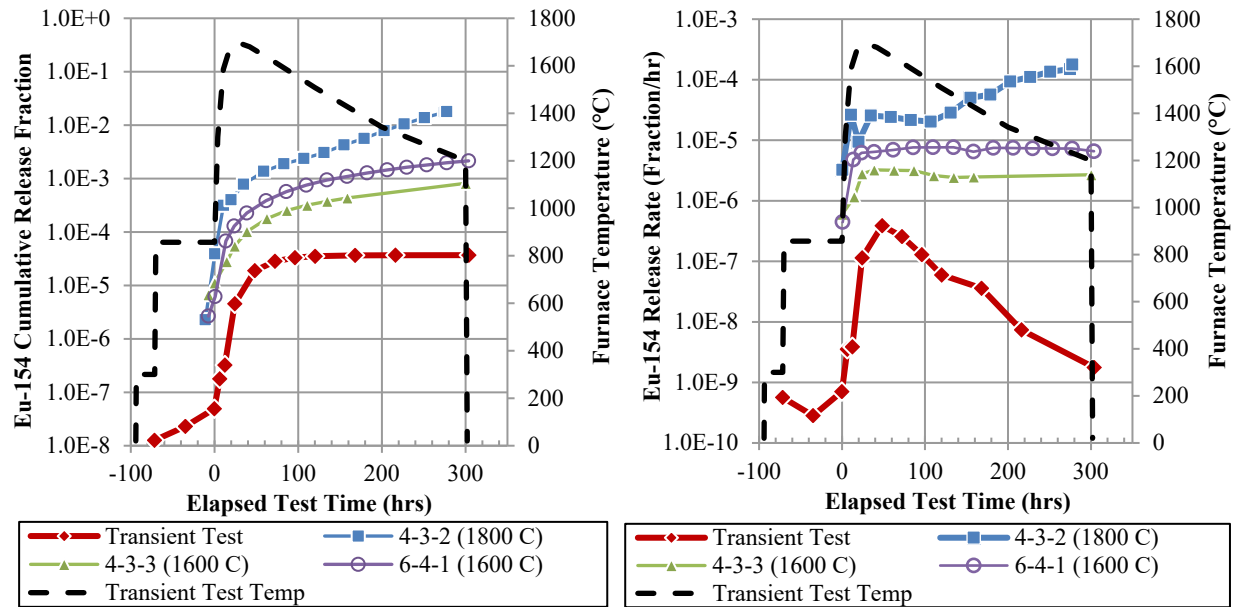


Figure 16. (a) Release fraction of Eu-154 from AGR-1 transient test compared to isothermal tests of three other AGR-1 fuel compacts and (b) release rates of Eu-154 from the same tests (Stempien et al. 2016).

The results from the transient test of AGR-2 Compacts 5-1-1, 5-1-2, and 5-3-1 at ORNL were consistent with those from AGR-1 (Hunn, Morris, and Burns 2019, see also Stempien et al. 2021 for Sr-90 results from this test). A summary plot from this test is given below in Figure 17. A CCCTF furnace cooling-line leak occurred early in the run (~25 h of elapsed time). It was repaired, and the test was completed. Additionally, the test was terminated early after problems were encountered with the cold finger during the eighth deposition-cup exchange at about 286 h. Although the transient test reached a peak temperature of 1695°C, the sample temperature was between 1600 and 1695°C for only approximately 65 h, and fractions of most fission products released from this test were less than in the 300-h isothermal tests of AGR-2 Capsule 5 fuel at 1600°C. The Eu-154 fractional release at the end of the transient test was $1.37E-4$, compared to cumulative Eu-154 releases that ranged from $6.24E-4$ to $1.10E-3$ in the AGR-2 Capsule 5 isothermal tests. A Sr-90 fraction of $8.66E-5$ was released from the AGR-2 transient test, compared to $2.27E-4$ to $7.91E-4$ from AGR-2 Capsule 5 isothermal tests. The fraction of Cs-134 released from the transient test was $1.14E-5$, which was about twice the Cs-134 fractions released from the AGR-2 Capsule 5 isothermal tests. However, that quantity equates to only 0.1 particle-equivalent. The releases of Ag-110m were similar for the transient test (a fraction of $2.15E-2$) and the isothermal tests (fractions ranging from $1.63E-2$ to $2.12E-2$). This Ag-110m behavior is consistent with prior AGR-1 post-irradiation heating tests at lower temperatures (Hunn et al. 2014d and 2015a). Here the Ag-110m release rates were highest as the transient safety test temperature passed through approximately 1100–1300°C (for rate data, see Hunn, Morris, and Burns 2019).

In the AGR-1 and AGR-2 transient tests, no SiC or TRISO failures were observed. This indicates that the temperature transient does not impose additional stress on UCO fuel beyond that demonstrated in the isothermal heating tests. In fact, the temperature variations during the AGR-1 simulated core-conduction cooldown transient temperature heating tests caused less release of Cs-134, Eu-154, and Sr-90 than in the AGR-1 300-h 1600°C isothermal tests. In AGR-2, the Eu-154 and Sr-90 releases were lower than comparable AGR-2 300-h isothermal tests at 1600°C, and the Ag-110m release was similar to other AGR-2 isothermal tests.

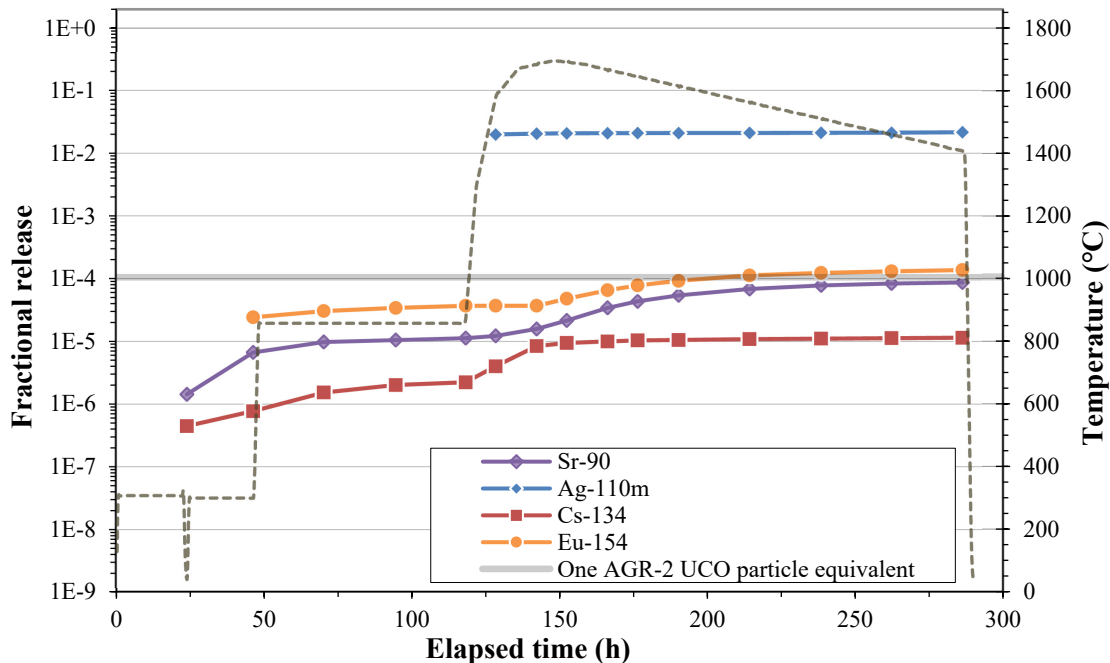


Figure 17. Summary of cumulative radionuclide releases from the simultaneous transient test of three Capsule 5 UCO compacts. Test and analysis performed at ORNL. Data from Hunn, Morris, and Burns (2019). Sr-90 data from Stempien (et al. 2021). One particle-equivalent in this test amounts to a fraction of $1.05\text{E-}4$.

4. FISSION-PRODUCT RELEASE RATES FROM UCO FUEL

One motivation for summarizing the available fission-product release data from AGR-1 and 2 (and some of the results from AGR-3/4) is to assess the feasibility of producing empirical relationships for the release or retention of key fission products from TRISO fuel over a range of nominal power-reactor conditions, margin conditions (i.e., high in-pile temperatures), and high-temperature conditions like those encountered in depressurized conduction-cooldown events. To estimate releases as a function of time, one requires rates. This section describes the development of release rates of key condensable fission products from the body of data collected from AGR-1 and AGR-2.^d

4.1 SiC and TRISO Failure Rates in UCO Fuel

TRISO coatings act as a functional containment, keeping fission products within the TRISO-coated particles to such a high degree that traditional reactor-containment structures may not be required (Petti et al. 2013). As the following sections will show, the retention of fission product Cs is directly tied to the integrity of these coatings. Europium and Sr retention is impacted by coating integrity, but some diffusion of Eu and Sr can occur through intact coatings, making overall retention or release of Eu and Sr less sensitive to coating integrity than Cs. Fission product silver transport is most sensitive to irradiation time and temperature. Of the fission products of interest in this report, the retention of Ag-110m is least affected by coating integrity.

The integrity of TRISO coatings is tied to their performance during irradiation and any subsequent safety testing. Table 10 listed the number of SiC and TRISO failures for specific compacts from AGR-1 and 2. Table 14 and Table 15 listed the SiC and TRISO failures for each AGR-1 and AGR-2 safety test,

^d In cases where fission-product activities were below detection, MDAs (see Section 1.3.1) were usually produced and reported. The true value for a fission product below detection is unknown and less than the MDA. MDAs and values derived from MDAs will not be used in the generation of fission-product release rates or empirical relationships.

respectively. Table 16 summarizes the SiC and TRISO failure fractions of AGR-1 and 2, separately and for a combination of the AGR-1 and 2 data. These are not time-dependent rates, but they give the total particle-failure fraction by the end of the irradiation and safety tests. Significant discussion on the methods and enumerations of these values is available in Demkowicz et al. (2015a) and Stempien et al. (2021). The safety-test temperatures represented are 1600, 1700, and 1800°C. There are also rows to represent the SiC and TRISO failures during irradiation. The temperatures given for those rows are the average TAVA temperatures for AGR-1, AGR-2, and the combination of AGR-1 and 2 UCO fuel compacts. The AGR-2 UO₂ fuel was not included in this table.

Figure 18 shows a plot of the SiC- and TRISO-failure fractions as a function of the irradiation temperature and the safety-test temperatures for the combination of the AGR-1 and 2 UCO fuel data. No AGR-2 safety tests were conducted at 1700°C; therefore, the values at 1700°C come only from AGR-1. Table 16 shows that the number of particles tested at 1700°C is the lowest among all safety-test temperatures. Thus, despite there being zero measured TRISO failures at 1700°C, the upper 95% confidence limit for TRISO failures at 1700°C is slightly higher than at 1800°C.

Table 16. Summary of SiC- and TRISO-failure fractions after irradiation and after safety testing for AGR-1 and 2 individually and for their combination into a single population. AGR-1 data are from Demkowicz et al. (2015a), and AGR-2 data are from Stempien et al. (2021). Combined data were calculated here. The 95% confidence values were calculated from binomial statistics. UCO fuel only.

		Temp (°C)	Number of Particles	SiC			TRISO		
				Number of Failures	Measured Failure Fraction	95% Confidence (≤)	Number of Failures	Measured Failure Fraction	95% Confidence (≤)
AGR-1	Irrad ^a	1044	298,000	4	1.50E-5	3.10E-5	0	0	1.10E-5
	ST ^b	1600	33,100	3	9.10E-5	2.40E-4	0	0	9.10E-5
		1700	12,400	7	5.60E-4	1.10E-3	0	0	2.50E-4
		1800	16,500	23	1.40E-3	2.00E-3	2	1.20E-4	3.90E-4
AGR-2	Irrad ^a	1142	114,336	≤6	5.25E-5	1.04E-4	≤4	≤3.50E-5	8.01E-5
	ST ^b	1600	19,056	0	0	1.58E-4	1	0	1.58E-4
		1800	15,880	5	3.15E-4	6.62E-4	≤1	≤6.30E-5	2.99E-4
AGR-1 and AGR-2 Combined	Irrad ^a	1077	412,336	10	2.43E-5	4.11E-5	≤4	≤9.70E-6	2.22E-5
	ST ^b	1600	52,156	3	5.75E-5	1.49E-4	1	1.92E-5	9.10E-5
		1700 ^c	12,400	7	5.60E-4	1.10E-3	0	0	2.50E-4
		1800	32,380	28	8.65E-4	1.19E-3	≤3	≤9.26E-5	2.39E-4

a. Irrad = irradiation.

b. ST = safety test.

c. Only AGR-1 had safety tests at 1700°C.

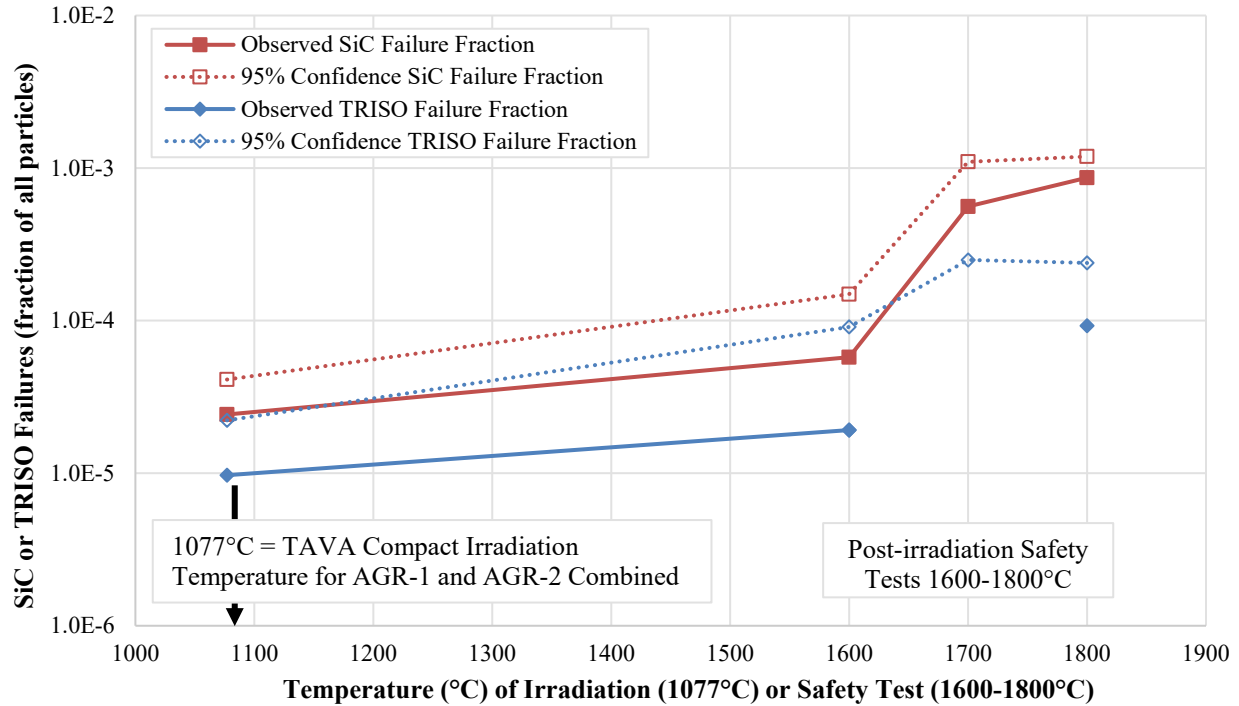


Figure 18. Plot of observed and SiC- and TRISO-failure fraction and the upper 95% confidence limits from the combined results from the AGR-1 and AGR-2 irradiations and safety tests. UCO fuel only.

4.2 In-pile Compact Release Rates

Typically, the best indicator of in-pile release from compacts comes from determining the fission-product mass balance in the irradiation capsule (see Section 2.2). Because of uncertainties in the gamma spectrometric methods (commonly on the order of 5%) and known biases in the calculated fission-product inventories, measuring the gamma inventory of individual compacts and comparing that to the calculated inventory is only effective in instances where fission-product release from a compact is on the order of 10% or greater. This can be the case for Ag-110m, but it is not the case for any other nuclides in AGR-1, 2, and 3/4. In this section, the fission-product mass balances from AGR-1, 2, and 3/4 were used to construct release rates as a function of time, burnup, and average irradiation temperature.

Here the EOI fission-product inventories measured on capsule components were normalized by irradiation time expressed in effective full-power days (EFPD) and burnup (% FIMA). This gives an average release rate over the period of irradiation that considers differences in burnup rate. The burnup rate is an important consideration given that AGR irradiations were accelerated compared to typical power-reactor burnup rates (Maki et al. 2007). These rates were then plotted versus inverse temperature, and exponential fits were applied. Data from all AGR capsules except the UO₂ capsule from AGR-2 and the unopened FBs from AGR-3/4 were combined in this analysis.

Data from the AGR-3/4 mass balances required a correction for the DTF particles that made up about 1% of all the particles in AGR-3/4. This correction was done by subtracting the inventory equivalent to 80 DTF particles per capsule from the mass balances in all AGR-3/4 capsules. If the difference was >0 , that value was retained as an estimate of the fission-product release from the compact due to the TRISO-coated driver-fuel particles. This implicitly assumes that the total inventory from the DTF particles was released from the compacts, and if the difference between the capsule mass balance and the DTF inventory was >0 , it meant the release from the driver particles exceeded the total DTF inventory. This is the case for Ag-110m in some AGR-3/4 capsules and for Eu-154 and Sr-90 in the high-irradiation temperature Capsule 7. If the difference was <0 (as was the case for most AGR-3/4 data sets), the value was rejected because there is no way of estimating the contribution from the DTF particles versus that from the driver particles.

Because no Ag-110m was measured in DLBLs of AGR-3/4 compacts, the AGR-3/4 mass balance and AGR-1 and AGR-2 results suggest the correction applied here for DTF fuel in AGR-3/4 capsules is a reasonable assumption in any capsules with average fuel temperatures $>1000^{\circ}\text{C}$. Comparing AGR-1 and 2 DLBL measurements (Section 2.1) to AGR-1 and 2 mass-balance measurements shows that the amount of Ag-110m released from the compacts exceeds that retained in the OPyC and matrix by one to three orders of magnitude. This means Ag-110m, no longer bound by intact TRISO coatings (the same as all the Ag-110m in the DTF particles), seems to be readily released from the compact rather than retained in the compact by the OPyC or matrix. No attempts to correct the AGR-1 and 2 mass balances for in-pile SiC or TRISO failures were made. Therefore, the AGR-1 and 2 compact release rates here implicitly represent the effects of SiC- and TRISO-failure statistics in addition to releases from intact fuel and should be somewhat conservatively high estimates for release rates from compacts with zero SiC or TRISO failures. Additionally, any release due to dispersed uranium also contributed to the total release from the compact.

Figure 19 shows an exponential fit to all the Ag-110m compact release rates for all AGR capsules versus inverse temperature. Values from five AGR-3/4 capsules are included here because release of Ag-110m from TRISO-coated driver particles exceeded the inventory in the DTF particles in those capsules. Figure 20 shows compact release rates of Cs-134. The number of points in this plot is less than in the plot for Ag-110m because some AGR-1 and 2 capsules had no measurable Cs-134 on components outside of the fuel. Furthermore, the Cs-134 release in AGR-3/4 capsules was dominated by the DTF particles, making it impossible to distinguish any small release of Cs-134 from intact driver fuel from that due to the DTF particles. Thus, Figure 20 only contains data on Cs-134 from AGR-1 and 2. Figure 21 and Figure 22 are plots of Eu-154 and Sr-90 compact release rates, respectively.

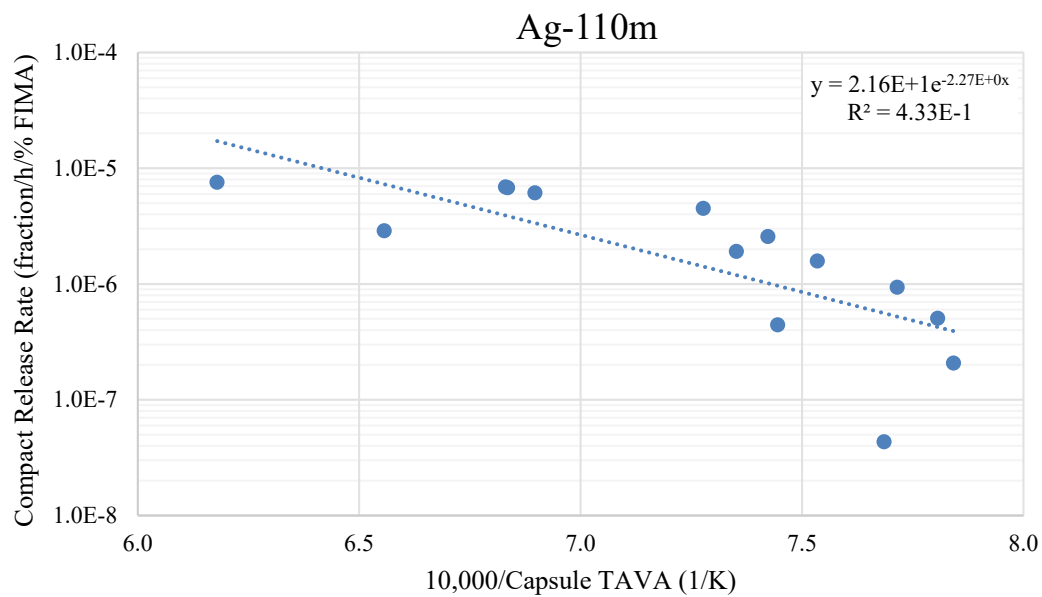


Figure 19. Compact release rates for Ag-110m. Data points come from AGR-1 Capsules 1-6; AGR-2 Capsules 2, 5, and 6; and AGR-3/4 Capsules 3, 4, 7, 8, and 10.

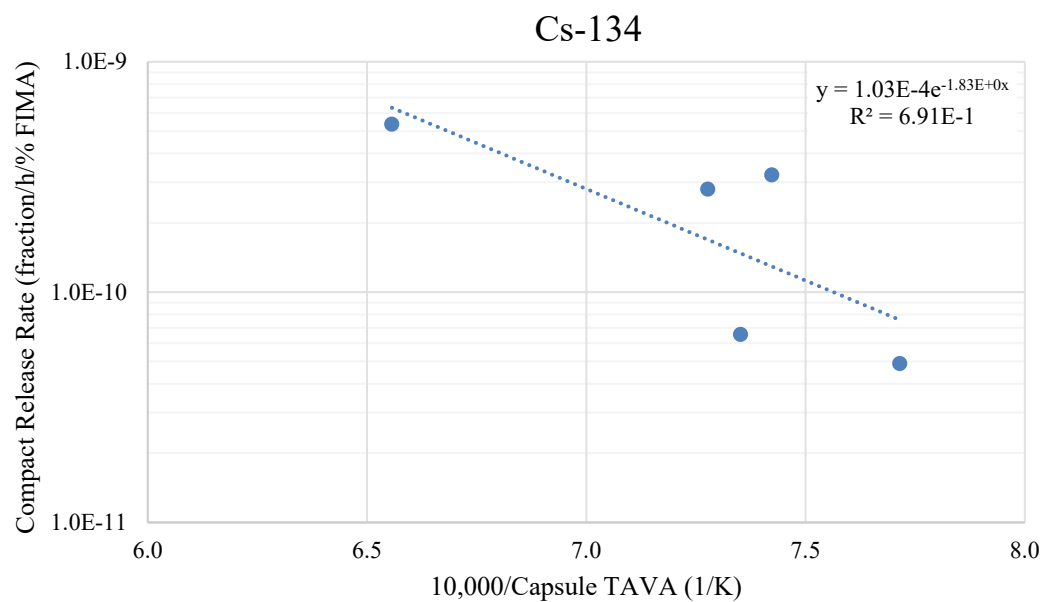


Figure 20. Compact release rates for Cs-134. Data points come from AGR-1 Capsules 5 and 6 and AGR-2 Capsules 2, 5, and 6.

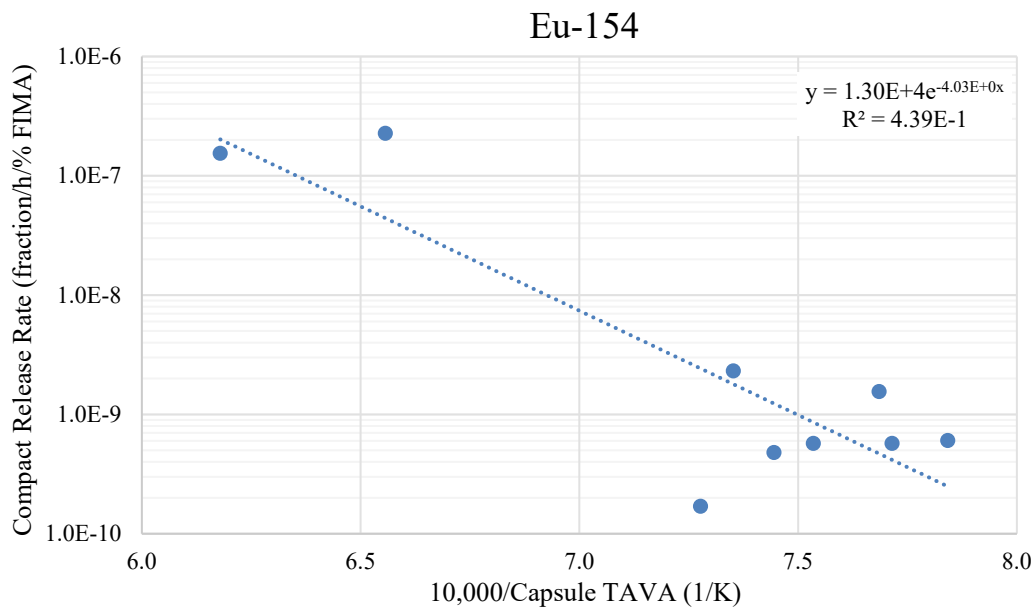


Figure 21. Compact release rates for Eu-154. Data points come from AGR-1 Capsules 1-6; AGR-2 Capsules 2 and 5; and AGR-3/4 Capsule 7.

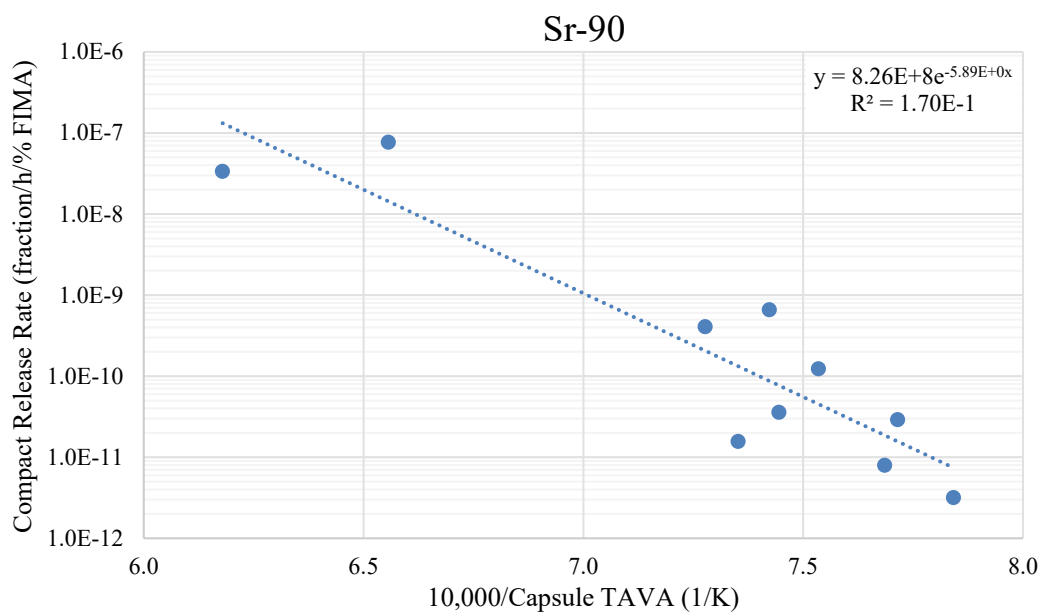


Figure 22. Compact release rates for Sr-90. Data points come from AGR-1 Capsules 1-6; AGR-2 Capsules 2, 5, and 6; and AGR-3/4 Capsule 7.

4.3 Accumulation of Fission Products in Compact Matrix

Multiple compacts from AGR-1 and 2 were subjected to as-irradiated DLBL as summarized in Section 2.1 and Table 9. This process establishes the inventory of fission products retained in the fuel compact outside of the SiC coatings. In compacts with SiC or TRISO failures (see Table 10), this allows the enumeration of these failures and the possibility of recovering the failed (or partially failed) particles for analysis. In compacts with no SiC or TRISO failures, this process gives the inventory of fission products released through intact SiC layers that was retained in the OPyC and compact matrix. To assess only the buildup of fission products in the matrix from intact TRISO particles, AGR-1 and 2 compacts with failed SiC or TRISO particles were excluded from this analysis. Similarly, no AGR-3/4 compacts were considered here because they each contained 20 DTF particles.

By knowing the EOI fission-product inventory in the compact matrix (given in Table 9) and the duration of the irradiation expressed in EFPD, an effective rate of fission-product accumulation in the compact matrix during the irradiation can be estimated by dividing the EOI DLBL inventories by the EFPD of the irradiation. The AGR-1 and AGR-2 irradiations were 620.2 and 559.2 EFPD, respectively. The two experiments had compact burnups overlapping in the 11–15% FIMA range. However, AGR-2 burnups extended down to 7.3% FIMA, and AGR-1 burnups extended up to about 19.6% FIMA. Therefore, the burnup rates can vary from one experiment to another. A further normalization by burnup is proposed here so that the rate of fission-product buildup in the compact matrix and OPyC is expressed as compact fraction per hour per % FIMA. The burnup normalization also accounts for the buildup of fission-product inventory in the fuel as the irradiation progresses.

The fission-product inventories of compacts with no SiC or TRISO failures were normalized by irradiation time and burnup, plotted against the calculated TAVA temperatures, and fit with an exponential function in Figure 23 through Figure 26. In the case of Cs-134, the fraction measured in all the AGR-2 DLBLs and some of the AGR-1 DLBLs was similar to or less than the DUF (discussed in Section 2.1). In those cases, the DLBL may more closely represent the amount of Cs-134 contributed from fission of as-fabricated dispersed uranium than from small release through intact particles. Thus, in Figure 24, two data series are depicted: one includes all AGR-1 and 2 DLBLs with no failed SiC or TRISO particles (regardless of how the Cs-134 fractions compared to DUF), and the other pools only the AGR-1 DLBLs with no failed SiC or TRISO where the Cs-134 inventory exceeded the DUF. The latter is the more conservative of the two data groupings for estimating Cs-134 buildup in the OPyC and compact matrix from intact particles.

A limitation of this approach is that the accumulation rate in the OPyC and compact matrix is a competition between the release rate from the SiC and that from the matrix. At lower temperatures, the release rate from SiC is slower, and presumably, the release rate from the matrix is also slower. At higher temperatures, the release rate from the SiC may be faster, but the release rate from the matrix may also be faster. To have significant accumulation in the matrix, the release rate from the SiC must be significant, but the release rate from the matrix must be lower. AGR-3/4 shows that if the temperature is high enough, significant release from the fuel will happen, but what is released may be driven farther from the fuel if the temperatures are very hot (Stempien et al. 2018, Stempien 2021). For example, in AGR-3/4, Capsule 7 had the highest total release of Ag-110m from the fuel, but it had the lowest amount of Ag-110m out of all AGR-3/4 inner rings that had measurable quantities of Ag-110m. The AGR-3/4 capsules that had the most Ag-110m in the inner rings were those with more-moderate temperatures (e.g., Capsules 3, 8, and 10). These were hot enough to see significant release from the fuel compacts, but not so hot that the Ag-110m was driven out of the inner ring. A similar kind of temperature range may exist for matrix accumulation where, at temperatures higher than this range, there is more release from particles, but also more release from the matrix, resulting in a smaller matrix inventory. At temperatures below this range, there would be little release from the particles, and while what is released from the particles may be retained in the matrix, the relatively small release from particles results in little

accumulation in the matrix. It is not clear what this temperature range for maximum matrix accumulation is for each nuclide.

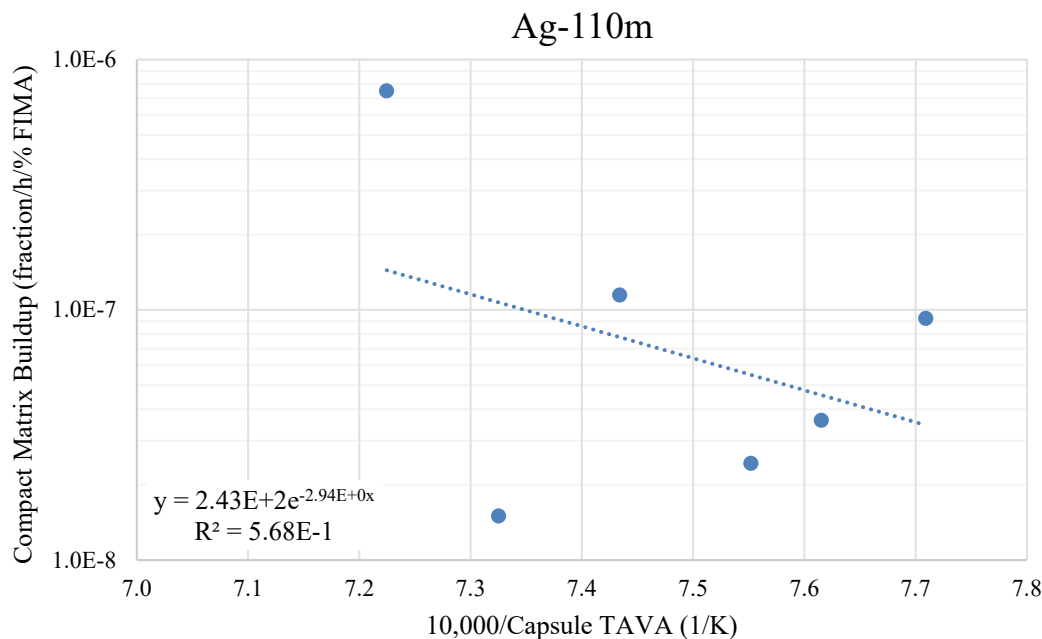


Figure 23. Rate of Ag-110m buildup in the fuel-compact matrix and OPyC from AGR-1 compacts subjected to as-irradiated DLBL that did not have any SiC or TRISO failures. The AGR-2 compacts with no SiC or TRISO failure did not have measurable Ag-110m in the matrix and OPyC.

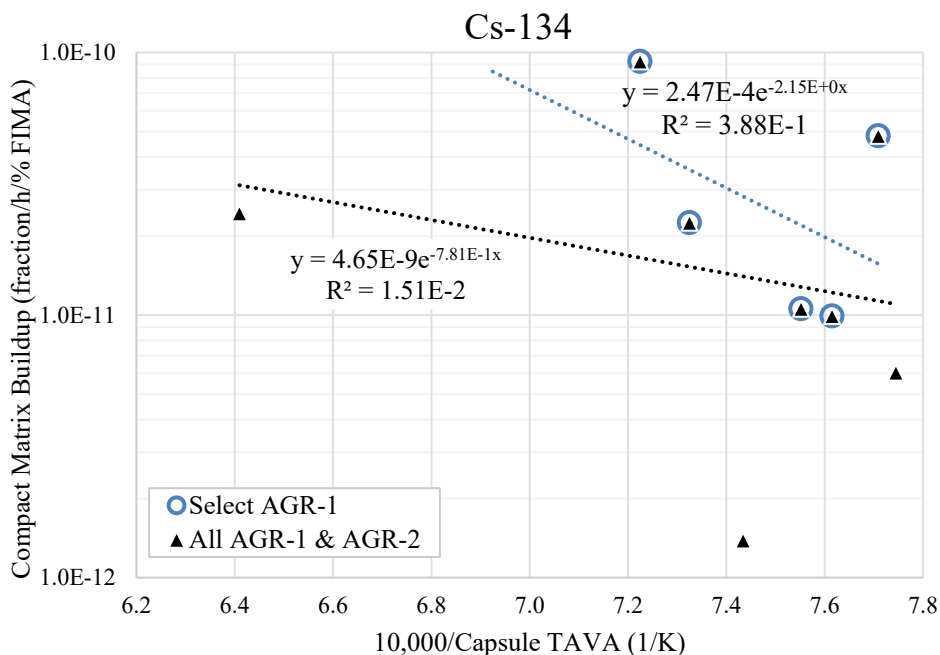


Figure 24. Rate of Cs-134 buildup in the fuel-compact matrix and OPyC from AGR-1 and 2 compacts subjected to as-irradiated DLBL. The data series “Select AGR-1” contains only data points where the Cs-134 content was in excess of what would be expected from dispersed uranium.

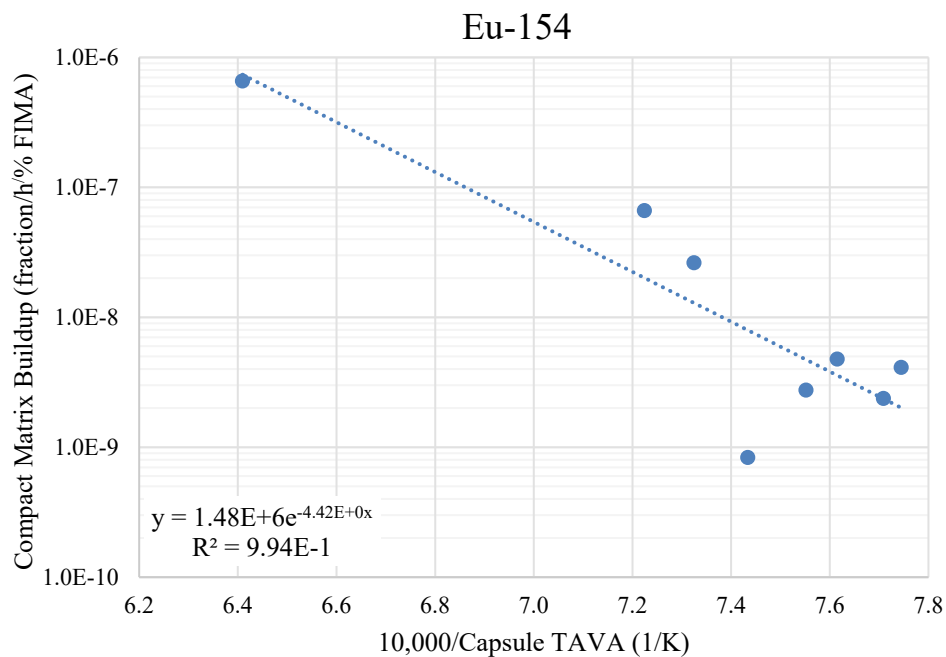


Figure 25. Rate of Eu-154 buildup in the fuel-compact matrix and OPyC from AGR-1 and 2 compacts subjected to as-irradiated DLBL.

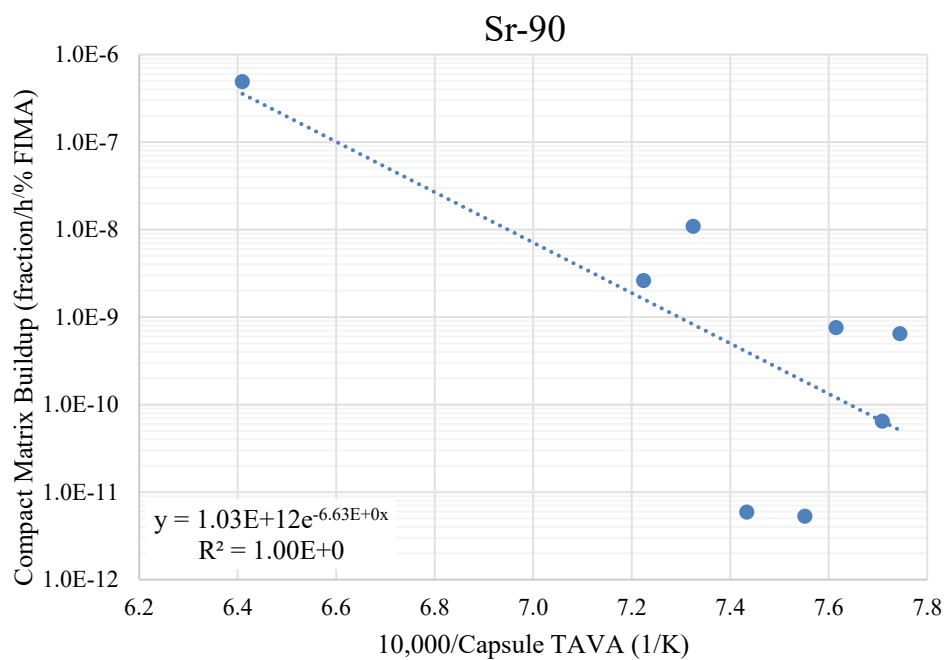


Figure 26. Rate of Sr-90 buildup in the fuel-compact matrix and OPyC from AGR-1 and 2 compacts subjected to as-irradiated DLBL.

4.4 In-pile through-SiC Release Rates

Section 4.2 developed rates of fission-product release from fuel compacts during irradiation as a function of irradiation temperature. Section 4.3 estimated the rate of fission-product accumulation in the matrix and OPyC of the fuel compacts during irradiation as a function of irradiation temperature. The mass balance dictates that the rate of release from compacts (Section 4.2) is equal to the rate of release from the particles, minus the rate of accumulation in the compact matrix and particle OPyC (Section 4.3). Thus, if desired, the release rate through the SiC of the particles can be estimated by adding the matrix accumulation rates determined in Section 4.3 to the compact release rates determined in Section 4.2. Note that the rate of matrix accumulation was determined from DLBL of the specific compacts listed in Table 9, but the rate of release from the compacts was determined from capsule components and represents a capsule-wide average-compact fission-product release rate that is not specific to the individual compacts listed in Table 9.^e

4.5 Release Rates from High-Temperature Safety Testing

Section 3.3 summarized the cumulative fractional fission product release as a function of time for several different test temperatures. Some of the time-dependent behaviors are more easily observed when looking at the derivative of the total-release-versus-time data sets (i.e., the release rates). These rates can be used to estimate fission product releases as a function of time at elevated temperatures.

4.5.1 Cs-134 Safety Test Release Rates

Generally, four types of cesium release behaviors were observed during safety testing. In the first type, there were no SiC- or TRISO-layer failures, and the initial Cs release rate was the result of compact matrix inventory. The release rate then decreased as the matrix inventory was depleted. The rate reached a relatively constant value at a lower level or continued to decrease as the matrix inventory was depleted in the presence of an extremely low rate of release through intact SiC. Figure 27 shows two examples of this type of behavior from AGR-1 and 2 compacts.

^e In attempting to determine the Cs-134 accumulation rate in the OPyC and matrix in Section 4.3, compacts with SiC or TRISO failures were neglected and compacts with Cs-134 inventories measured via DLBL that were \leq DUF were also neglected. Thus, Section 4.3 gives the rate of Cs-134 accumulation for fission products originating in the TRISO particles and does not include the contribution from DUF. In Section 4.4, the total compact Cs-134 release includes the contribution from dispersed uranium. Other key radionuclides measured in DLBL were present in quantities exceeding the DUF by 100 times or more, and DUF is only a small contribution to those nuclides.

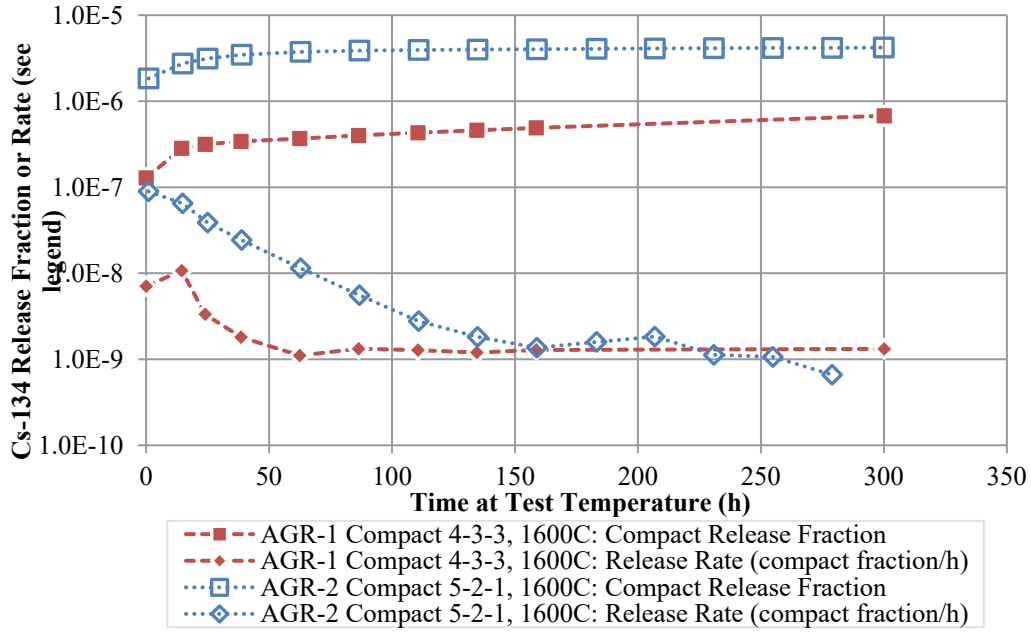


Figure 27. Release fractions and release rates for AGR-1 Compact 4-3-3 and AGR-2 Compact 5-2-1, showing typical 1600°C Cs-134 release behavior in the absence of any SiC or TRISO failures.

The second type is when a SiC or TRISO failure (or multiple failures) occurs during the rise to test temperature or very shortly after reaching the isothermal hold. In this case, the shape of the cumulative release-versus-time plot may be similar to that in the first type (where there are no failures); however, the rates involved are two to four orders of magnitude higher than in a similar test with no failures. Examples of this are given in Figure 28. Here, both compacts had a single SiC failure at the very beginning of the test.

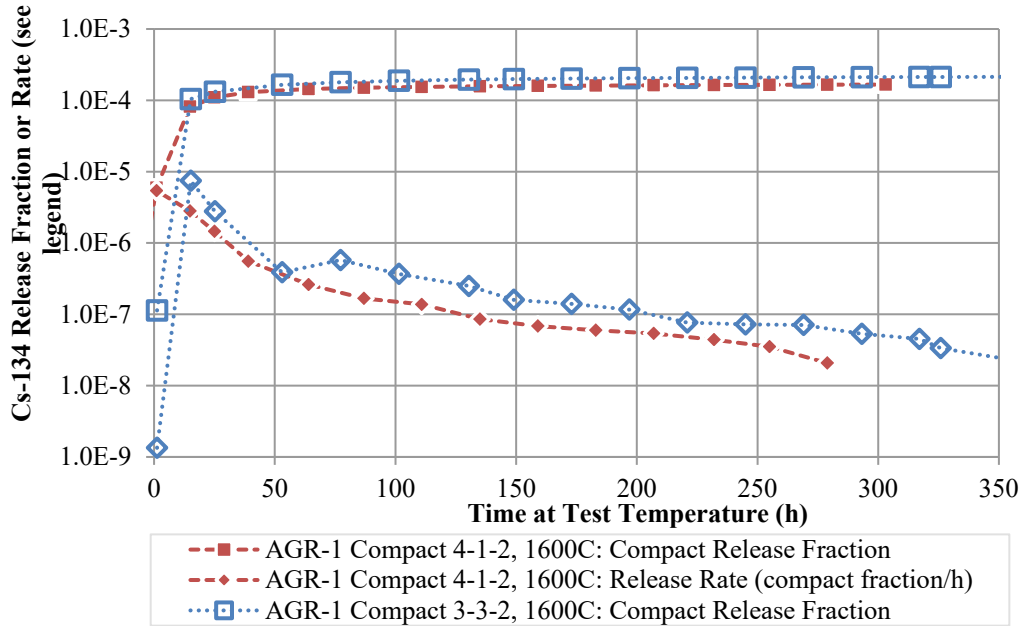


Figure 28. Release fractions and release rates for AGR-1 Compact 4-1-2 and AGR-1 Compact 3-3-2, each of which suffered a single SiC failure at the beginning of the test.

The third type of cesium release behavior is dominated by multiple failures involving the SiC coating occurring at any stage of the test. When multiple SiC or TRISO failures occurred in a test, the time dependent release from individual particle failures could not be resolved. Figure 29 shows the cesium release behavior from the 1800°C safety test of AGR-1 Compact 3-2-3, which experienced an estimated 11 SiC failures throughout the duration of the test (Hunn et al. 2016b, Demkowicz et al. 2015a), and AGR-2 Compact 6-2-1, which experienced a TRISO failure and three SiC failures (Hunn et al. 2019a, Stempien et al. 2021). The typical maximum Cs release rate observed at the start of tests without SiC failures is masked by multiple SiC failures and the resultant higher Cs release rates at the start of the AGR-1 Compact 3-2-3 test. The AGR-2 Compact 6-2-1 test shows a local maximum in the Cs release rate upon the start of the test followed by a sharp reduction in rate until additional failures occur and cause an increase in rate. After about 100 h at 1800°C, the Cs-release rates in these two tests are relatively steady at values about four orders of magnitude greater than in the 1600°C tests that did not have any SiC failures (see Figure 27).

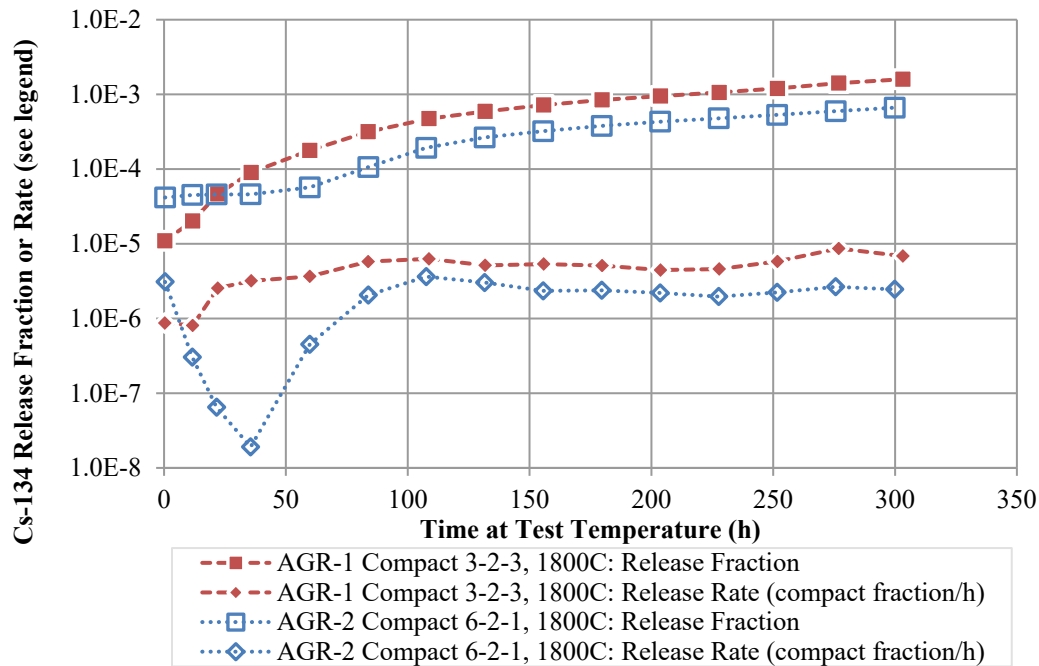


Figure 29. Release fractions and release rates for AGR-1 Compact 3-2-3 and AGR-2 Compact 6-2-1, at 1800°C. The AGR-1 Compact 3-2-3 test had 11 SiC failures. The AGR-2 Compact 6-2-1 test had three SiC failures and one TRISO failure.

The fourth type of cesium release behavior occurs when SiC and TRISO failures occur after the test temperature has been reached, and they are few in number and separated by enough time during a test that individual failures can be resolved. Figure 30 shows total releases and release rates for the AGR-1 Compact 4-4-1 test (which experienced two SiC failures, one after about 60 h at 1800°C and one after about 200h at 1800°C) (Hunn et al. 2013b, Hunn et al. 2013c), and for the AGR-2 Compact 2-1-2 test, which had one SiC failure after about 100 h at 1800°C (Hunn et al. 2019b, Stempien et al. 2021). In the Compact 2-1-2 test, a local maximum in Cs-134 release rate was reached after the first 10 h of time at 1800°C. The rate then began to decrease until the SiC failure occurred after about 100 h.

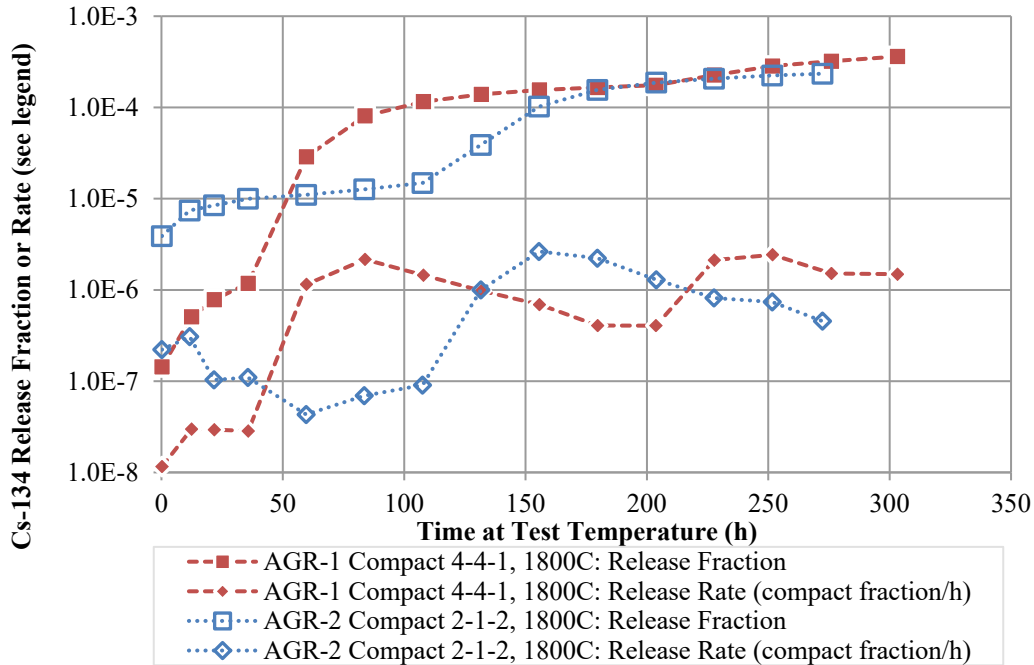


Figure 30. Release fractions and release rates for AGR-1 Compact 4-4-1 and AGR-2 Compact 2-2-1, at 1800°C. The AGR-1 Compact 4-4-1 test had two SiC failures, and the AGR-2 Compact 2-1-2 test had one SiC failure.

From each available safety test, regions of relatively steady Cs-134 release rate were used to establish average Cs-134 release rates for that test by fitting a line to the cumulative release vs time data points. Figure 31 gives an example of how this was done for two 1600°C tests with no SiC or TRISO failures. These types of tests give the clearest indication of Cs release at accident temperatures in the absence of degraded particles. The majority of safety tests were fit in this manner, including the Type 3—where multiple SiC or TRISO failures occurred and the time-dependent release from individual failures in individual particles could not be resolved—and Type 2 tests—where SiC or TRISO failure occurs during the rise to test temperature or upon reaching the isothermal hold. As long as the second derivative of the cumulative release versus time was steady for a period, a linear fit tended to approximate the behavior well. The compacts that did not fit into this simple process include AGR-1 Compacts 4-3-2, 4-4-3, and 6-4-3 and AGR-2 Compacts 2-1-2, 2-3-2, 5-4-1, and 6-2-1. Furthermore, Cs-134 measured during the AGR-2 Compact 6-4-2 test was not considered here because it was determined that cross contamination from a preceding test affected this test (Stempien et al. 2021). Compacts with very low release rates often did not have measurable Cs-134 on at least some of the condensation plates or deposition cups. In these tests, an average release rate was estimated by taking the slope between the last data point of the initial release in the early phase of the test (typically about 30–50 h after reaching the isothermal hold) and the total release at the end of the test. This was done for AGR-1 Compacts 4-4-3 and 6-4-3 and AGR-2 Compact 2-3-2. Release rates from other tests were taken by fitting a line to areas away from the influence of particle failures. These included AGR-1 Compact 4-3-2 and AGR-2 Compacts 2-1-2, 5-4-1, and 6-2-1. In tests like AGR-1 Compact 4-3-2 and AGR-2 Compact 2-1-2, rates were fit before and after SiC failures.

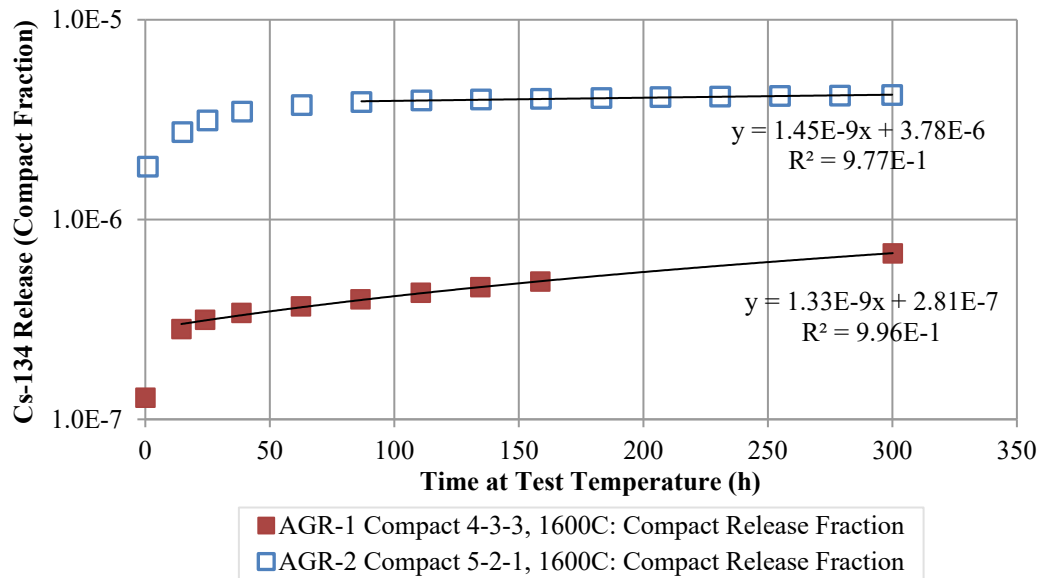


Figure 31. Compact release fraction versus time for two safety tests. Linear fits were made to relatively linear portions of the tests after the initial increase in release rate upon reaching the isothermal holds.

After establishing average Cs-134 release rates during the pseudo-steady-state period for each test during their isothermal holds, these rates were plotted versus inverse test temperature in Figure 32. Compacts with no layer failures were grouped separately from compacts that experienced one or more failures. Arrhenius equations were fit to each group. In the absence of SiC failures, the average compact cesium release rates are low (generally $<1E-8$ compact fraction/h). When SiC failures do occur, cesium release rates may be up to about four orders of magnitude higher for a period of time. The data set made up of results from tests with failed SiC and failed TRISO particles includes failure statistics embedded in the release rates.

The maximum release rate from each test was also plotted versus inverse temperature in Figure 32. Typically, the maximum release rate persists for 12–48 h and is commonly about 5–50 times greater than the pseudo-steady-state average for tests with no SiC (or TRISO) failures and roughly 2–30 times greater for tests with one or more SiC (or TRISO) failures). In tests with no SiC (or TRISO) failure, the maximum release rate tends to occur as the isothermal hold is reached (about 30 total hours into the test). In tests with SiC or TRISO failures, the maximum rate occurs a little later (about 15 h into the isothermal hold on average).

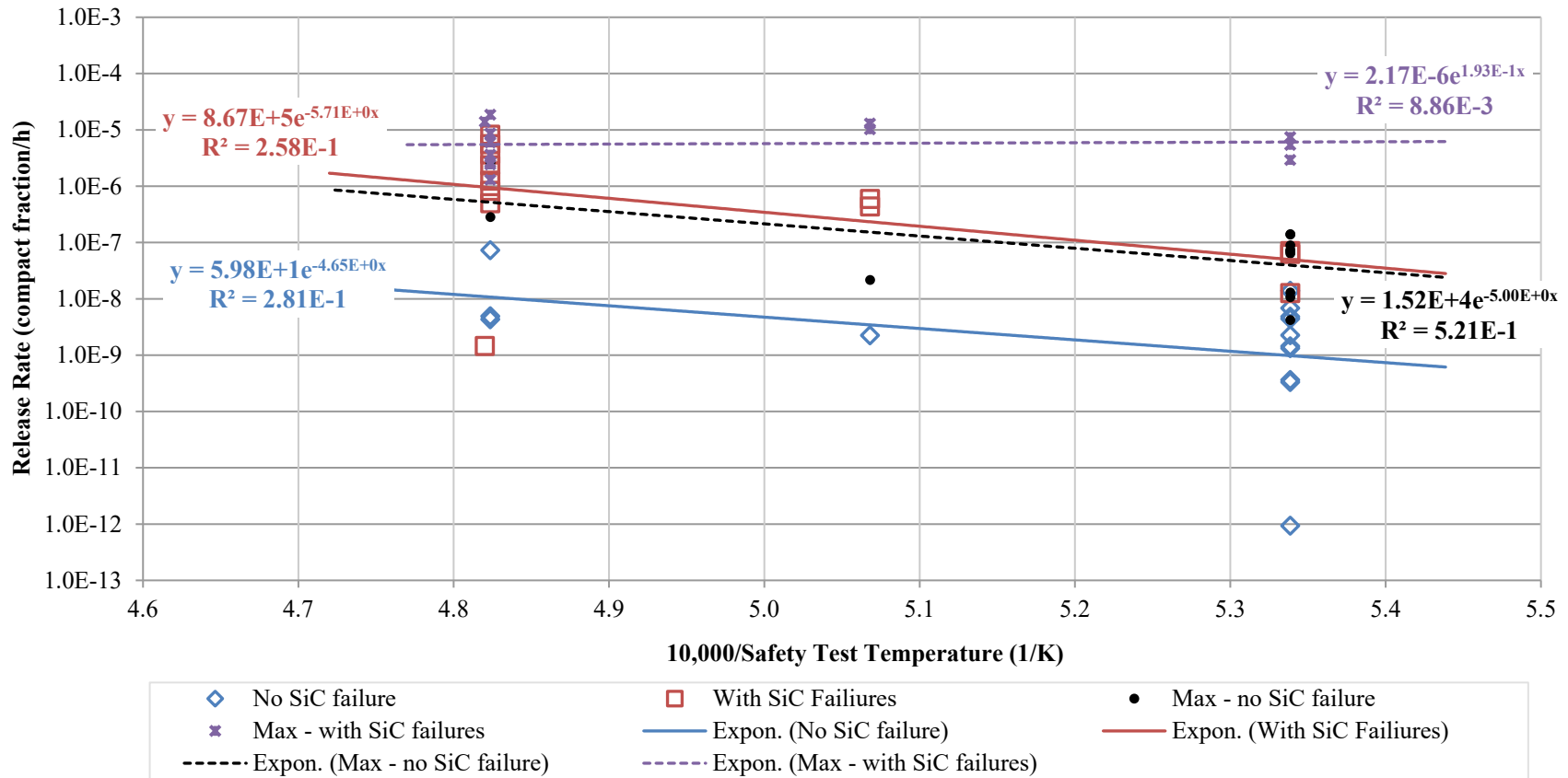


Figure 32. Average pseudo-steady-state release rates of Cs-134 from AGR-2 and 1 fuel compacts subjected to safety testing at temperatures of 1600, 1700, and 1800°C at INL and ORNL. The maximum release rate from the entirety of each test is also plotted.

4.5.2 Ag-110m Safety-Test Release Rates

A process similar to that used to establish average Cs-134 release rates during isothermal holds was used here for Ag-110m. Lines were fit to the cumulative Ag-110m release-versus-time data points for each test, and the slopes were used as the average rate during the isothermal hold for each test. Figure 33 uses AGR-1 Compact 4-1-2 as an example of a data set for which this process was successful. In the majority of the AGR-1 and 2 safety-test data sets, the data points after 35 h at the isothermal hold and beyond were fit with a line to give a rate. For the majority of safety tests, the initially high Ag-110m release rate characteristic of these tests during heating and upon first reaching the isothermal hold had decreased and become steadier after 35–50 h at the hold temperature.

The instances where this approach did not work were the following: the 1700°C test of AGR-1 Compact 5-1-1 and the 1800°C tests of AGR-2 Compacts 5-4-1, 6-2-1, and 6-4-3. To show why a different approach was needed for these tests, the cumulative Ag-110m release and release rate (calculated from the slope between adjacent points) is plotted for the 1800°C test of AGR-2 Compact 6-4-3 in Figure 33 where the rate of Ag-110m release increased with time as the test went on. In these cases, the slope between a point between 35 and 50 h at the isothermal hold and the last point in the test for which the cumulative Ag-110m increased was used to represent the average rate at the test temperature.

In Figure 34, the pseudo-steady-state rates from each test were plotted versus inverse safety-test temperature and fit with exponential functions. Figure 34 has five data series, and in the first three, one is for safety tests where there was one or more SiC failures, one for safety tests with no SiC and no TRISO failures, and one where all data were grouped. There is no meaningful difference between these series, which corroborates the conclusions made in earlier sections of this report that Ag-110m may significantly transport through intact TRISO coatings; thus, the Ag-110m release behavior at high temperatures is much-less dependent on the integrity of the coatings than the Cs-134 release behavior. The fourth series plots the local maximum rate within the time interval of the test used to establish the pseudo-steady-state test average. An exponential function was also fit to this data set to give an even more conservative (higher) release-rate estimate. The fifth series shows that the maximum rate may be considerably higher than the pseudo-steady-state average. This maximum rate is only a little higher for the 1800°C than it is for 1600°C tests. Generally, the maximum rate persists for about 12–24 h upon the rise to test temperature, and then it drops off. The only cases where the Ag-110m rate increased as a test proceeded were 1800°C tests of AGR-1 Variant 3 fuel and AGR-2 fuel. Figure 35 shows the pseudo-steady-state average release rates for AGR-1 fuel, AGR-1 Variant 3 fuel, and all other AGR-1 fuel types besides Variant 3. The fine-grain SiC in the AGR-1 Variant 3 fuel exhibits the highest release rates, followed by AGR-2 (which had SiC fabricated under similar process to AGR-1 Variant 3). The other AGR-1 types had the lowest Ag-110m release rates. For a given safety-test temperature, the release rate during a safety test did not seem to be dependent on prior irradiation temperature or burnup.

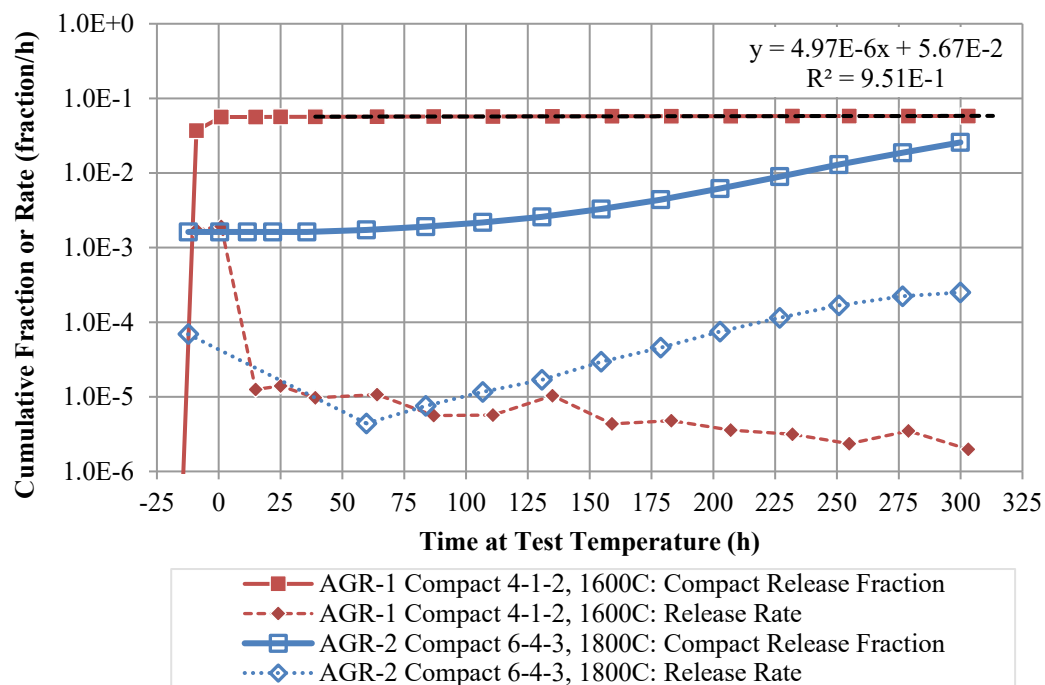


Figure 33. Cumulative fractional release of Ag-110m and release rates (calculated as the slopes between adjacent cumulative releases) for two compacts.

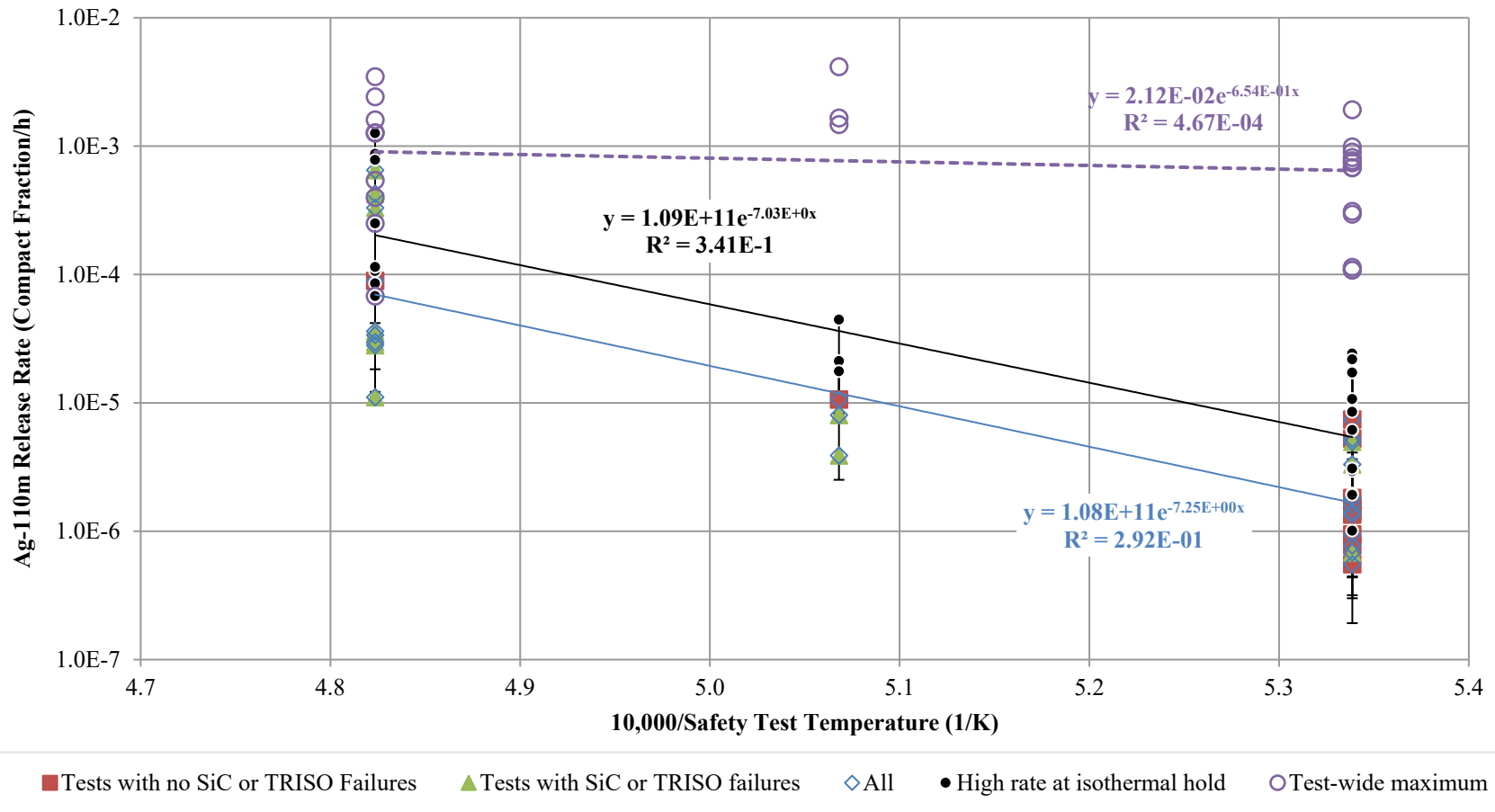


Figure 34. Pseudo-steady-state release rates of Ag-110m from AGR-2 and AGR-1 fuel compacts subjected to safety testing at temperatures of 1600, 1700, and 1800°C at INL and ORNL. Error bars represent the maximum and minimum release rates over the safety-test time interval used to generate the average rate from each test. Local maxima from the time interval used to generate the pseudo-steady-state averages are plotted. The global maximum from each test is also plotted.

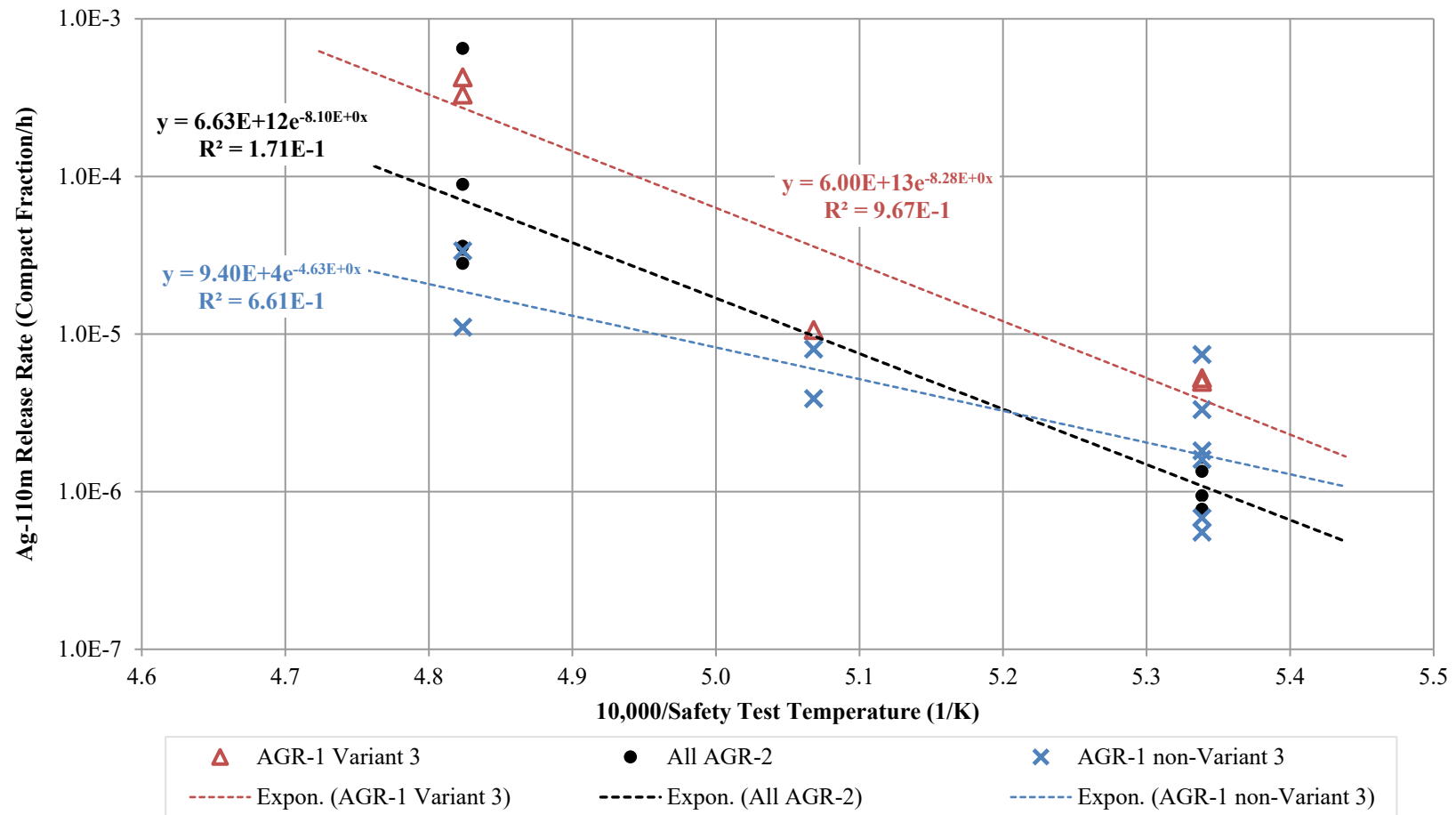


Figure 35. Pseudo-steady-state release rate of Ag-110m from AGR-2 and AGR-1 fuel compacts subjected to safety testing at temperatures of 1600, 1700, and 1800°C at INL and ORNL. Data are grouped for AGR-1 Variant 3 only, all AGR-2, and all non-Variant 3 AGR-1 fuel.

4.5.3 Eu-154 Safety Test Release Rates

The strategy employed to establish average Eu-154 release rates is similar to that used for Cs-134. After the high release rates during the earlier parts of a test as the temperature is being raised, linear fits to the cumulative release-versus-time curves were made. Typically, this was done for total elapsed times from about 100 h to the end of the test at about 330 h. This corresponds to fitting to the data points from about 70 h to 300 h of the isothermal hold. In some cases, particularly when the test temperature was 1800°C, the linearity in the cumulative release-versus-time curves was reached earlier (after perhaps 10–40 h at the isothermal hold), and fits from that point in time to the end of the test were made.

Figure 36 shows three examples of fits made to AGR-1 and 2 data. In the 1600°C test of AGR-1 Compact 5-3-3, there were no SiC or TRISO failures, and a single linear fit was made from the data point at 94 h to the end of the test at 334 h. In the 1800°C test of AGR-1 Compact 4-4-1, there were two SiC failures. The first occurred after about 71 h of total elapsed time, and the second occurred after about 239 h. Given the total release of Eu-154 from Compact 4-4-1 was already about 1 particle-equivalent inventory by 57 h and 15 particle-equivalent inventories by 239 h, any clear effect of the SiC failures on the Eu-154 release rates is imperceptible in Figure 36. Two fits were made to the Compact 4-4-1 data set, one in the earlier phase of the test from 95 to 191 h and another from 215 to 339 h. The difference between the two rates is about a factor of six, and the larger of the two was taken as the conservative average for the test. The Eu-154 data from the 1800°C test of AGR-1 Compact 4-3-2 received similar treatment. The increase in rate later in a test was observed with 1800°C tests of AGR-1 Variant 3 fuel (e.g., Compact 4-4-1 and 4-3-2) and in the 1800°C test of AGR-2 Compact 5-4-1. The third example in Figure 36 is the AGR-2 Compact 2-1-2 1800°C test where there was little change in the Eu-154 release rate after 50 h of total elapsed time, and no apparent influence from the SiC failure at 167 h. In this case, a linear fit was applied from 47 to 309 h.

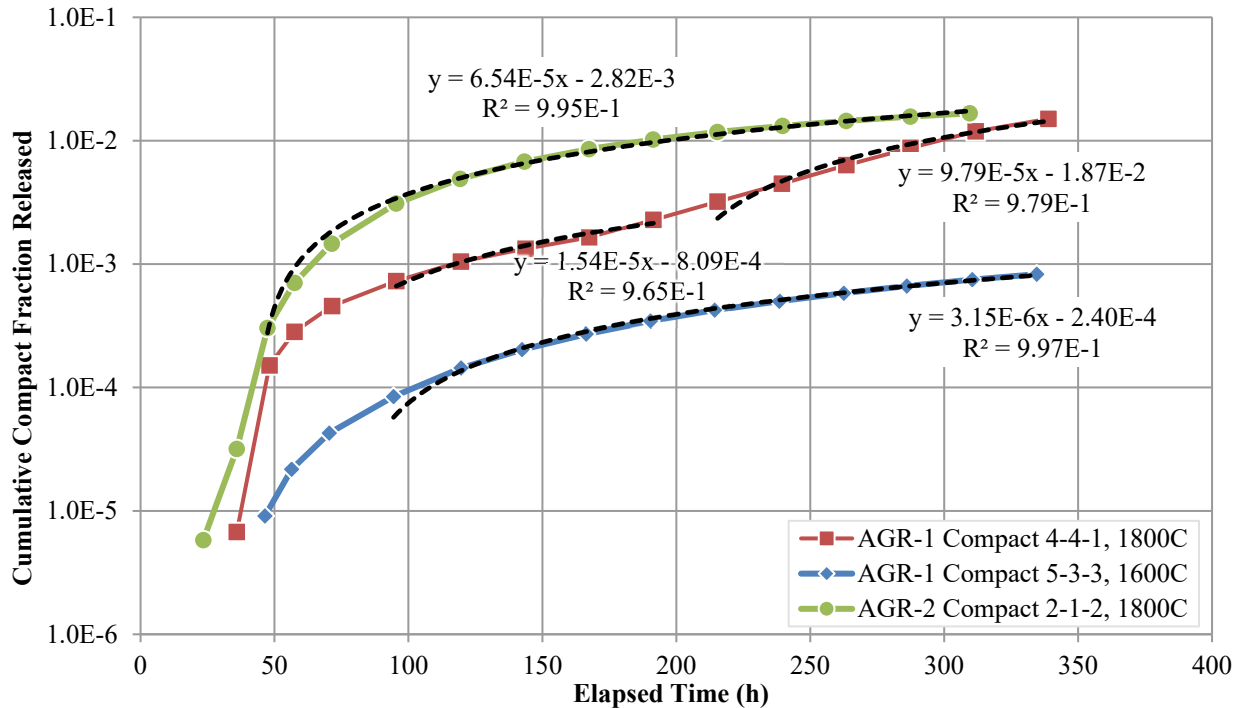


Figure 36. Examples of Eu-154 release vs time data from three different safety tests and the linear fits applied to establish average rates of release.

Unlike Ag-110m, for instance, the release rates of Eu-154 during safety testing have some dependence on the irradiation temperature of the compacts prior to the safety test. Figure 37 shows the pseudo-steady-state Eu-154 release rates from 1600°C AGR-1 and AGR-2 safety test versus the compact irradiation temperature. Data were grouped according to whether SiC or TRISO failures occurred. Here there is a tendency for the release rate to be higher during a safety test with higher irradiation temperature. This shows that at 1600°C, most of the release of Eu-154 during a safety test is from inventory that diffused through intact fuel particles and was retained in the compact matrix during irradiation in the Advanced Test Reactor (ATR). This plot also shows that there is a little impact from SiC layer failures. The data are few, but on average, fuel with SiC failures that was irradiated between 1000 and 1050°C has a slightly higher release rate than fuel with the same irradiation temperature and no SiC failure.

Figure 38 shows the pseudo-steady state Eu-154 release rates for 1700 and 1800°C tests of AGR-1 and AGR-2 fuel versus the compact TAVA irradiation temperature. Here it seems the tendency for release rates to increase with increasing irradiation temperature is weaker than it was at 1600°C in Figure 37. If the data point in Figure 38 for AGR-2 Compact 2-3-2 at a TAVA temperature of 1296°C were to be removed, there would be no apparent dependence on irradiation temperature. This suggests that the higher safety test temperature may elicit diffusive release from fuel particles to an extent that makes the contribution of the OPyC and matrix inventory to the safety-test release less dominant at 1800°C. Additionally, at these higher safety test temperatures, there are insufficient data to conclude that small quantities of SiC failures noticeably alter the release rate from the compact.

Figure 39 shows a plot of the pseudo-steady state average Eu-154 release rates versus inverse safety test temperature. Figure 37 showed a small difference between the rates for 1600°C safety tests with and without SiC failures. Figure 38 showed there are insufficient data to assert a difference in Eu-154 release rates with and without SiC failures. Since there is little difference in the Eu-154 release rate with and without SiC failure, data were only grouped based on the TAVA irradiation temperature of the fuel compacts in Figure 39. One series combines all the data regardless of compact irradiation history and in-safety test SiC failure status. A second series combines data from all compacts with TAVA irradiation temperatures <1200°C, and the third series is composed only of safety-test results from compacts with irradiation temperatures >1200°C (i.e., AGR-2 Capsule 2 compacts). Thus, these groupings implicitly include the effects (however small) of the SiC and TRISO failure rates. Figure 39 shows that there appears to be a threshold where safety tests (especially 1600°C safety tests) of compacts that were irradiated at TAVA temperatures >1200°C have distinctly higher release rates than those from compacts irradiated at TAVA temperatures <1200°C. The reason this hotter fuel has higher rates was illustrated in Figure 25 where the rate of Eu-154 accumulation in the OPyC and fuel compact matrix increases with temperature and accelerates dramatically above 1200°C. An exponential fit through the results from safety tests of compacts with irradiation temperatures >1200°C is shown mostly as a visual aid. Given the available data, the Eu-154 release rate for a 1600-1800°C safety test of fuel similar to AGR-2 Capsule 2 fuel would be about 3E-4/h.

The maximum release rate during all the test has also been plotted in Figure 39. The average ratio of the pseudo-steady state Eu-154 release rate to the maximum release rate is 2.1 ± 2.2 , and the median ratio is 1.29. The tests where the maximum-to-average release rate ratios were largest were those conducted at 1800°C. Comparing the exponential functions fit to the averages over all tests and the maximum from each test reveals the averages are not much smaller than the maxima. The maximum release rates are reached after about 150 h at the isothermal hold, and they tend to persist for 100 h.

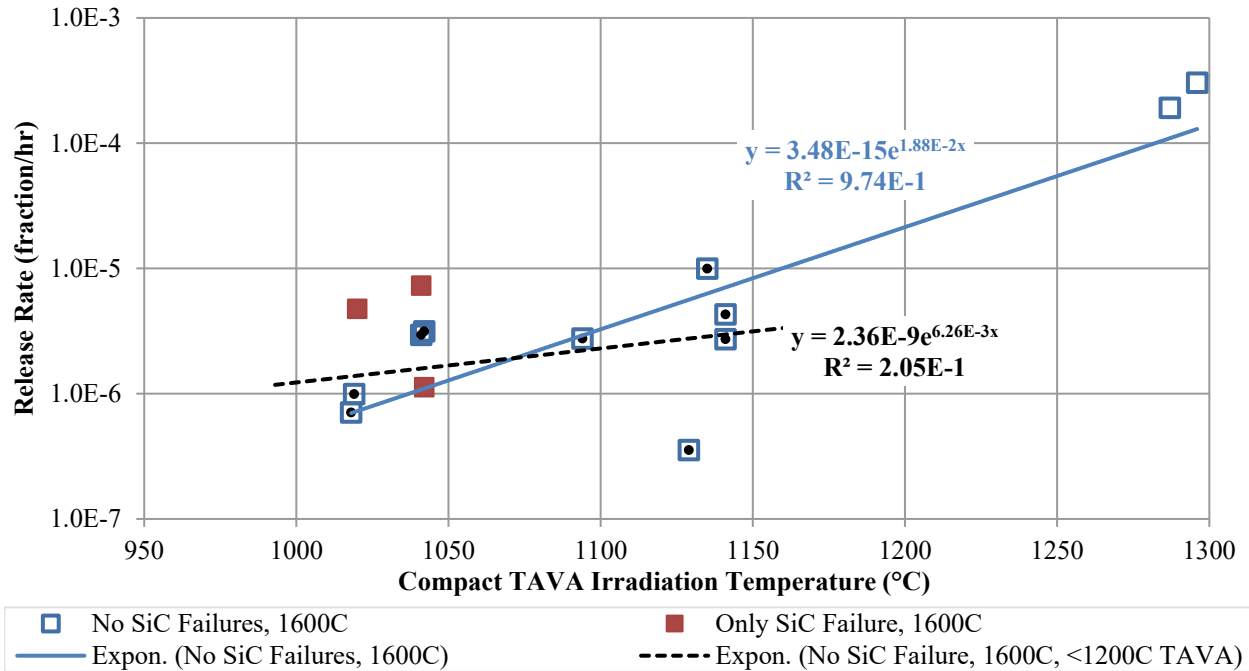


Figure 37. Eu-154 pseudo-steady-state release rates from 1600°C AGR-1 and AGR-2 safety tests versus compact TAVA irradiation temperature. Note that here any kind of failure that involves SiC failure is called “SiC” failure. A particle with a TRISO failure would be included as one with a SiC failure here. The exponential fit shown in black is the fit if fuel with TAVA > 1200°C is neglected.

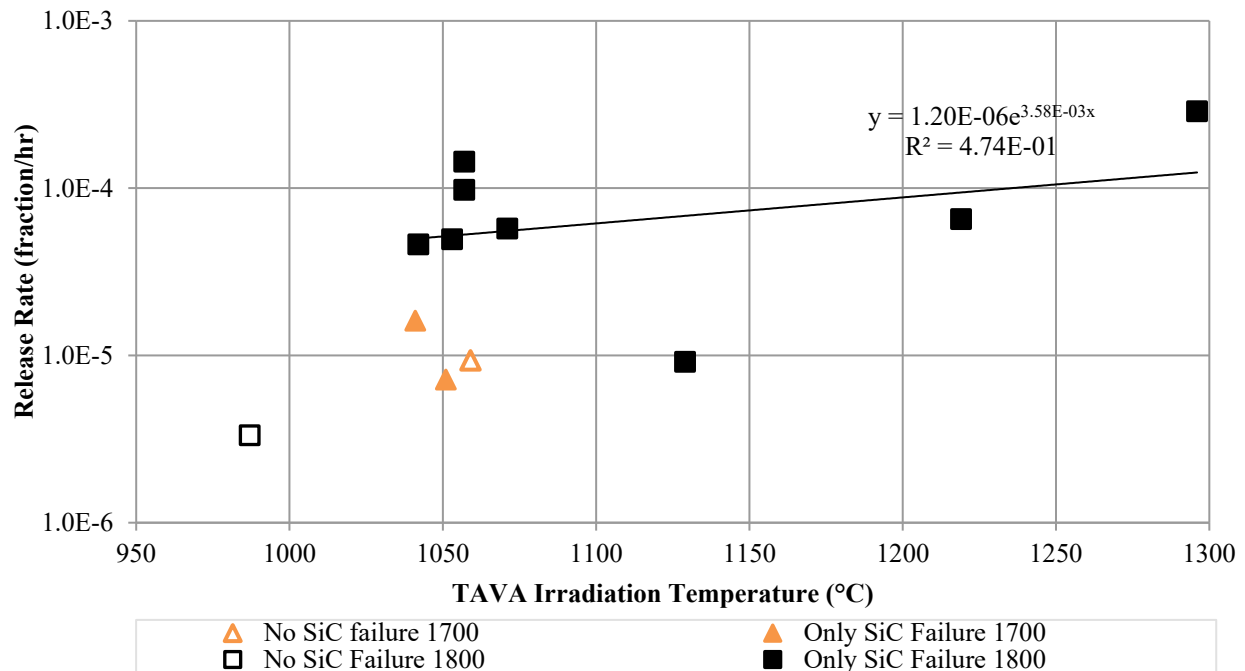


Figure 38. Eu-154 pseudo-steady-state release rates from 1700 and 1800°C AGR-1 and AGR-2 safety tests versus compact TAVA irradiation temperature. Any kind of failure that involves a SiC failure is called “SiC” failure here (including TRISO failures).

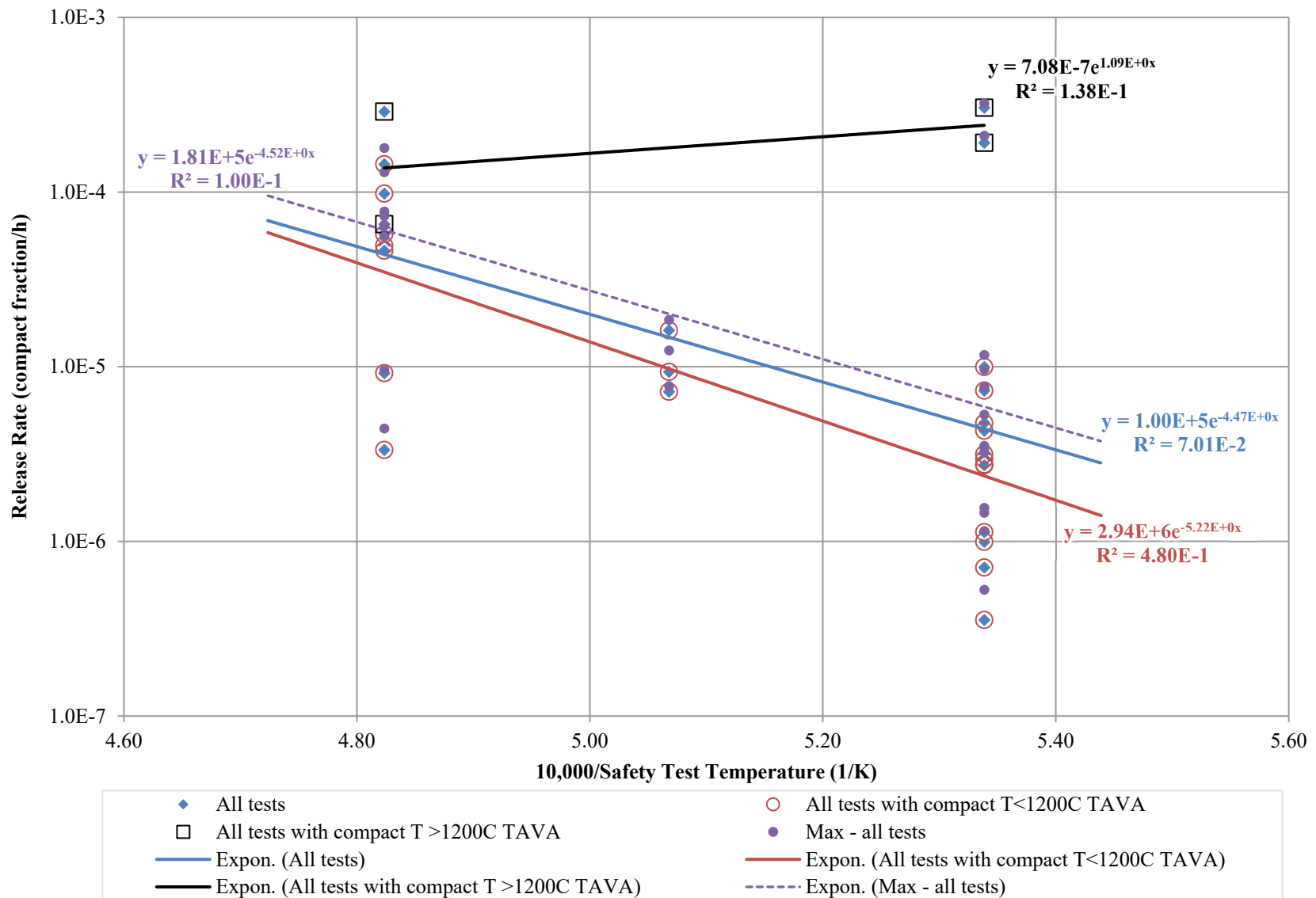


Figure 39. Pseudo-steady state Eu-154 release rates versus inverse safety test temperatures including exponential fits for different groupings of compacts based on TAVA temperature. Maximum rates from each test are also plotted.

4.5.4 Sr-90 Safety Test Release Rates

The methodology used to get Sr-90 release rates during the isothermal hold for the AGR-1 and AGR-2 compacts was nearly identical to that used for Eu-154. After the high release rates during the earlier parts of a test, as the temperature is being raised, linear fits to the cumulative release-versus-time curves were made. Typically, this was done for total elapsed times from about 100 h to the end of the test at about 330 h. This corresponds to fitting to the data points from about 70 to 300 h of the isothermal hold. In some cases, particularly when the test temperature was 1800°C, the linearity in the cumulative release-versus-time curves was reached earlier (after perhaps 10 to 40 h at the isothermal hold), and fits from that point in time to the end of the test were made.

Figure 40 gives examples of fits made to AGR-1 and AGR-2 data. In the 1600°C test of AGR-1 Compact 5-3-3, there were no SiC or TRISO failures, and a single linear fit was made from the data point at 94 h to the end of the test at 334 h. In the 1800°C test of AGR-1 Compact 4-4-1, there were two SiC failures. The first occurred after about 71 h of total elapsed time, and the second occurred after about 239 h. Given the total release of Eu-154 from Compact 4-4-1 was already about 70% of a particle equivalent inventory by 57 h and 12 particle equivalent inventories by 239 h, any obvious effect of the SiC failures on the Eu-154 release rates is imperceptible in Figure 36. Similar to the AGR-1 Compact 4-4-1 Eu-154 behavior shown in Figure 36, there is a change in the Sr-90 release rate at about the 200-h mark. Here again, two fits were also made to the Compact 4-4-1 Sr-90 data set: one in the earlier phase of the test from 95 to 191 h and another from 215 to 339 h. The difference between the two rates is about a factor of seven, and the larger of the two was taken as the conservative average for the test. The Sr-90 data from the 1800°C test of AGR-1 Compact 4-3-2 received similar treatment. The increase in Sr-90 and Eu-154 release rates later on in a test was observed with 1800°C tests of AGR-1 Variant 3 fuel (e.g., Compact 4-4-1 and 4-3-2) and in the 1800°C test of AGR-2 Compact 5-4-1.

The third example in Figure 40 is the AGR-2 Compact 2-1-2 1800°C test where a SiC failure occurred after about 167 h of total elapsed time; however, the impact of the SiC failure was not apparent in the Sr-90 release rate versus time plot. In this case, a linear fit was applied from 119 to 309 h. Other cases like these three existed among the data, and similar approaches were taken for those.

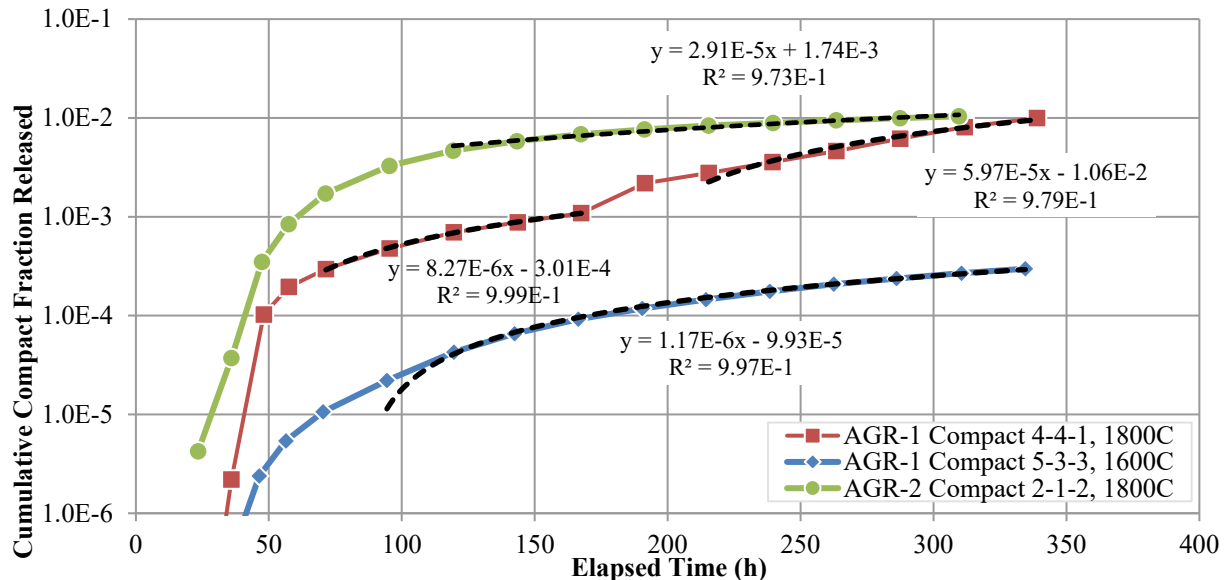


Figure 40. Examples of Sr-90 release vs time data from three different safety tests and the linear fits applied to establish average release rates at the isothermal holds.

In a few cases, the starting and ending points used for the Sr-90 fits were different by one or two deposition-cup or condensation-plate changes from those used for Eu-154. The biggest difference between the points used for Sr-90 and those used for Eu-154 was for the 1800°C test of AGR-2 Compact 6-4-3 where the points at ~50–250 h of elapsed time were used for Sr-90 compared to those from ~50–340 h for Eu-154. Figure 41 shows the time-dependent releases and the release rates for the 1600°C safety test of AGR-1 Compact 6-4-3 and the 1800°C safety test of AGR-2 Compact 6-4-3.

These tests were unique in that they had some of the lowest total fractional releases of Sr-90 and the lowest Sr-90:Eu-154 ratios. From all AGR-1 and 2 safety tests, the average ratio of the Sr-90 release fraction to the Eu-154 release fraction was 0.51. The AGR-1 Compact 6-4-3 Sr-90:Eu-154 ratio was 0.008, and that ratio was 0.06 for AGR-2 Compact 6-4-3.^f The 1600°C test of AGR-1 Compact 6-4-3 was the only 1600°C test to have an increase in the Sr-90 release rate toward the end of the test. AGR-1 Compact 6-4-3 had among the lowest burnup and irradiation temperature from AGR-1 and it was held for 400 h at 1600°C (100 h longer than any other compact). The increase in its Sr-90 release rate occurred after about 350 h of total elapsed time, after all the 300 h isothermal holds would have already ended. Thus, the longer hold time of this test and the overall low release fraction allowed this small increase in release rate to be observed at the end of the test. AGR-2 Compact 6-4-3 had the lowest irradiation temperature and, by far, the lowest burnup of all AGR-1 and AGR-2 compacts safety tested. In these two instances, the higher rates were used as conservative estimates of the average rate when compiling rates from all the tests into Figure 42, Figure 43, and Figure 44. The higher release rates at the ends of these two tests could be useful in investigating diffusivities.

Figure 42 shows the pseudo-steady-state Sr-90 release rates from each AGR-1 and AGR-2 1600°C safety test versus the compact-irradiation temperature. Data were grouped according to whether SiC or TRISO failures occurred. There is a tendency for the release rate to be higher during a safety test with higher irradiation temperature. This suggests that at 1600°C, most of the release of Sr-90 during a safety test is from inventory that diffused through intact fuel particles and was retained in the compact matrix during irradiation in ATR. That is why the compacts with the higher TAVA temperatures had higher release rates. This plot does not show evidence of any meaningful difference in the Sr-90 release rate with or without a SiC (or TRISO) failure.

Figure 43 shows the pseudo-steady-state Sr-90 release rates for 1700 and 1800°C tests of AGR-1 and AGR-2 fuel versus the compact TAVA irradiation temperature. At 1600°C, there was a little evidence that the release rate increases with increasing irradiation temperature. There is no such evidence when the safety-test temperatures are 1700 and 1800°C. This suggests that the higher safety-test temperature may elicit diffusive release from fuel particles to an extent that makes the OPyC and matrix inventory less dominant at 1800°C. Additionally, at these higher safety-test temperatures, there are insufficient data to conclude that small quantities of SiC failures noticeably alter the release rate from the compact.

^f Note that AGR-1 Compact 6-4-1 had a Sr-90:Eu-154 ratio of 0.09. Its total fractional release of Eu-154 was about average for AGR-1, and its Sr-90 release was on the low end. However, that Sr-90 fraction was similar to or greater than a couple other AGR-1 compacts.

Figure 44 shows a plot of the pseudo-steady-state Sr-90 release rates versus inverse safety-test temperature. As with Eu-154, this plot for Sr-90 shows an irradiation temperature threshold where compacts that were irradiated at TAVA temperatures $>1200^{\circ}\text{C}$ have distinctly higher release rates during safety tests (especially during 1600°C safety tests) than those from compacts irradiated at TAVA temperatures $<1200^{\circ}\text{C}$. Figure 42 and Figure 43 showed little compelling evidence that fuel compacts with SiC failures had higher Sr-90 release rates. Thus, the data in Figure 44 were only grouped based on the TAVA irradiation temperature and without regard to SiC or TRISO failures. One series combines all the data regardless of compact irradiation history and in-safety test SiC failure status. A second series combines data from all compacts with TAVA irradiation temperatures $<1200^{\circ}\text{C}$, and the third series is composed only of safety-test results from compacts with irradiation temperatures $>1200^{\circ}\text{C}$ (i.e., AGR-2 Capsule 2 compacts).

The fourth data series in Figure 44 is a plot of the maximum Sr-90 release rate during all the tests as a function of inverse test temperature. An exponential function was also fit to this series to give a conservative estimate of the Sr-90 release for comparison to the average pseudo-steady state Sr-90 release rates. The average ratio of the pseudo-steady state Sr-90 release rate to the maximum release rate is 7.2 ± 18 , and the median ratio is 2.03. The tests where the maximum-to-average release rate ratios were largest were those conducted at 1800°C . Comparing the exponential functions fit to the averages over all tests and the maximum from each test reveals the averages are not much smaller than the maxima, especially for the 1600°C tests. The maximum release rates are reached after about 130 h at the isothermal hold, and they tend to persist for about 120 h.

As with Eu-154, the Sr-90 data available from AGR-1 and 2, suggest that fuel irradiated at TAVA temperatures $>1200^{\circ}\text{C}$ needs to be considered separately from fuel irradiated at cooler temperatures (especially for 1600°C safety tests). The reason this hotter fuel has higher rates was illustrated in Figure 26 where the rate of Sr-90 accumulation in the OPyC and fuel-compact matrix increases with temperature and accelerates dramatically above 1200°C .

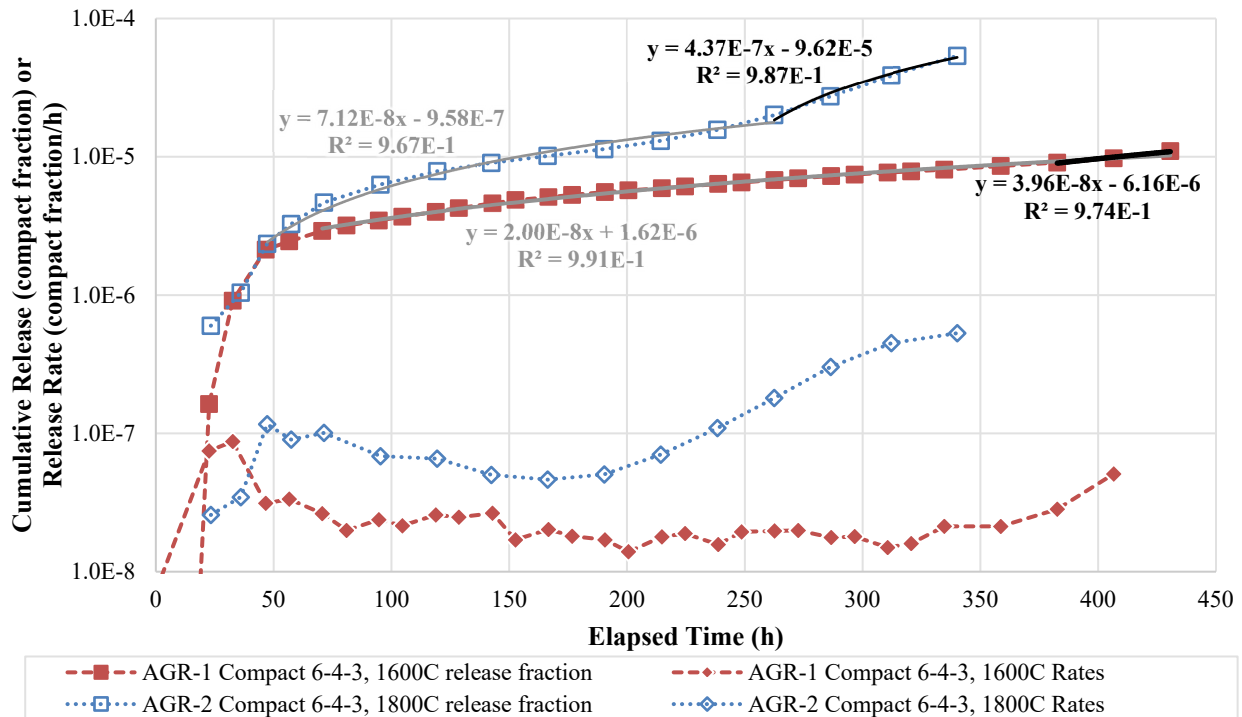


Figure 41. Cumulative fractional release and release rates for unique tests with late increases in Sr-90 release rate.

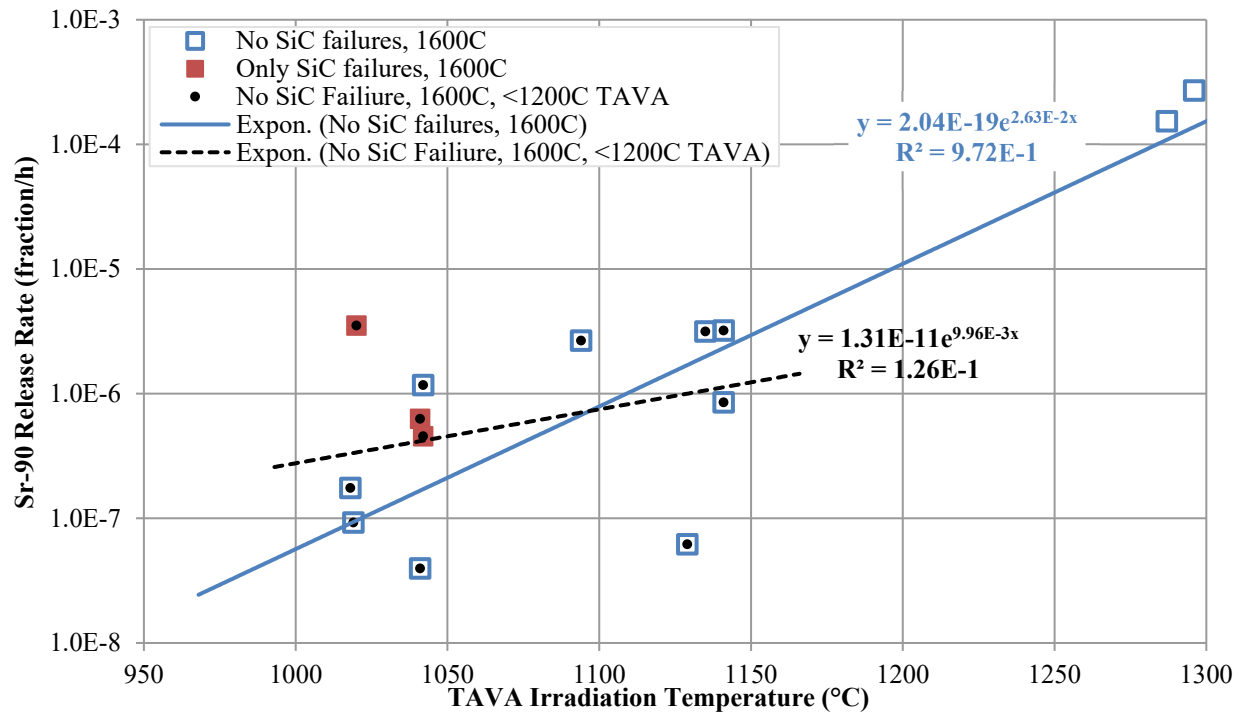


Figure 42. Sr-90 pseudo-steady-state release rates from AGR-1 and 2 safety tests versus compact TAVA irradiation temperature. Here any kind of failure that involves SiC failure is called SiC failure. Thus, a particle with a TRISO failure would be included as one with a SiC failure here.

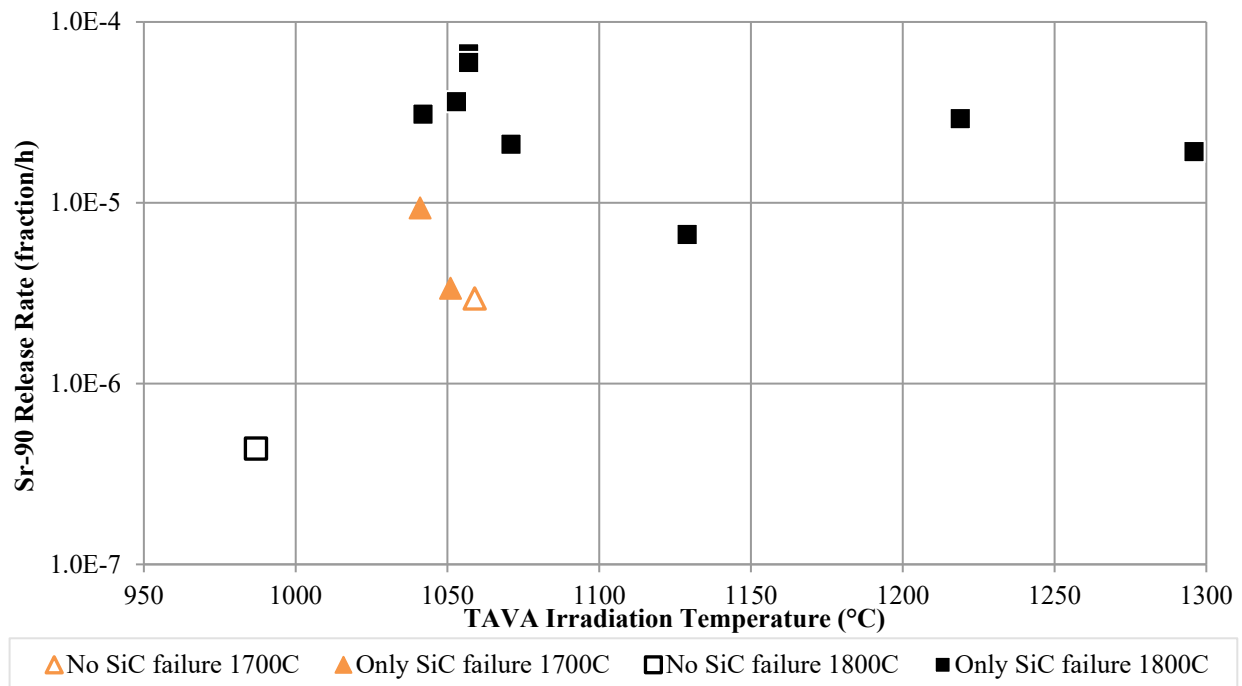


Figure 43. Pseudo-steady-state Sr-90 release rates from 1700 and 1800°C AGR-1 and 2 safety tests versus compact TAVA irradiation temperature. Any kind of failure that involves a SiC failure—including TRISO failures—is called SiC failure here.

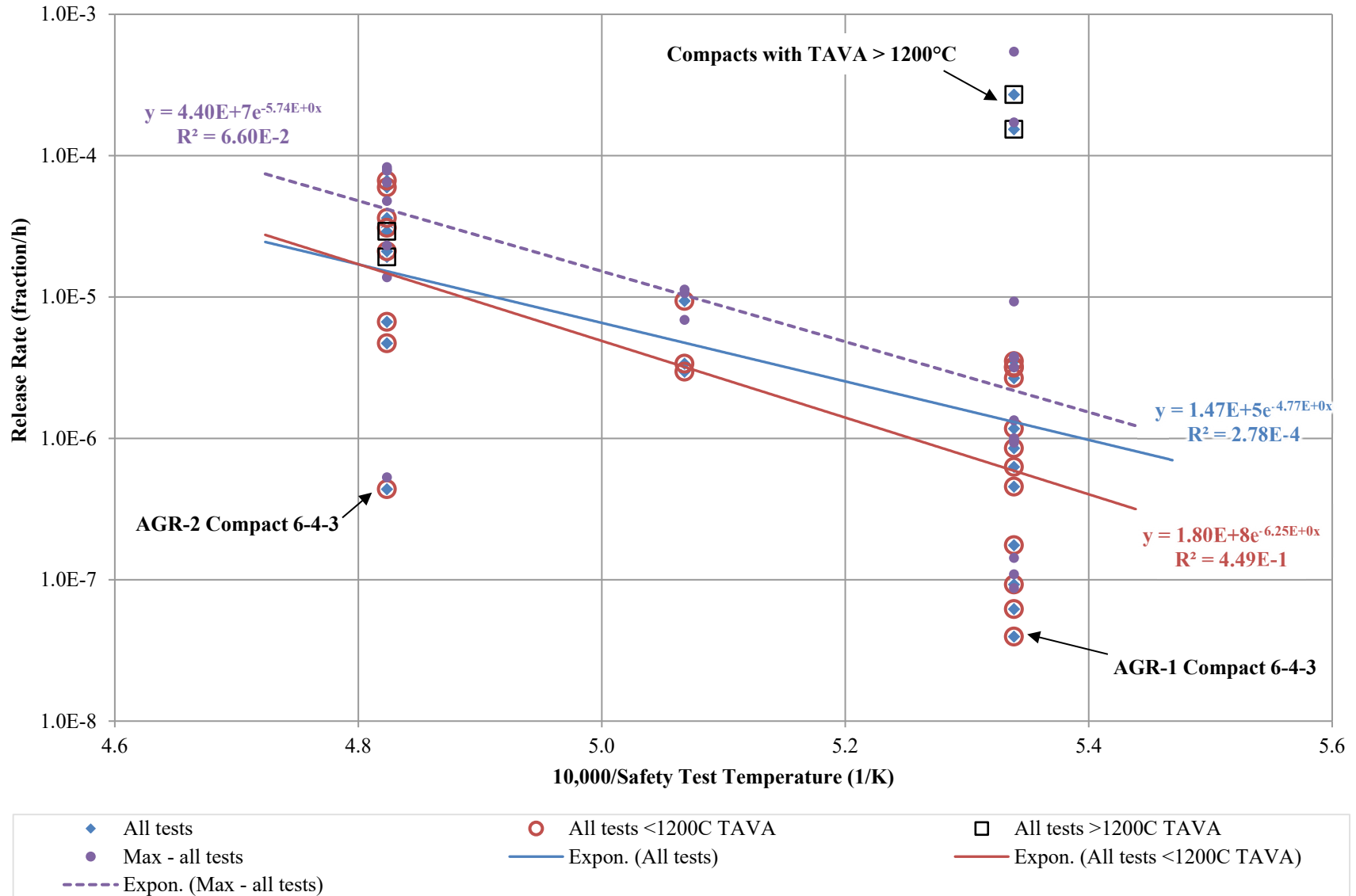


Figure 44. Sr-90 pseudo-steady-state release rates versus inverse safety-test temperatures, including exponential fits for compacts with irradiation temperatures > or < 1200°C. The maximum release rate from each test is also plotted.

5. SUMMARY AND CONCLUSIONS

Knowledge of fission-product retention in and release from TRISO fuel under normal and off-normal conditions is needed for reactor-safety analyses. This is important for coated-particle fuel used in high-temperature reactors relying on the functional containment strategy. Data on the release and retention of key fission products (e.g., Ag-110m, Cs-134, Eu-154, and Sr-90) in AGR UCO TRISO fuels have been summarized in this report, and empirical relationships with respect to time and temperature were developed. This included fission-product accumulation in the OPyC and compact graphitic matrix during irradiation, release from compacts during irradiation, and release during post-irradiation safety testing at temperatures from 1600–1800°C. The frequencies of SiC failure and TRISO coating failure from irradiation and post-irradiation safety testing were also summarized because they have bearing on the quantities of Cs release from the fuel. In a forthcoming publication, a framework for combining and using these empirical relationships as part of a source-term analysis will be presented.

The compact matrix is an important part of the coated-particle fuel system and has been shown to retain some fission products that may have diffused out of the particles. The type of matrix in the AGR-1, 2, and 3/4 fuel compacts is similar to the A3-3 formulation historically referred to as the German TRISO program's reference matrix. Data collected from DLBL were used to determine the fission-product inventory in the compact matrix and particle OPyC layers (outside of the SiC layer) as a function of irradiation conditions. An effective rate of fission-product accumulation in the compact matrix during irradiation was estimated by dividing the EOI DLBL inventories by the EFPD of the irradiation and the EOI burnup of the compacts. This gives the rate of fission-product accumulation in the matrix as a function of time and burnup. Burnup was included here because AGR irradiations were accelerated compared to typical power-reactor burnup rates.

Looking at all the components other than the fuel compacts themselves (i.e., the mass balance) enabled a determination of the fission-product inventory that migrated out of the compacts during irradiation. Here the EOI fission-product inventories measured on capsule components were normalized by irradiation time and burnup. This gave an average release rate over the duration of irradiation that took differences in burnup rate into account. These rates were then plotted versus inverse temperature, and exponential fits were applied. Data from all AGR capsules except the UO₂ capsule from AGR-2 and the unopened fuel bodies from AGR-3/4 were combined in this analysis. If desired, the fission-product release rates through the SiC layer in the particles could be estimated by adding the matrix accumulation rates derived from DLBL results to the compact release rates derived from the mass-balance results.

Both isothermal and temperature-transient safety tests were conducted on fuel compacts after irradiation at INL and ORNL. Isothermal tests of UCO fuel were conducted at 1600, 1700, and 1800°C. Two transient tests mimicking a core-conduction cooldown event with a peak temperature of 1695°C were conducted via simultaneous heating of three AGR-1 compacts at INL and three AGR-2 compacts at ORNL. From the perspective of time-at-temperature, the high-temperature (1600–1800°C) isothermal tests lasting 300 h are more severe than actual core-conduction cool-down events in traditional HTGRs. In the AGR-1 and 2 transient tests, no SiC or TRISO failures were observed, indicating the temperature transient did not impose additional stress on UCO fuel beyond that demonstrated in the isothermal heating tests. In fact, the temperature variations during the AGR-1 transient-temperature heating test caused less release of Cs-134, Eu-154, and Sr-90 than in the AGR-1 300-h 1600°C isothermal tests. In AGR-2, the Eu-154 and Sr-90 releases were lower than comparable AGR-2 300-h isothermal tests at 1600°C, and the Ag-110m release was similar to other AGR-2 isothermal tests.

The results from all AGR-1 and 2 isothermal tests were compiled and rates of release were determined for each test for Ag-110m, Cs-134, Eu-154, and Sr-90 as a function of test temperature. After the safety-test isothermal holds were achieved, and the typically higher initial rates of release early in the tests had subsided, pseudo-steady-state release rates were determined. The maximum rates for each key nuclide in each test were also determined and compared to the pseudo-steady-state release rates. The biggest differences between the maximum and pseudo-steady-state release rates were seen for Ag-110m in tests with isothermal-hold temperatures $<1800^{\circ}\text{C}$. Under these conditions, the ratio of the maximum rate to the pseudo-steady-state rate was up to about a factor of 100. The difference between the maximum rate and the pseudo-steady-state rate for Cs-134 was on the order of a factor of 10. For Sr-90 and Eu-154, the difference between the maximum release rate and the pseudo-steady-state rate tended to be about 15–25% for the 1600°C tests, and on average a factor of 2–15 for Eu and Sr, respectively, for tests at 1700 and 1800°C .

The Cs-134 pseudo-steady state release rates showed some dependence on safety-test temperature. Of the key fission products considered here, those for Cs were the most dependent on the integrity of the SiC layer. In the absence of particles with failed SiC layers, Cs releases originated with dispersed uranium in the compact matrix from fabrication. In the relatively few tests with observed SiC or TRISO failures, it was those failures that dominated the Cs release, and it was shown that those failures increase with increasing safety-test temperature as well.

A key determinant in the safety-test releases of Eu-154 and Sr-90 was the inventory that had been released through intact TRISO particles during irradiation that was retained in the compact matrix and particle OPyC layers after irradiation. The Sr-90 releases paralleled the Eu-154 releases, though at about 50% of the total Eu-154 release. The release rates of Sr-90 and Eu-154 during safety testing increased with increasing irradiation temperature of the compacts. Fuel compacts with higher irradiation temperatures ($\geq 1200^{\circ}\text{C}$) were shown to have especially high matrix inventories and, therefore, higher rates of release of Eu-154 and Sr-90 during the safety tests. SiC and TRISO failures had a mostly negligible impact on the rates. In AGR-1 and 2 fuel with lower irradiation temperatures ($\leq 1100^{\circ}\text{C}$), the matrix inventories of Sr-90 and Eu-154 may have been small enough that release from intact TRISO coatings could amount to a few percent of the relatively small total Eu and Sr releases from a safety test. This effect was small at 1600°C , but in 1800°C tests, the effect was more pronounced. In developing Eu-154 and Sr-90 release rates as a function of safety-test temperature, fuel with irradiation temperatures $\geq 1200^{\circ}\text{C}$ should be regarded separately from fuel with cooler irradiation temperatures.

The Ag-110m release behavior was characterized by rapid early release. In most safety tests at 1600°C , the majority of the Ag-110m is released during the rise to the isothermal hold or by 1 h into the hold. Some of this silver came from what had been released in-pile through intact TRISO coatings that was retained in the compact matrix material after irradiation, but some additional release through intact TRISO coatings also occurred. The phenomenon of Ag-110m release through intact TRISO coatings was particularly noticeable in the 1800°C tests of UCO compacts where the Ag-110m release had not leveled off after 300 h. Furthermore, AGR-1 Variant 3 fuel was shown to have the highest Ag-110m release rates of all AGR fuel types. This has been previously attributed to the relatively fine, equiaxed grains in the AGR-1 Variant 3 SiC layers. Ag-110m may significantly transport through intact TRISO coatings; thus, the Ag-110m release behavior at high temperatures was much less dependent on the integrity of the SiC coating than the Cs-134 release behavior.

6. REFERENCES

Baldwin, Charles A., et al., 2014. “First elevated-temperature performance testing of coated particle fuel compacts from the AGR-1 irradiation experiment.” *Nuclear Engineering and Design*. Vol. 271, 131–141.

- Chadwick, Mark B., et al. 2011. "ENDF/B-VII.1 Nuclear Data for Science and Technology: Cross Sections, Covariances, Fission Product Yields and Decay Data." Nuclear Data Sheets 112: 2887–2996, specific decay data accessed 2013-07-09 at <http://www.nndc.bnl.gov/endl/b7.1/>.
- Collin, Blaise P., 2015a. "AGR-1 Irradiation Test Final As-Run Report," INL/EXT-10-18097, Rev. 3, Idaho National Laboratory.
- Collin, Blaise P., 2015b, "AGR-3/4 Irradiation Test Final As-Run Report", INL/EXT-15-35550, Rev. 0, Idaho National Laboratory.
- Collin, Blaise P. 2018. "AGR-2 Irradiation Test Final As-Run Report." INL/EXT-14-32277, Rev. 4, Idaho National Laboratory.
- Demkowicz, Paul A., Jason Harp, Phil L. Winston, and Scott A. Ploger. 2012. "AGR-1 Fuel Compact 6-3-2 Post-Irradiation Examination Results." INL/EXT-12-27123. Idaho National Laboratory.
- Demkowicz, Paul A., Jason M. Harp, Philip L. Winston, and Scott a. Ploger. 2013. "Analysis of Fission Products on the AGR-1 Capsule Components." INL/EXT-13-28483.
- Demkowicz, Paul A., John D. Hunn, Rober N. Morris, Isabella van Rooyen, Tyler Gerczak, Jason M. Harp, and Scott A. Ploger. 2015a. "AGR-1 Post Irradiation Examination Final Report," INL/EXT-15-36407, Rev. 0, Idaho National Laboratory.
- Demkowicz, Paul A., Scott A. Ploger, Philip L. Winston, and Jason M. Harp. 2015b, "AGR-1 Compact 3-2-1 Post-Irradiation Examination Results." INL/EXT-15-36352, Idaho National Laboratory.
- Demkowicz, Paul A., Philip L. Winston, Jason M. Harp, and Scott A. Ploger. 2015c. "AGR-1 Compact 5-3-1 Post-Irradiation Examination Results." INL/EXT-15-36354. Idaho National Laboratory.
- Demkowicz, Paul A., Jason M. Harp, Philip L. Winston, Scott A. Ploger, and Isabella J. van Rooyen. 2015d. "AGR 1 Compact 4-1-1 Post-Irradiation Examination Results." INL/EXT-15-36169, Idaho National Laboratory.
- Demkowicz, Paul A., Scott A. Ploger, Philip L. Winston, and Jason M. Harp. 2015e. "AGR-1 Compact 1-3-1 Post-Irradiation Examination Results." INL/EXT-15-36365. Idaho National Laboratory.
- Demkowicz, P.A., et al., 2015f, "First high temperature safety tests of AGR-1 TRISO fuel with the Fuel Accident Condition Simulator (FACS) furnace." Journal of Nuclear Materials, vol. 464, 320-330.
- Demkowicz, Paul A., Scott A. Ploger, Philip L. Winston, and Jason M. Harp. 2015g. "AGR-1 Safety Tested Compact 4-3-3 Post-Irradiation Examination Results." INL/EXT-15-36457. Idaho National Laboratory.
- Demkowicz, P.A., John D. Hunn, Robert N. Morris, Charles A. Baldwin, Jason M. Harp, Philip L. Winston, Scott A. Ploger, Tyler Gerczak, Isabella J. van Rooyen, Fred C. Montgomery, Chinthaka M. Silva, 2016. "Irradiation performance of AGR-1 high temperature reactor fuel." Nuclear Engineering and Design, Vol 306, pp. 2-13.
- Gerczak, Tyler J., John D. Hunn, Richard A. Lowden, and Todd R. Allen. 2016. "SiC Layer Microstructure in AGR-1 and AGR-2 TRISO Fuel Particles and the Influence of its Variation on the Effective Diffusion of Key Fission Products." Journal of Nuclear Materials 480: 1–14.
- Gerczak, Tyler J., Anne A. Campbell, Grant W. Helmreich, Gerald E. Jellison Jr., and John D. Hunn. 2022. "Texture Analysis of AGR Program Matrix Materials." Journal of Nuclear Materials 398: 111965.
- Harp, Jason M., Paul A. Demkowicz, and John D. Stempien. 2020. "Fission product Inventory and Burnup Evaluation by Gamma Spectrometry of the AGR-2 Irradiation." INL/EXT-16-39777, Rev. 1. Idaho National Laboratory.

- Harp, Jason M., John D. Stempien, Paul A. Demkowicz. 2021. "Gamma Spectrometry Examination of the AGR-3/4 Irradiation." INL/EXT-20-58254, Rev. 1. Idaho National Laboratory.
- Hawkes, Grant L. 2012. "AGR-1 Daily As-Run Thermal Analyses." ECAR-968 Rev. 3, Idaho National Laboratory.
- Hawkes, Grant L. 2014a. "AGR-1 Daily As-Run Thermal Analyses." ECAR-9638, Rev. 4, Idaho National Laboratory.
- Hawkes, Grant L. 2014b. "AGR-2 Daily As-Run Thermal Analyses." ECAR-2476, Rev. 1, Idaho National Laboratory.
- Hawkes, Grant L. 2016. "AGR-3/4 Daily As-Run Thermal Analyses." ECAR-2807, Rev. 1, Idaho National Laboratory.
- Hunn, John D., Lowden, R.A., 2007, "Data Compilation for AGR-3/4 Driver Fuel Coated Particle Composite LEU03-09T", ORNL/TM-2007/019, Oak Ridge National Laboratory.
- Hunn, John D., G.E. Ellison, and R.A. Lowden. 2008. "Increase in pyrolytic carbon optical anisotropy and density during processing of coated particle fuel due to heat treatment." *Journal of Nuclear Materials*. 374: 445-452.
- Hunn, John D., Miller, J.H., 2009, "Data Compilation for AGR-3/4 Designed-to-Fail (DTF) Fuel Particle Batch LEU04-02DTF", ORNL/TM-2008/193, October 2009, Oak Ridge National Laboratory.
- Hunn, John, Trammell, M.P., Montgomery, F.C., 2011, "Data Compilation for AGR-3/4 Designed-to-Fail (DTF) Fuel Compact Lot (LEU03-10TOP2/LEU03-07DTF-OP1)-Z", ORNL/TM-2011/124, Oak Ridge National Laboratory
- Hunn, John D., Robert N. Morris, Charles A. Baldwin, Fred C. Montgomery, Chinthaka M. Silva, and Tyler J. Gerczak. 2012a, "AGR-1 Irradiated Compact 6-1-1 PIE Report: Evaluation of As-Irradiated Fuel Performance using Leach Burn Leach, IMGA, Materialography, and X-ray Tomography." ORNL/TM-2012/233, Oak Ridge National Laboratory.
- Hunn, John D., Robert N. Morris, Charles A. Baldwin, Fred C. Montgomery, and Chinthaka M. Silva. 2012b, "PIE on Five Irradiated AGR-1 Compacts." ORNL/LTR-2012/397, Oak Ridge National Laboratory.
- Hunn, John D., Robert N. Morris, Charles A. Baldwin, Fred C. Montgomery. 2012c. "Safety Tests on Irradiated AGR-1 Compacts 3-3-2, 3-2-2, and 6-2-1." ORNL/LTR-2012/396. Oak Ridge National Laboratory.
- Hunn, John D., Robert N. Morris, Charles A. Baldwin, Fred C. Montgomery. 2012d. "Summary of PIE on AGR-1 Compact 3-2-2," ORNL/LTR-2012/928. Oak Ridge National Laboratory.
- Hunn, John D., Robert N. Morris, Charles A. Baldwin, Fred C. Montgomery. 2012e. "Summary of Safety Test on Irradiated AGR-1 Compact 3-3-1." ORNL/LTR-2012/926. Oak Ridge National Laboratory.
- Hunn, John D., Robert N. Morris, Charles A. Baldwin, Fred C. Montgomery, Chinthaka M. Silva, and Tyler J. Gerczak. 2013a. "AGR-1 Irradiated Compact 4-4-2 PIE Report: Evaluation of As-Irradiated Fuel Performance with Leach Burn Leach, IMGA, Materialography, and X-ray Tomography." ORNL/TM-2013/236. Oak Ridge National Laboratory.
- Hunn, John D., Robert N. Morris, Charles A. Baldwin, Fred C. Montgomery, Chinthaka M. Silva, and Tyler J. Gerczak. 2013b. "PIE on Three Irradiated AGR-1 Compacts in FY2013." ORNL/LTR-2013/291, Oak Ridge National Laboratory.
- Hunn, John D., et al., 2013c. "Safety Tests on Irradiated AGR-1 Compacts 4-1-2, 4-4-3, and 4-4-1," ORNL/LTR-2013/290. Oak Ridge National Laboratory.

- Hunn, John D., Robert N. Morris, Charles A. Baldwin, and Fred C. Montgomery. 2013d. "Safety Tests on Irradiated AGR-1 Compacts 5-3-3 and 5-1-3." ORNL/LTR-2013/603. Oak Ridge National Laboratory.
- Hunn, John D., Charles A. Baldwin, Tyler J. Gerczak, Fred C. Montgomery, Robert N. Morris, and Chinthaka M. Silva. 2014a. "AGR-1 Irradiated Compacts 5-2-3 and 5-2-1 PIE Report: Evaluation of As-Irradiated Fuel Performance with Leach Burn Leach, IMGA, Materialography, and X-ray Tomography." ORNL/TM-2014/171, Oak Ridge National Laboratory.
- Hunn, J. D., R. N. Morris, C. A. Baldwin, F. C. Montgomery, and T. J. Gerczak, 2014b, PIE on Safety-Tested AGR-1 Compacts 5-3-3, 5-1-3, and 3-2-3, ORNL/TM-2014/484, Oak Ridge National Laboratory, Oak Ridge, Tennessee, 2014
- Hunn, John D., Robert N. Morris, Charles A. Baldwin, Fred C. Montgomery, and Tyler J. Gerczak, 2014c. "PIE on Safety-tested AGR-1 Compacts 4-1-2 and 4-4-3." ORNL/LTR-2014/101 Rev. 0. Oak Ridge National.
- Hunn, John D., Robert N. Morris, Charles A. Baldwin, and Fred C. Montgomery. 2014d. "Safety Test on Irradiated AGR-1 Compact 4-2-2." ORNL/LTR-2014/485. Oak Ridge National Laboratory.
- Hunn, J.D., Lowden, R.A., Miller, J.H., Jolly, B.C., Trammell, M.P., Kercher, A.K., Montgomery, F.C., and Silva, C.M., 2014e, "Fabrication and Characterization of Driver Fuel Particles, Designed-to-Fail Fuel Particles, and Fuel Compacts for the US AGR-3/4 Irradiation Test, Nuclear Engineering and Design 271 (2014) 123-130.
- Hunn, John D., Robert N. Morris, Charles A. Baldwin, Fred C. Montgomery, Tyler J. Gerczak, 2015a. "PIE on Safety-Tested AGR-1 Compact 4-2-2." ORNL/TM-2015/033, Rev. 0. Oak Ridge National Laboratory.
- Hunn, John D., Robert N. Morris, Charles A. Baldwin, and Fred C. Montgomery. 2015b. "Safety Testing of AGR-2 UO₂ Compacts 3-3-2 and 3-4-2." ORNL/TM-2015/388, Oak Ridge National Laboratory.
- Hunn, John D., Robert N. Morris, Charles A. Baldwin, Fred C. Montgomery, and Tyler J. Gerczak. 2015c. "PIE on Safety-Tested AGR-1 Compact 5-1-1." ORNL/TM-2015/317. Oak Ridge National Laboratory.
- Hunn, John D., Robert N. Morris, Charles A. Baldwin, and Fred C. Montgomery. 2016a. "Safety Testing of AGR-2 UCO Compacts 5-2-2, 2-2-2, and 5-4-1." ORNL/TM-2016/423, Oak Ridge National Laboratory.
- Hunn, John D., Charles A. Baldwin, Tyler J. Gerczak, Fred C. Montgomery, Robert N. Morris, Chinthaka M. Silva, Paul A. Demkowicz, Jason M. Harp, and Scott A. Ploger. 2016b. "Detection and analysis of particles with failed SiC in AGR-1 fuel compacts." *Nuclear Engineering and Design*, Vol. 306, pp. 36-46.
- Hunn, John D., Robert N. Morris, Charles A. Baldwin, Zachary M. Burns, Fred C. Montgomery, and Darren J. Skitt. 2017. "Safety Testing of AGR-2 UCO Compacts 6-4-2 and 2-3-1." ORNL/TM-2017/439, Oak Ridge National Laboratory.
- Hunn, John D., Charles A. Baldwin, Fred C. Montgomery, Tyler J. Gerczak, Robert N. Morris, Grant W. Helmreich, Paul A. Demkowicz, Jason M. Harp, and John D. Stempfen. 2018a. "Initial Examination of Fuel Compacts and TRISO Particles from the US AGR-2 Irradiation Test." *Nuclear Engineering and Design* 329: 89–101.
- Hunn, John D., Robert N. Morris, Fred C. Montgomery, Tyler J. Gerczak, Darren J. Skitt, Charles A. Baldwin, John A. Dyer, Grant W. Helmreich, Brian D. Eckhart, Zachary M. Burns, Paul A. Demkowicz, and John D. Stempfen. 2018b. "Post-Irradiation Examination and Safety Testing of US

- AGR-2 Irradiation Test Compacts.” Paper 10 in Proceedings of the 9th International Topical Meeting on High Temperature Reactor Technology (HTR-2018), Warsaw, Poland, October 8–10, 2018.
- Hunn, John D., Tyler J. Gerczak, Fred C. Montgomery, Darren J. Skitt, Charles A. Baldwin, Grant W. Helmreich, Brian D. Eckhart, and John A. Dyer. 2018c. “AGR-2 As-Irradiated UCO Compact 5-4-2 PIE Report.” ORNL/TM-2018/863, Oak Ridge National Laboratory.
- Hunn, John D., Robert N. Morris, Fred C. Montgomery, Tyler J. Gerczak, Darren J. Skitt, Grant W. Helmreich, Brian D. Eckhart, and Zachary M. Burns. 2018d. “Safety Testing and Post-Safety-Test Examination of AGR-2 UCO Compact 2-3-2 and AGR-2 UO₂ Compact 3-4-1.” ORNL/TM-2018/956, Oak Ridge National Laboratory.
- Hunn, John D., Tyler J. Gerczak, Fred C. Montgomery, Darren J. Skitt, Charles A. Baldwin, Grant W. Helmreich, Brian D. Eckhart, and John A. Dyer. 2018e. “AGR-2 Safety-Tested UCO Compact 6-4-2 PIE Report.” ORNL/TM-2018/864, Oak Ridge National Laboratory.
- Hunn, John D., Robert N. Morris, and Zachary M. Burns. 2019. “Transient Temperature Safety Testing of AGR-2 UCO Compacts 5-1-1, 5-1-2, and 5-3-1.” ORNL/TM-2019/1292, Oak Ridge National Laboratory.
- Hunn, John D., Robert N. Morris, Tyler J. Gerczak, Fred C. Montgomery, Darren J. Skitt, Grant W. Helmreich, Brian D. Eckhart, Zachary M. Burns, and Charles A. Baldwin. 2019a. “Post-Irradiation and Post-Safety Test Examination of AGR-2 TRISO Performance.” Presented at Gas-Cooled Reactor Fuels and Methods Program Review at Idaho National Laboratory, June 18–19, 2019.
- Hunn, John D., Tyler J. Gerczak, Robert N. Morris, Fred C. Montgomery, Darren J. Skitt, Brian D. Eckhart, and Zachary M. Burns. 2019b. “Safety Testing and Destructive Examination of AGR-2 UCO Compact 2-1-2.” ORNL/TM-2019/1201, Oak Ridge National Laboratory.
- Hunn, John D., Tyler J. Gerczak, Robert N. Morris, Fred C. Montgomery, Darren J. Skitt, Brian D. Eckhart, and Zachary M. Burns. 2019c. “Safety Testing And Destructive Examination of AGR-2 UCO Compact 6-4-3.” ORNL/TM-2019/1200, Oak Ridge National Laboratory.
- Hunn, John D., Robert N. Morris, Fred C. Montgomery, Darren J. Skitt, and Zachary M. Burns. 2020a. “Safety Testing and Destructive Examination of AGR-2 UO₂ Compact 3-1-1.” ORNL/TM-2020/1451, Oak Ridge National Laboratory.
- Hunn, John D., Tyler J. Gerczak, Robert N. Morris, Fred C. Montgomery, Darren J. Skitt, Grant W. Helmreich, Brian D. Eckhart, and Charles A. Baldwin. 2020b. “Destructive PIE and Safety Testing of Six AGR-2 UO₂ Capsule 3 Compacts.” ORNL/TM-2020/1612, Oak Ridge National Laboratory.
- INL. 2022. “Technical Program Plan for INL Advanced Reactor Technologies Advanced Gas Reactor Fuel Development and Qualification Program.” PLN-3636, INL/MIS-10-20662, Rev. 11. Idaho National Laboratory.
- Kercher, A.K. and Hunn, J.D., 2006, “Results from ORNL Characterization of Nominal 350 μ m LEUCO Kernels (LEU03) from the BWXT G73V-20-69303 Composite”, ORNL/TM-2006/552, October 2006, Oak Ridge National Laboratory.
- Kercher, Andrew K., Jolly, Brian C., Montgomery, Fred C., Silva, G.W.C, and Hunn, John D., 2011. “Data Compilation for AGR-3/4 Designed-to-Fail (DTF) Fuel Particle Batch LEU03-07DTF”, ORNL/TM-2011/109, Oak Ridge National Laboratory.
- Maki, John T., David A. Petti, Darrell L. Knudson, and Gregory K. Miller. 2007. “The Challenges Associated with High Burnup, High Temperature and Accelerated Irradiation for TRISO-coated Particle Fuel.” *Journal of Nuclear Materials* 371: 207-280.

- Morris, Robert N., Paul A. Demkowicz, John D. Hunn, Charles A. Baldwin, Edward L. Reber, 2016. "Performance of AGR-1 high temperature reactor fuel during post-irradiation heating tests." *Nuclear Engineering and Design*, Vol 306, pp. 24-35.
- Morris, Robert N., John D. Hunn, Charles A. Baldwin, Fred C. Montgomery, Tyler J. Gerczak, and Paul A. Demkowicz. 2018. "Initial Results from Safety Testing of US AGR-2 Irradiation Test Fuel." *Nuclear Engineering and Design* 329:124–133.
- Petti, David A., Richard R. Hobbins, Peter Lowry, and Hans Gougar. 2013. "Representative Source Terms and the Influence of Reactor Attributes on Functional Containment in Modular High-Temperature Gas-cooled Reactors." *Nuclear Technology* 184: 181-197.
- Pham, Binh T., Jeffrey J. Einerson, and Grant L. Hawkes. 2013. "Uncertainty Quantification of Calculated Temperatures for the AGR-1 Experiment." INL/EXT-12-25169, Rev. 1., Idaho National Laboratory.
- Pham, Binh T., Jeffrey J. Einerson, Dawn M. Scates, John T. Maki, and David A. Petti. 2019. "AGR-1, AGR-2, and AGR-3/4 Release-to-Birth Ratio Data Analysis." INL/EXT-14-32970, Rev. 2. Idaho National Laboratory.
- Phillips, Jeffrey A., Charles M. Barnes, and John D. Hunn. 2010. "Fabrication and Comparison of Fuels for Advanced Gas Reactor Irradiation Tests." Paper 236 in *Proceedings of the 5th International Topical Meeting on High Temperature Reactor Technology (HTR-2010)*, Prague, October 18–20, 2010.
- Schenk, Werner, D. Pitzer, and H. Knauf. 1993. "Simulation der max. MODUL-Störfallaufheizkurve (AVR-GLE 3, 09/20) und deren Extrapolation auf 1700°C (AVR-GLE 3, 91/31)." IWE-TN-17/93 Forschungszentrum Jülich GmbH (KFA).
- Stempien, John D., Paul A. Demkowicz, Edward L. Reber, and Cad L. Christensen. 2016. "High-Temperature Safety Testing of Irradiated AGR-1 TRISO Fuel." Paper HTR2016-18595. *Proc. 8th International Topical Meeting on High Temperature Reactor Technology (HTR-2016)*, Las Vegas, Nevada, November 6–10, 2016.
- Stempien, John D., Paul A. Demkowicz, Jason M. Harp, and Philip L. Winston. 2018. "AGR-3/4 Experiment Preliminary Mass Balance." INL/EXT-18-46049, Rev. 0, Idaho National Laboratory.
- Stempien, John D. and Paul A. Demkowicz. 2020. "AGR-2 Irradiation Experiment Fission Product Mass Balance." INL/EXT-19-53559, Rev. 1, Idaho National Laboratory.
- Stempien, John D. 2020. "AGR-2 Compact 6-4-1 Post-Irradiation Examination Results." INL/EXT-18-45418, Idaho National Laboratory.
- Stempien, John D. 2021. "Measurement of Fission Product Concentration Profiles in AGR-3/4 TRISO Fuel Graphitic Matrix and Nuclear Graphites." INL/EXT-21-62863, Idaho National Laboratory.
- Stempien, John D., John D. Hunn, Robert N. Morris, Tyler J. Gerczak, and Paul A. Demkowicz. 2021. "AGR-2 TRISO Fuel Post-Irradiation Examination Final Report." INL/EXT-21-64279, Rev. 0, Idaho National Laboratory.
- Sterbentz, James W. 2013. "JMOCUP As-Run Daily Depletion Calculation for the AGR-1 Experiment in ATR B-10 Position." ECAR-958, Rev. 2, Idaho National Laboratory.
- Sterbentz, James W. 2014. "JMOCUP As-Run Daily Depletion Calculation for the AGR-2 Experiment in ATR B-12 Position." ECAR-2066, Rev. 2, Idaho National Laboratory.
- Sterbentz, James W. 2015. "JMOCUP As-Run Daily Physics Depletion Calculation for the AGR-3/4 TRISO Particle Experiment in ATR Northeast Flux Trap." ECAR-2753, Rev. 1, Idaho National Laboratory.